PREDICTION OF DOWNHOLE GAS WELL PITTING CORROSION IN CO_2 AND H_2S ENVIRONMENT

By

MOHSEN HEDI ACHOUR

Bachelor of Science
In Chemical Engineering
Oklahoma State University
Stillwater, Oklahoma
1986

Master of Science
Oklahoma State University
Stillwater, Oklahoma
1987

Submitted to the Faculty of the
Graduate College of the
Oklahoma State University
in partial fulfillment of
the requirements for
the Degree of
DOCTOR OF PHILOSOPHY
May, 1992

PREDICTION OF DOWNHOLE GAS WELL PITTING CORROSION IN CO2 AND H2S ENVIRONMENT

Thesis Approved:

Thesis Advisor

Dean of the Graduate College

ACKNOWLEDGMENTS

I wish to express my sincere gratitude and appreciation to my major advisor, Dr. R. C. Erbar, for the continuous support and assistance throughout this work. Unfortunately, she did not have a chance to sign this document since she passed away just as this work was finished. God bless her soul. I am grateful to my committee members, Drs. A. H. Johannes, K. J. Bell, K. A. M. Gasem, C. E. Price, and J. H. Kolts for their technical assistance. I would like to thank the industrial sponsors from Conoco, Phillips, Marathon, Arco, Exxon, and Norsk Hydro for their financial support and technical help. I am also thankful to all the staff of the corrosion and materials section - production division of Conoco at Ponca City, and to Dr. R. L. Robinson Jr. and the School of Chemical Engineering at Oklahoma State University. I would like to extend my thanks to Dr. Guohai Liu for discussing technical matters pertaining to this work.

I wish to express my sincere thanks and appreciation to my dearest family: my loving mother, Hamdouna, my caring sister, Jamila, and her family, and my dear brothers, Wahab and Hamadi, and their families for their continuous encouragment. My sincere thanks and gratitude to all my friends, here in the U.S.A. and in Tunisia, for their moral

support and continued caring.

I dedicate this work to my loving mother, Hamdouna, and to my memorable father, Hedi, who always encouraged me to further my education but unfortunately did not have the chance to see my accomplishments. God bless his soul.

TABLE OF CONTENTS

LIST OF TABLES

LIST OF FIGURES

NOMENCLATURE

C_i	Concentration of species i
d	Depth of pit
D_i	Diffusion coefficient of species i
E_c	Critical pitting corrosion
f	Friction factor
F	Faraday's constant, 96500 C/sec
f_i	Fugacity of species i
F_D	Distribution function
h	Pit depth
h^+	Boundary layer thickness
H_i	Henry's constant of species i
i	Current density; number of samples
I	Ion strength
i_a	Anodic current density
i_{ao}	Exchange current density
i_c	Corrosion current
J_i	Flux of species i
k	Ratio of outer to inner radius; rate constant
K	Equilibrium constant; mass transfer coefficient
m	Constant
m_i	Molality of species i
n	Constant
N	Number of data points

N_T	Total number of specimens
N_c	Number of pitted specimens
P	Probability of occurrence; total pressure
P_i	Plotting position of data point i
$P(X_i)$	Probability of occurrence of element X_i
P_s	Probability that a pipe has not leaked
Q	Charge density
Q(E)	Probability to observe a potential E
R	Outer cylinder radius; universal gas constant; Risk of occurrence
R_i	Rank of data point number i
R_e	Reynold number
R_i	Rate of depletion or production of species i
r_p	Pit radius, i.e., half of the width
t	Exposure time, time
T	Temperature
u	Velocity
v	Potential sweep rate
V	Characteristic age
V_p	Fluid velocity in a pipe
W	Pipe thickness
x_m	Mean value
y_i	Mole fraction of species i in the vapor phase
Y	Reduced Variate, also denoted as y
z_i	Charge of species i
α	Shape parameter
α_c	Risk factor
ß	Scale parameter

ρ	Density
τ	Wall shear stress
μ	Viscosity
μ_n	Mode of the whole pitting data population
μ_e	Mean of the extreme value distribution
σ_e	Variance of the extreme value distribution
η_a	Overpotential
ω_o	Angular velocity
Y	Characteristic age
Φ	Electrostatic potential
Φ_i	Activity coefficient of species i
$\Phi(x)$	Probability distribution of x
ε_D	Eddy diffusivity
$\mathfrak{R}$	Radius of curvature of the spherical pit

CHAPTER I

INTRODUCTION

Over the years, premature failures of different types of structures have increased the public awareness and fear of the lack of technical reliability within the design stage. Such calamities are often caused by either a deliberate neglect of minor problems or an incomplete understanding of the phenomena at hand. To overcome such problems, engineers in different disciplines have been specifying well detailed designs and researchers have strived to find sound and thorough solutions to existing problems. Within the corrosion area, research efforts have been enormous, covering advanced topics in corrosion modeling, measurement, control, and prevention. Specifically, several corrosion models have been developed mainly to predict uniform corrosion rates in gas and oil wells and pipelines exposed to various internal environments. Such predictions are used to provide for better designs and to facilitate corrosion prevention and control. However, it is often found difficult to fully describe and predict localized corrosion, such as crevice corrosion, stress corrosion cracking, pitting corrosion, and intergranular attack due to the inherent random occurrences of such phenomena.

In particular, pitting attack is a form of localized corrosion in which metal is removed preferentially from vulnerable areas on the surface. More specifically,

pitting corrosion is the local dissolution of material leading to the formation of cavities in protected metals which are exposed to aqueous solutions containing aggressive anions, primarily chlorides. In general, the protection of the metal is the result of the presence of an inhibitor film, a metal oxide film, an iron carbonate or sulfide scale, or a coating layer. This work concentrates on modeling pitting corrosion of untreated bare carbon steel tubing in CO_2 and H_2S environments for downhole applications.

Firstly, the initiation of CO_2 pitting corrosion has been experimentally investigated in both chemically inhibited and uninhibited systems. The essence of the experimental work is to show the fluid flow effects on the initiation mode of pitting in CO_2 environments. A second goal consists of testing the viability of using some traditional electrochemical methods, usually employed for stainless steel pitting susceptibility analysis, to study pitting initiation and propagation on carbon steel in CO_2 systems. The experimental work and the results are described in detail in the next chapter.

Secondly, a statistical model has been developed in order to analyze the inherent probabilistic behavior of pitting corrosion observed at the macro level. This model is based on the Extreme Value Theory, which has been found viable for studying the behavior of the deepest pits present in a chosen structure. Given experimental data or a caliper survey analysis, the model is capable of fitting the data into the appropriate distribution function and providing the analysis and predictions for the given data. Predictions of time to first leak and of corrosion allowance can be made for time dependent data. The model is fully described in chapter III.

Finally, a theoretical model has been formulated in order to predict the extent

of pit growth under the effect of high turbulence regimes. Given the flow conditions in the main stream and an initial shape of a pit along the pipe, the model predicts the hydrodynamics inside the pit and the extent of propagation or repassivation, accounting for the equilibrium condition, the surface kinetics, the electrochemical process at the surface, and the fluid flow inside the cavity. The hydrodynamics model is based on the phenomenon of flow separation and reattachment for shallow and medium size pits, whereas the skimming flow analysis is applied in the case of deep pits. The model has been used to study the effect of velocity on the wall shear stress, the pit surface concentration of ferrous ion, the mass transfer coefficient in and out of the cavity, and the overall propagation rate of the existing pit. The model has also been tested to predict the severity of actual gas wells. For a given downhole string, the model calculations are performed at subsections of the tubing in order to predict the dynamic behavior of an existing pit along the wall under the effect of the fluid flow regime. Chapter IV covers a full description of the model.

The development of the experimental work and the two models will allow some understanding of the phenomenon of pitting corrosion in CO_2 and H_2S environments. Such a localized attack, even though having caused enormous numbers of failures, has not been fully understood because of the theoretical complexities involved and its inherent random behavior. The following chapters describe an approximate picture of pitting corrosion occurring in downhole environments in the presence of CO_2 and H_2S containing brines. The treatment is nearly complete as it presents an experimental study of pit initiation, a statistical analysis of the phenomenon, and a predictive mechanistic model of pit growth under flow effects.

CHAPTER II

LITERATURE REVIEW

Pitting Initiation in CO_2 Environments

In the past few years, electrochemical measurements of pitting corrosion of stainless steels have been studied extensively. Less work has been done on carbon steels, especially in CO_2 environments, in which case it is difficult to distinguish between the contributions of uniform corrosion and pitting attack to the overall weight loss. However, in the case of stainless steels, almost all the weight loss during pitting comes from the localized corrosion. It is important to determine how and where pitting occurs in CO_2 environments in downhole tubing. From field observations, i.e., caliper survey analysis and failed structures, pitting most often occurs at joints and occasionally along the tubing. To explain such occurrences, two experimental procedures have often been used. Several authors (Strutt et al. 1985, Marsh et al. 1988) studied pitting corrosion by immersing carbon steel in stagnant seawater-oil solutions saturated with CO_2. Others (Videm and Dugstad 1988) had built high velocity flow loops to simulate the environment at the connection between two joints along the tubing. The former practice is valid only if the samples are soaked in the solution for a long period, otherwise the "pits" may simply represent early nucleation sites of uniform corrosion. At long exposure times, the localized attack can be

legitimately taken as pitting corrosion. The results from a typical caliper survey show that pits are formed at the upper and lower ends of the joints, apparently because of the higher density of gas bubbles and the high velocities at those locations. This effect could be a result of the existence of swirling type flow or eddy turbulence.

Pitting corrosion is hypothesized to initiate in CO_2 environments at downhole tubing following two mechanisms: either from mechanical disturbances occurring at locations where high turbulence exists, or at sites where localized defects have been introduced in a protective film. Example defects in carbon steels include inherent metal flaws, i.e. inclusions (Gösta 1969, 1974, Berendson et al.1980), or a reticulated iron carbonate film (Videm et al. 1987). The electrochemical methods, traditionally used in the examination of pitting corrosion of stainless steels, have been tested for viability in the case of carbon steels. Obviously, the protective films, i.e., chromium oxide versus iron carbonate, are quite different in structure and behavior. It is possible that both films, if locally destroyed, can create a corrosion cell where the pit is the anode and the metal surface is the cathode. The initiation step itself can be either due to the hydrodynamics or to the electrochemical effects. In the case of chemical inhibition, pit growth will proceed if either the inhibitor does not repassivate the surface inside the pit or if the hydrodynamics result in continuous removal of the inhibitor. The corrosion cell between the surface and the pit is more pronounced in stainless steel than carbon steel (Pourbaix 1974). Nevertheless, the presence of iron carbonate on the surface of steel and its local removal from the pit site can form a concentration cell which causes the pit to enlarge.

Statistical Modeling of Pitting Corrosion

The use of statistical theories in analyzing and interpreting plant or experimental corrosion data has been of great importance since the early thirties. The application of probability concepts to describe the corrosion probability and velocity was first introduced by Evans, Mears, and Queneau back in 1933. Mears and Brown (1937) quantified the corrosion probability and applied it to pitting corrosion in aluminum. The chance of attack experienced by specimens of a specific size under a known set of conditions has been termed the corrosion probability and expressed in percentage from the following equation:

$$P = 100 * \frac{N_c}{N_T} \qquad (2.1)$$

N_T being the total number of specimens and N_c the number of specimens showing any traces of localized attack. It was postulated and experimentally verified that an increase in the area of metal increases the probability of pitting occurrences at some locations on the specimen but decreases the number of breakdowns per unit area.

Aziz and Godard (1952) emphasized that the corrosion probability is solely a measure of the metal tendency to initiate pitting and gives no indication of the rate of penetration once pitting has occurred. Such a rate was termed pitting or growth rate. For short periods, this rate is given roughly by:

$$d = Kt^{1/3} \qquad (2.2)$$

where d is the depth of pit, K is a constant depending on the alloy structure and the environment, and t represents time of exposure. This relation indicates that doubling the thickness of a structure will increase the time to penetration by a factor of eight. The experimental results concluded that the addition of 1.0 % magnesium and 1.25 % manganese; or 0.5% magnesium and 0.5 % manganese reduces the pitting susceptibility of 99.5 to 99.7 % pure aluminum. It was also concluded that above 99.7 % purity, pitting probability is reduced as the purity increases without any alloying.

By the early forties, the extreme value statistical methods, as described by Gumbel (1954, 1958) for the prediction of naturally occurring calamities, had been successfully applied to corrosion work. Chilton and Evans (1955), Streicher (1956), Greene and Fontana (1959), and Sato (1976) had used the concepts of statistics in analyzing the stochastic process of pitting corrosion in wrought iron and stainless steels.

It was shown that the population of pits observed on a given corroded sample follow an exponential type distribution. In addition the statistical theory of extremes can be applied to maximum pit depth data. It was also postulated and shown that the maximum pit depth observed on replicate samples is the most satisfactory measure of the rate of growth of a pit despite the uncertainty introduced as a result of the statistical nature of the phenomenon. The maximum pit depths measured on each of the samples were analyzed according to the statistical theory of extreme values using the corresponding probability paper and were shown to fit the extreme value distribution. This led to the following mathematical expression for the distribution:

$$\Phi(x) = e^{-e^{-y}}, \tag{2.3}$$

where

$$y = \alpha(x-u). \tag{2.4}$$

The reduced variate is y, and u and α are the parameters of the distribution. The mode or highest point of the distribution is u, and α is the scale parameter defined such that $(1/\alpha)$ is the product of $(\sqrt{6}/\pi)$ and the standard deviation of the distribution. The information from such an analysis on aluminum was used by Aziz (1956) to predict the probability of occurrence of a pit of a certain depth, the number of samples needed before a pit of a specified depth can be detected, and the frequency of pits of any chosen depth. Most importantly, he showed that the probability of occurrence of deep pits varies linearly with the logarithm of the exposed area; therefore it would be legitimate to extrapolate pitting data obtained in the laboratory on small samples to large scale field installations.

Eldredge (1957) applied the extreme value statistical method in analyzing caliper survey data collected for the investigation of corrosion in oil and gas wells. He devised a new method for presenting and plotting such data in order to provide the expected deepest pit, as a single-value representative of the survey data. This was called the Pit Depth Rank Chart.

Godard (1960) verified, through laboratory pitting test methods, the existence

of a cube root dependency rate curve for the pitting of aluminum in water with respect to time. The analysis of the laboratory data suggested that the maximum pit depth, d, was proportional to the cubic root of time, t. The equation

$$d^3 = Kt \tag{2.5}$$

should be used in preference to equation (2.2) in order to avoid the assumption that pitting initiates at the time of immersion, therefore accounting for the inevitable induction time. This pitting rate law, if used in parallel with the results from the extreme value distribution method, allows the determination of time to initial leak.

Finley and Toncre (1964) used the extreme value statistical analysis to correlate the time-to-first perforation on 2500 miles of pipelines submerged in Lake Maracaibo, Venezuela. In their analysis, the pipeline was divided into several lines. In order to predict the time-to-first leak for each line, a probability distribution function was needed to describe the behavior of the deepest pits in each line. Gumbel's theory of extreme values presents three choices for the initial distribution function:

(1) The exponential type is chosen if the probability of deep pits drops off exponentially as the pit depth increases. The prototype of this category is the exponential function itself. The most important distributions are the normal, the chi-square, and the log normal distributions.

(2) The Cauchy type is selected if the above rate of probability drop is faster than the exponential function but approaches the power function. The Cauchy distribution is

chosen as the prototype.

(3) The third type is selected if there exists a pit depth that is approached but not exceeded, i.e., the probabilities of all deeper pits become zero. This type of distributions are denoted as "limited distributions". The first and second type of distributions are not bounded to the left or to the right, whereas this type of limited distributions presents limit values to the right for largest values and to the left for smallest values. Such criterion was found appropriate in describing the behavior of the deepest pits and it was used by Finley and Toncre in predicting the time-to-first leak for each section of the pipeline.

The cumulative probability of survival, i.e., the probability that a line has not leaked at age x was expressed as follows:

$$\Phi(x) = \exp[-(x/V)^k] \qquad (2.6)$$

The exponent, k, is a constant for all pipe sizes and is a measure of the density of the population of leaks around the mode, i.e., the skewness of the probability density curve. The characteristic age, V, is a function of the pipe thickness, W, and is an indication of the environment corrosivity. For coated steel pipeline in Lake Maracaibo, the following correlation had been used to calculate the general survival function:

$$\Phi(x) = \exp[-(x^{2.46}/53400W^{1.24})] \qquad (2.7)$$

Three years later, Finley (1967) continued the same work as above in an effort

to generalize the concept for different environments. If P_s is the probability of survival, t is the time to first leak in months, and V is the characteristic age in months, then the probability that a line has not leaked is as follows:

$$P_s = \exp[-(t/V)^k] \qquad (2.8)$$

Three different sets of data were fitted to the above expression and values for V and k were easily computed. Values of V range from 49 to 61, and k from 1.5 to 2.4. The outside diameter of the pipe, the weight per unit length, and the wall thickness have an effect on the magnitude of V, the characteristic age of the pipe. The paper also demonstrates that if the maximum pit depths conform to a Gumbel type 1 asymptotic distribution, i.e., follow the extreme value hypothesis, and the pits continue to deepen according to a logarithmic growth law, then the times-to-perforation of the samples conform to a Gumbel type 32 asymptotic distribution shown in the equation (2.6).

So far, all the experimental data collected from the above references were obtained by measuring the depths of pits generated on the surface of the structures. Such data have illustrated the stochastic behavior of pitting corrosion. On the other hand, Shibita and Takeyama (1977) were able to show the same random behavior of pitting corrosion through electrochemical measurements mainly to detect pitting initiation. Linear dependence of the pit generation rate on the potential suggested that the pitting process was controlled not only by an electrochemical reaction, but also by a mechanical breakdown of the passive film which is bound to be a stochastic process. The existing flaws of various sizes, i.e., the inherent cracks, can be considered as

precursors or active sites in the film which can yield to the generation of pits of different sizes. The statistical theory assumes that the pit generation process obeys the Markov property. This is based on the assumption that the probability of initiating a pit in the future is independent of the past state of the structure and can fully be specified once the probability of the pit generation at present is known.

Provan and Rodriguez (1989) have recently proposed a new Markov stochastic process to describe the growth of maximum pit depth with time in pitting corrosion systems. Again, the extreme value distribution analysis was used, and in this work the distribution function, F_D, was expressed as follows:

$$F_D(d) = e^{-e^{-\alpha(d-\beta)}}, \qquad (2.9)$$

where α and ß are the parameters of the distribution , D is the random variable maximum pit depth, and d is a specific outcome of D. The details of the model tend to be complicated by virtue of using principles from set theory, measure theory, the axiomatic definitions of probability and conditional probability, random variables, and distribution functions. But, the main essence of a Markov process is that it is a stochastic process which has no memory that would allow it to use past information to modify the probabilities which follow. In other words, the knowledge of the present state of the process makes its future independent of the past. In order to formulate the problem, the above assumption is used along with the implementation of the idea that if the maximum pit on a certain area of observation is in state (j-1) at time t, then during the time interval (t,t+dt), it grows to state j with probability P:

$$P = \delta(j-1)\frac{(1+\delta t)}{(1+\delta t^{\Phi})} \qquad (2.10)$$

The model is found fully operational with the determination of the two parameters, δ and ϕ, called the corrosion system parameters, which can be computed through fitting the experimental data to an absolute probability equation formulated following the Markov process hypothesis. The study of the statistical behavior of pitting corrosion is continuously being carried out due to its attractive capability to predict structure reliability (Nathan 1971, Stetler 1980, Sheikh et al. 1990, Gabrielli 1990, and Boffardi 1989-90).

Flow Induced Pit Propagation

The rapidity with which pitting corrosion can lead to the a premature failure of a given structure and the extreme unpredictability of the time and location of the attack has necessitated the need for a detailed study of the phenomenon. Due to the various difficulties associated with the experimental simulations and measurements needed for a full understanding of the pitting process, several investigators have developed theoretical models in an attempt to predict the rate of growth of localized corrosion in different environments. Sharland (1987) provided a complete review of the theoretical modelling of pitting corrosion performed before 1986, as an attempt to highlight both the usefulness and the weaknesses of the state of the art work. Even though various authors have developed different theoretical models to fit their applications, a common aim has dominated the focus of their studies. Mainly, the

mathematical models have been developed to predict the solution chemistry and electrochemistry within the restricted geometries of the pits as a function of several parameters such as cavity dimensions, bulk solution compositions, fluid velocity, etc. Such information is used to predict pit penetration rates. The developed models vary from simple to complex and from semi empirical to purely theoretical. The latter models, based on more rigorous physical arguments, are found more useful and viable to provide reliable answers related to a given corrosive environment.

Although the detailed models might be different in application, the same fundamental equations governing the mass transport of aqueous chemical species in electrolyte solutions are used. The general mass balance equation for a species i can be written as

$$\frac{\partial C_i}{\partial t} = -\nabla \left[-D_i \nabla C_i - \frac{z_i D_i F}{RT} C_i \nabla \Phi + u C_i \right] + R_i \qquad (2.11)$$

where C_i is the concentration of the ion i, D_i is the diffusion coefficient, z_i is the charge, ϕ is the electrostatic potential, u is the velocity describing the motion of the electrolyte, and R_i represents the rate of production or depletion of species i by chemical reaction. The electrostatic potential is governed by Poisson's equation,

$$\nabla^2 \Phi = \frac{Q}{\epsilon_o} \qquad (2.12)$$

where Q is the charge density. Poisson's relation is approximated by satisfying the local electroneutrality equation (Levich 1962):

$$\sum_i z_i C_i(x) = 0 \qquad (2.13)$$

The flux of the species is related to the current density by applying Faraday's law:

$$i = F \sum_i z_i J_i \qquad (2.14)$$

the flux of species i, J_i, includes the terms for concentration gradient, potential difference, and convection effects:

$$J_i = -D_i \nabla C_i - \frac{Z_i D_i F}{RT} C_i \nabla \Phi + u C_i \qquad (2.15)$$

The specification of the boundary conditions usually consists of fixing the species concentrations at the bulk solution outside the cavity and describing the active species fluxes at the metal surface. The resulting problem is a set of highly nonlinear partial differential equations to be solved, in the most general form, by a suitable numerical method. In summary, when formulating a general model which simulates the growth process of an existing pit, several factors are to be accounted for:

1) The solution chemistry within and outside the pit.

2) The electrochemical and the chemical reaction rates occurring between the existing species. The dependence of such rates on different parameters, such as pH and electrostatic potential, is to be also incorporated.

3) The variation of species concentrations with time, i.e., the unsteady state behavior.

4) The transfer or the migration of ions under potential and concentration gradients.

5) The formation of reaction products and their effects on pit propagation.

6) The fluid flow effects on the mobility of ions and of reaction products.

7) The significance of the changing shape of the pit as it enlarges.

Melville (1979) developed a simple model based on transport by electromigration only. The resulting equation was solved analytically to predict the variation of potential in the pit and compare the results to measured experimental data. The usefulness of this model is to verify and validate some electrochemical fundamentals associated with the dynamics of the cathodic and anodic sites. It was concluded that the anodic reactions at the crack tip had to balance the cathodic charges generated both at the specimen surface and at the sides.

On the other hand, several models have considered ionic transport by diffusion only (Faita 1974, Tester and Isaacs 1975, Alkire et al. 1978, Alkire and Siitari 1979). The justifications are either that the potential drop associated with the system is negligible, or that a supporting electrolyte is present in enough excess to carry all the charges, i.e., the concentration of the electrolyte ions is greater than those of the reactive species. Faita had derived the concentration profiles in a wedge-shaped crack by solving the simplified mass balance equation. He had not tested his predictions against experimental data. Tester and Isaacs had experimentally simulated a parallel-sided cavity and proven that the potential drop in the crack was insignificant. Alkire modeled the pit as a circular cylinder filled with a solution of electrolyte containing a soluble salt of the corroding metal. The electropotential variation was not included directly in the mass equation, yet its influence was considered with respect to the

electrode reaction rate. A one dimensional transport model was developed specifically to predict the location of the cathodic activity in the corroding cavity. It was concluded that the cathodic processes occurred both inside the cavity and outside on the surface metal. If a significant amount of cathodic activity occurs inside the pit, then both the potential and the concentration distributions are influenced.

Several models were developed including both the electromigration and diffusion terms. The hydrogen reduction rate in a system under cathodic protection conditions, i.e., at low metal potential, was investigated considering both diffusion and electromigration (Ateya and Pickering 1975). The calculated solutions, performed on a narrow deep slot filled with an acidic electrolyte HY, showed increasing H^+ and Y^- ions with the distance into the slot. Six years later, the authors duplicated the work at higher metal potential (Ateya and Pickering 1981). A more complex model was developed with particular application to cathodically polarized steels in chloride solutions (Turnbull and Thomas 1979). The pit was modeled as a parallel-sided slot and the two dimensional transport equations were reduced to a one dimensional problem through an approximation procedure developed by the authors.

In a subsequent paper, the work was improved by using more accurate expressions for the electrode reaction rates and by determining the effect of the ferrous hydroxide (Turnbull and Thomas 1980). A similar series of papers, by Galvele et al. (1976), Galvele (1981) and Gravano and Galvele (1984), presented several steady state solutions to the problem of diffusion and anodic dissociation and hydrolysis of metal ions in parallel-sided slots with passive and active walls. The addition of the ferrous hydroxide reaction had been also implemented, so had the reactive role of the more

aggressive chlorine and sodium ions. A similar type of modelling was performed by Alkire and co-workers using different metals, e.g. stainless steels and aluminum (Alkire et al. 1978, Alkire and Siitari 1979, Hebert and Alkire 1983).

A more empirical and less predictive model has been developed mainly for material selection purposes (Oldfield and Sutton 1978). The model predicted the occurrence and severity of crevice corrosion by estimating the pH value and the oxygen concentration in the cavity. The testing and evaluation of the model was performed later by studying the effect of environmental variables such as temperature, pH value in the bulk, chlorine content, dissolved oxygen level, and solution velocity on crevice corrosion.

In the previous models, the convection term had been neglected by the virtue of using deep narrow parallel-sided slots. Few studies were performed in order to investigate the effect of fluid flow on pit growth. The convection effect was simulated either by considering a fast growing pit in a stagnant fluid or a dynamic flow over an existing pit on the metal surface (Silverman 1984, Shuck and Swedlow 1974, Smyrl and Newman 1974, Alkire and Cangellari 1983).

Most of the developed models were specific to particular environments and metals where either diffusion or electromigration was neglected, nevertheless, such models were experimentally validated within the specified conditions. Recently, various other models had were developed for different applications, and their usage and validity were predominantly system dependent (Galvele 1981, Turnbull et al. 1982, Sharland 1989, Sharland et al. 1988, Provan and Rodriguez III 1989, Rodriguez and Provan 1989, Gabriel et al. 1990, Shiekh et al. 1990, Kondo 1989, Beavers et al.

1987, Turnbull 1980, Beck 19882, Li 1974, Walton 1990, Pan and Acrivos 1967, Batchelor 1956, Alkire et al. 1990).

From the above discussion, it is evident that a general model, accounting for all the effects, can not be easily formulated. Moreover, most of the systems simulated by the models, described above, have been restricted to oxygenated water. No theoretical models have been developed to predict pitting corrosion in CO_2 and/or H_2S environments. However, some experimental efforts have been attempted to study the susceptibility of carbon steel to pitting corrosion in CO_2 containing NaCl brine (Xia et al. 1989). The primary reaction product, identified within short test durations inside the pit, was $Fe(HCO_3)_2$. This product forms a tight and adherent film on the metal. With time, it decomposed to form iron carbonate film, $FeCO_3$, a porous, non-adherent, and non-protective layer. In addition, Johnson et al. (1991) performed some experimental measurements in order to study the wall shear stress and its effects on the corrosion rate of an X-52 steel. Corrosion rates as high as 300 mils per year (mpy) were obtained at wall shear stresses of about 500 N/m^2. A mil is one inch divided by a thousand.

As part of this work, the fundamental equations of ion transport along with the above experimental observations and measurements are utilized in the development of a mechanistic model in order to predict pit propagation rates in CO_2 and H_2S environments under high turbulence effects.

CHAPTER III

EXPERIMENTAL INVESTIGATION OF PIT INITIATION IN CO2 ENVIRONMENTS

Objectives

In this laboratory work, two types of experiments have been designed to study pitting corrosion in CO_2 environments. The corrosive environment used is ASTM synthetic seawater mixed with 10 percent LVT oil and saturated with CO_2 at one atmosphere and a controlled operating temperature. At stagnant conditions, the Greene cell apparatus has been used to electrochemically introduce defects to an inhibitor protective film, hence initiate pitting and follow its propagation rate. On the other hand, in order to test the role of hydrodynamics in pit initiation, the concentric cylinder apparatus has been modified to produce a high turbulence regime with direct bombardment of the steel sample with CO_2 bubbles. This experiment serves as an alternative to the typical high velocity flow loops, usually used to study high velocity effects on corrosion. A detailed experimental procedure and the results of the laboratory investigation are described in the following sections.

Experimental Procedure

Experimental equipment

The Teflon concentric cylinder apparatus, schematically shown in Figure 1, and the rotating electrode in Figure 2 were the main components of the experiment used to simulate the flow induced pitting corrosion. Figure 3 is a photograph of the cylinder. The main characteristics of the apparatus are a centrifugal pump providing a solution inlet, a gas inlet, a solution and gas outlet, two counter electrodes, a temperature gage, and a reference electrode capillary. The sample is mounted on the arbor which is concentrically placed inside another fixed cylinder. The width of the annular space can be varied to determine the shear stress in conjunction with the rotating velocity and the fluid properties. The sample can be viewed through the windows as shown on Figure 4. The corrosive solution used is ASTM synthetic seawater with 10 volume percent LVT 200 oil at 160°F saturated with CO_2. Two separate vessels are connected to the concentric cylinder apparatus. These kettles are mounted in parallel so that the switch from one to the other could be applied without the introduction of oxygen to the system. In addition, each vessel is under a slight positive pressure of about an inch of water to prevent oxygen entry. A centrifugal pump mounted below the electrode keeps the oil and water in a mechanical emulsion. Such an emulsion simulates phase behavior in high velocity flow. The pump also enables the electrolyte to flow past the electrode through the annular space to wet the sample. The control valves are used to select a flow rate past the sample and to switch the flow from one vessel to the other. A photo and a schematic drawing of the

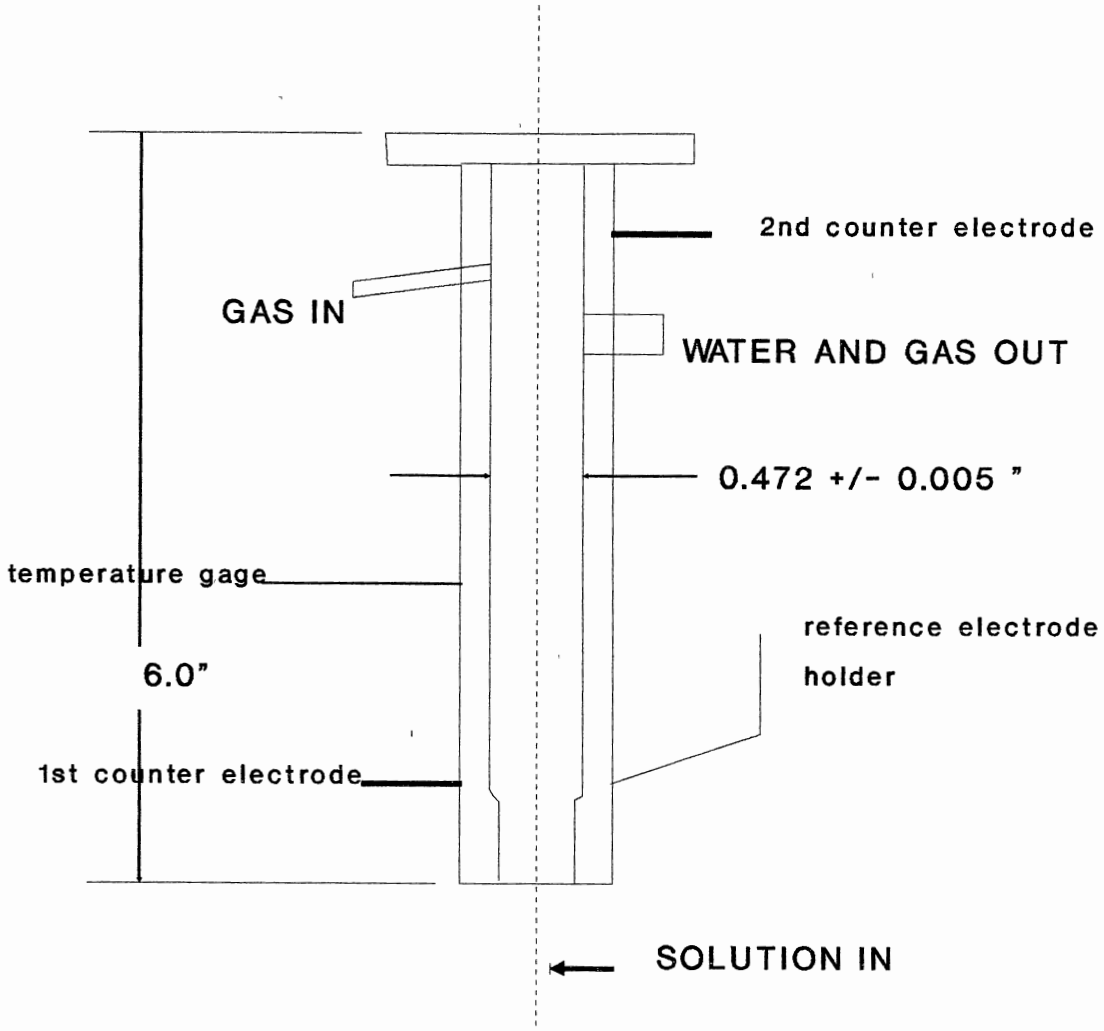

Figure 1. Drawing of Concentric Cylinder Apparatus

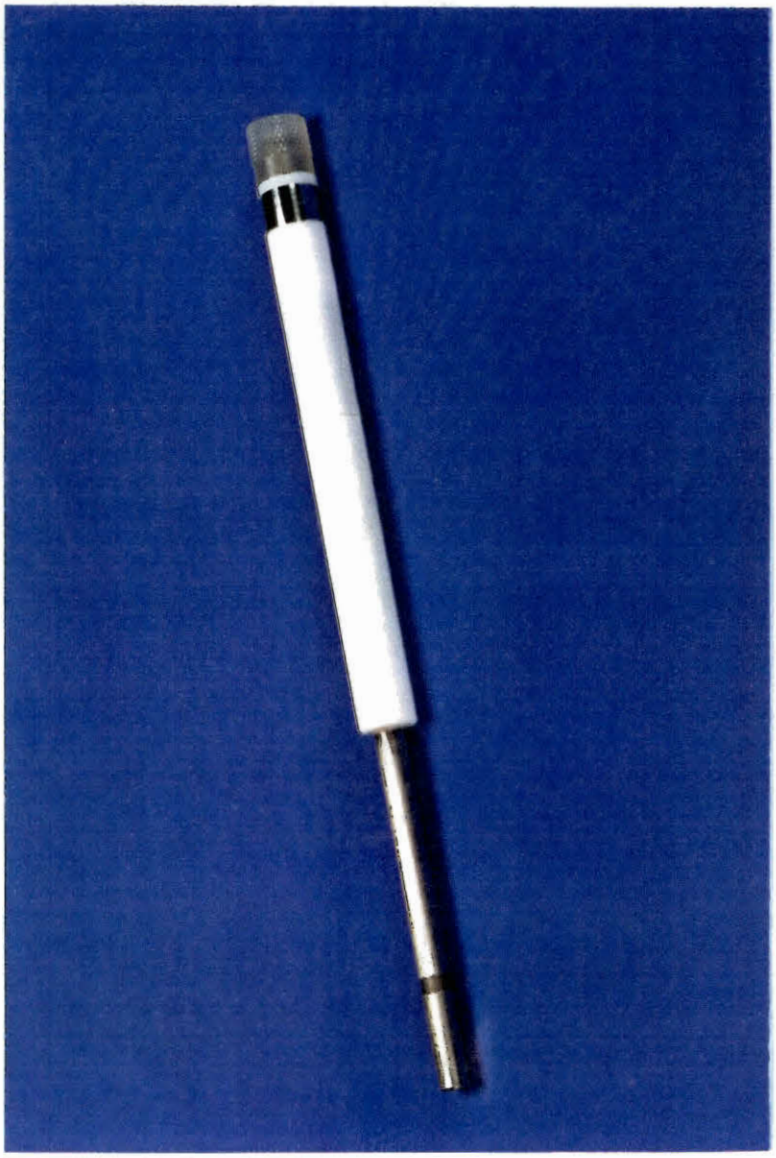

Figure 2. Photo of the Rotating Electrode

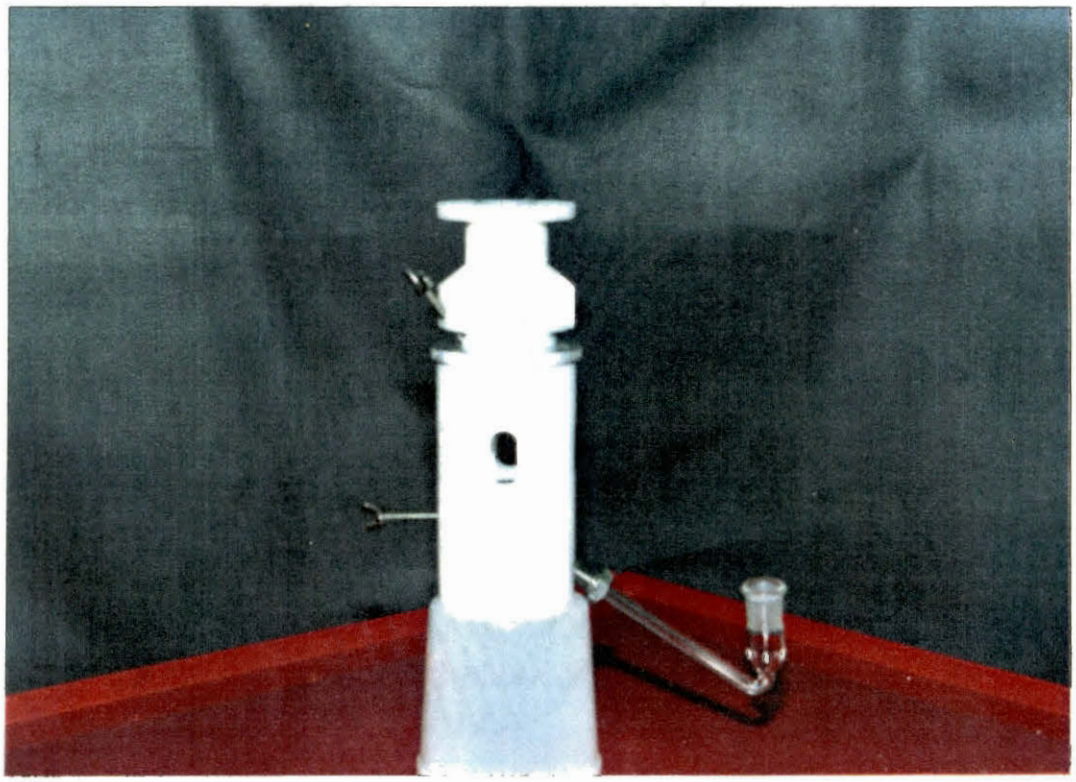

Figure 3. Photo of the Rotating Concentric Cylinder

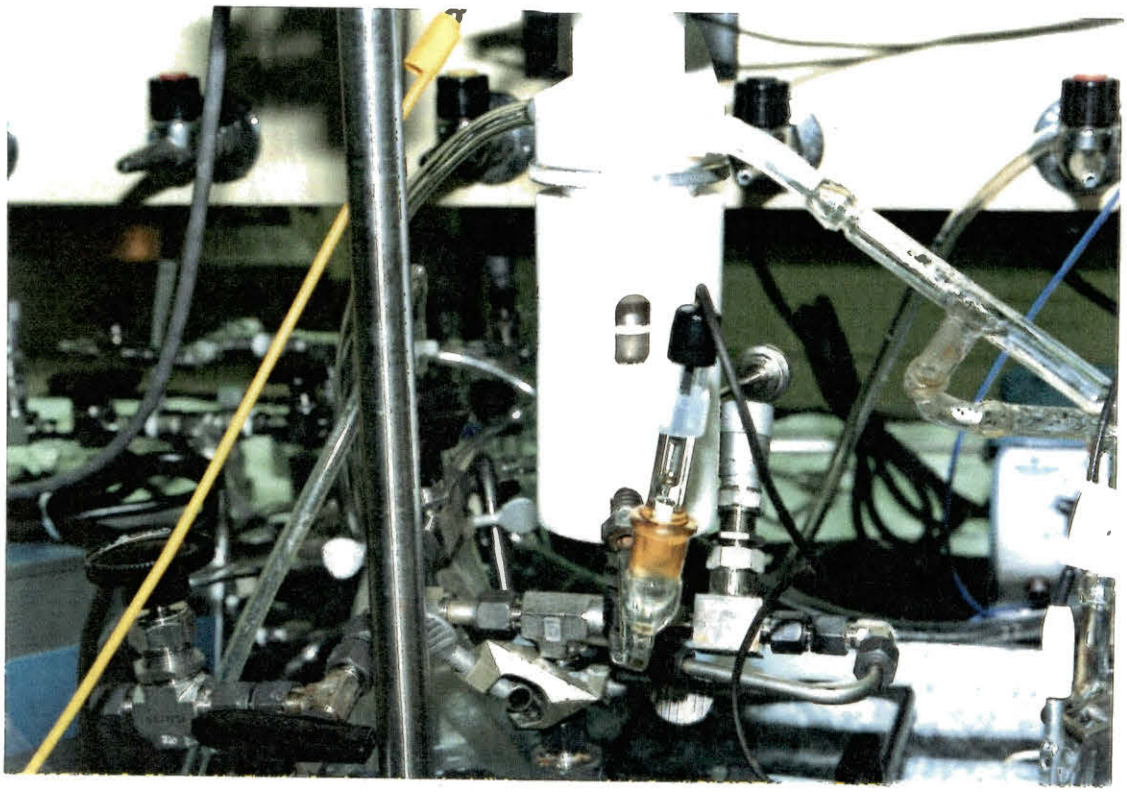

Figure 4. The Rotating Concentric Cylinder Apparatus

experiment are shown on Figures 5 and 6.

The second experimental apparatus, shown on Figure 7, is simply a series of Greene cells mounted on a bench and connected to a common CO_2 outlet. Each cell is placed in a heating mantle and contains 500 ml of solution, the X-60 steel sample holder, a calomel reference electrode, a platinum counter electrode, a temperature sensor, a magnetic stirrer, and a CO_2 inlet and an outlet. The composition of the carbon steel used throughout the experiment is shown in Table I.

All the equipment, before and after use, is washed with hot soapy water, methanol, 1:1 diluted hydrochloric acid solution and rinsed with deionized water. Finally acetone and 1,1,1-trichloroethane are used in the final cleaning step.

Assembly procedure

The pump head and the fittings are assembled first. The inlet and outlet tubing and valves are connected. Next, the solution vessels are mounted in parallel to the pump. The appropriate probes and measuring devices are inserted before the CO_2 purging. Meanwhile, the concentric cylinder is cleaned following the procedure described above. A cylindrical steel sample (0.472" in radius and 0.5" long) is wet polished progressively to 600 grit paper, inspected for pits and surface blemishes, and placed on the arbor. The arbor axis near the sample is slightly wetted with a thin ring of a low resistance contact cement for electrical contact between the sample and the arbor. Once the arbor is centered in the outer cylinder, it is bolted to the rotator motor. Finally, the entire motor and regulating valve assembly are positioned on the supporting rod and connected to the pump. After the sample is mounted, it is

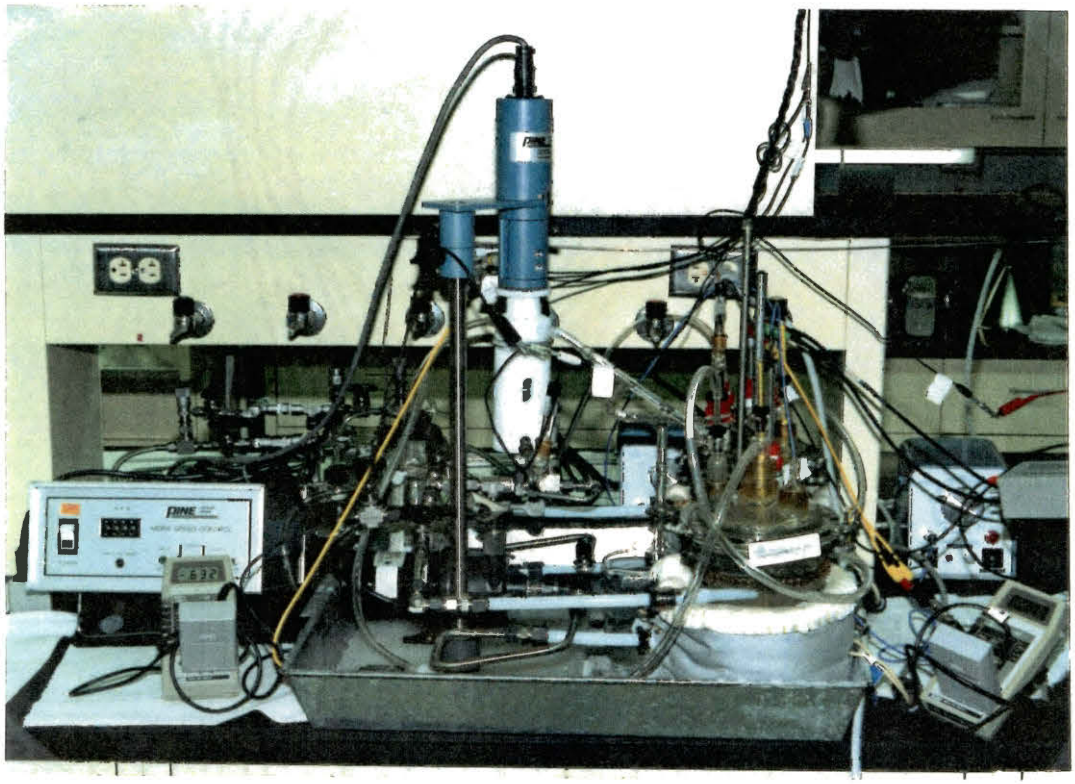

Figure 5. The Concentric Cylinder Apparatus Set up

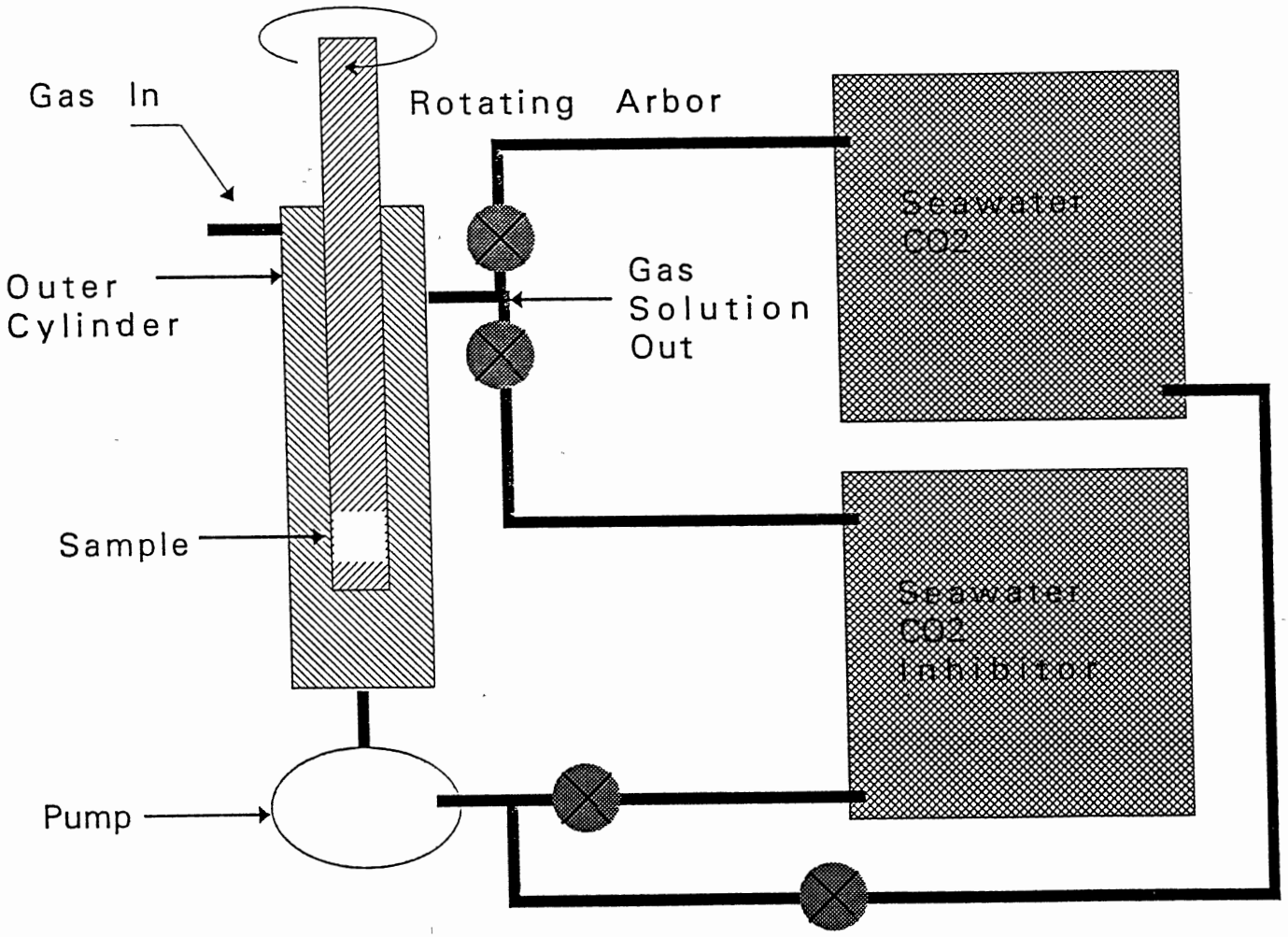

Figure 6. Schematic Drawing of Concentric Cylinder Apparatus

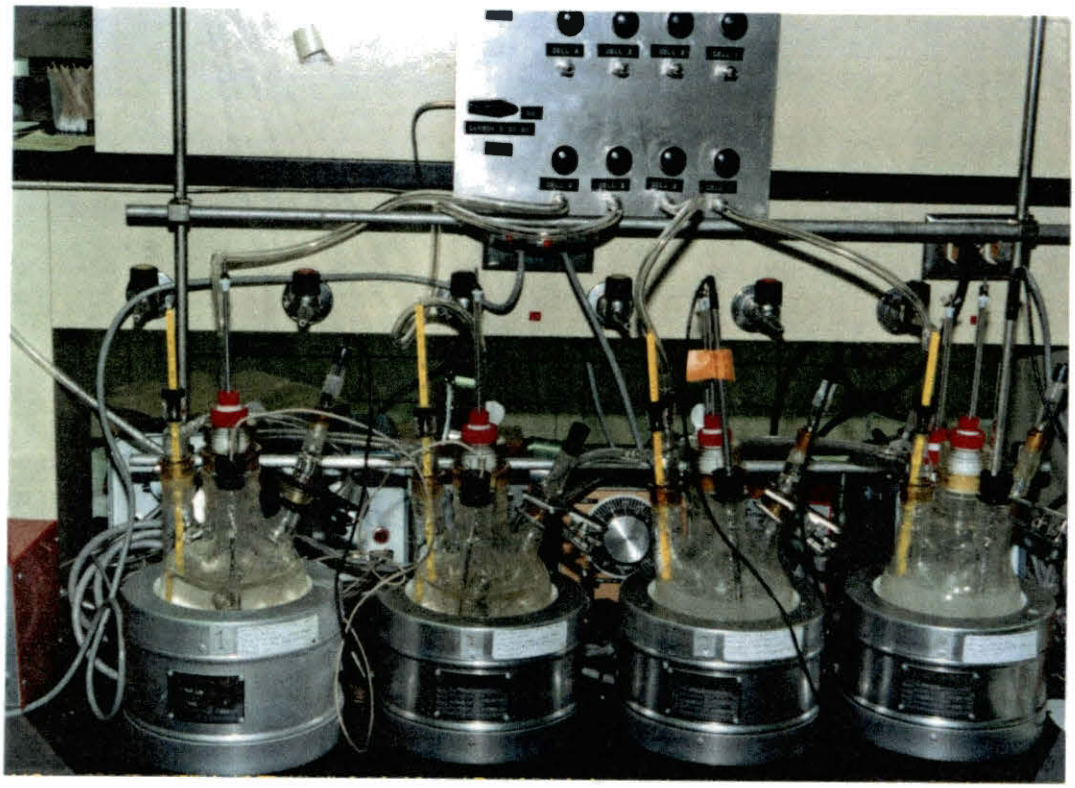

Figure 7. The Greene Cell Experimental Set up

TABLE I

STEEL COMPOSITION

Alloy	C	Mn	P	S	Si	Cu	Ni	Cr	Mo	V
X-60 Steel	*.12	1.25	.02	.017	.29	.02	.08	.03	.02	.009

* Weight percent

continuously exposed to CO_2 until the corrosive solution is introduced.

Calibration Curves

The concentric cylinder offers a variable operating temperature and a flowing velocity. Therefore, before any measurements are made, it is necessary to generate calibration curves for both parameters. First, figure 8 correlates the kettle temperature with the solution temperature just before the sample in order to correct for the heat loss between the two components through the tubing. The flow velocity past the sample at stagnant conditions has been calibrated against the control valve setting. Giving the gap and the height of the annulus, the solution residence time as a function of the valve opening has also been calculated and plotted on figure 9. The valve setting is chosen such that a fresh solution is introduced every four seconds. Such a residence time conserves the emulsion and keeps the corrosion products from settling and altering the pH in the solution.

The flow induced pitting corrosion is hydrodynamics dependent. The level of turbulence can be obtained by varying the angular velocities, i.e., rotating the cylinder shaft at different rpm values. A relationship between rpm and linear velocity is needed. To obtain such a correlation, the equation of motion (Byrd et al. 1960) has been solved for the concentric cylinder apparatus. The following expression gives the shear stress at the surface of the inner cylinder.

$$\tau_{r\theta} = \frac{-2\mu\omega_0}{1-k^2} \tag{3.1}$$

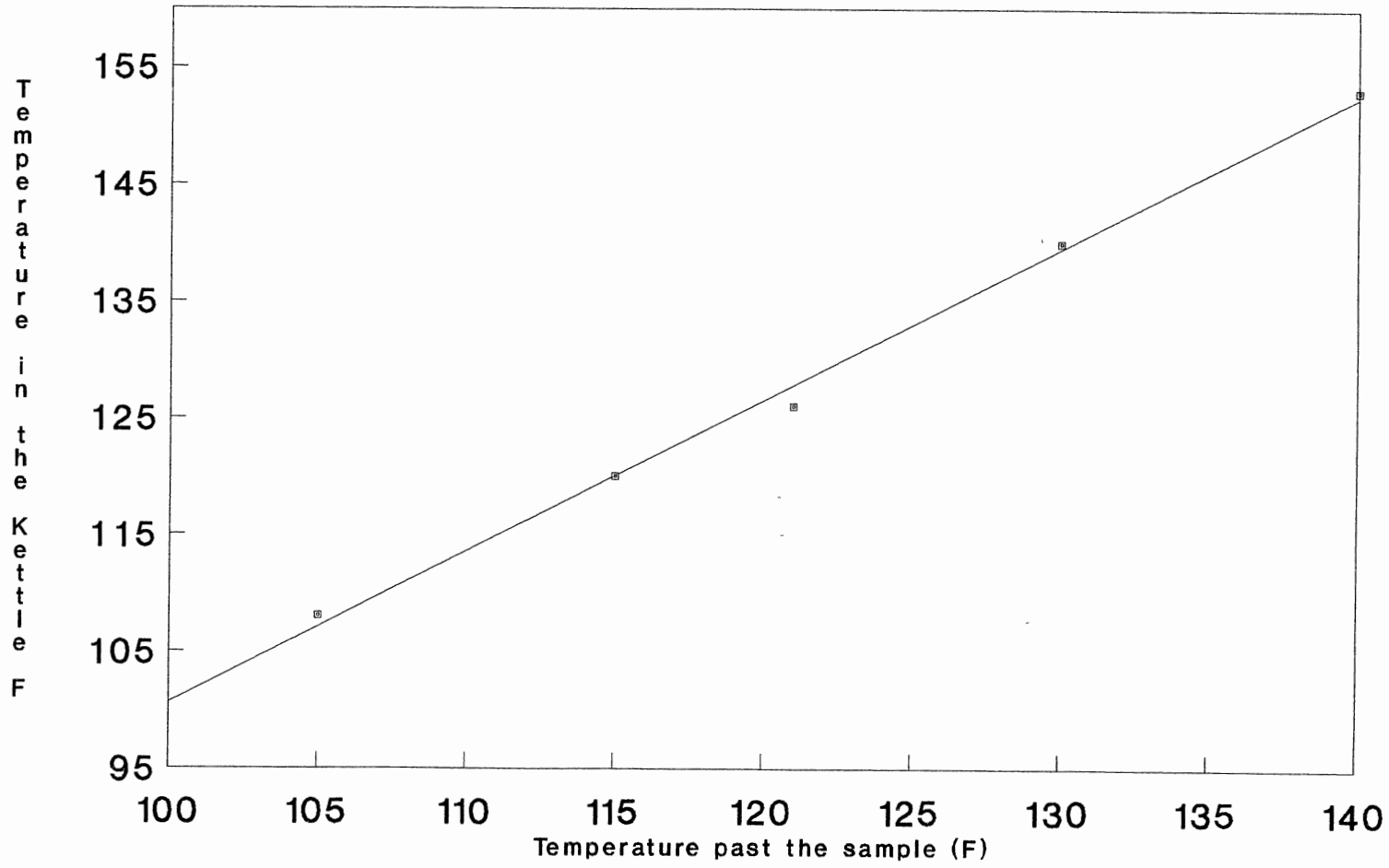

Figure 8. Temperature Calibration Curve

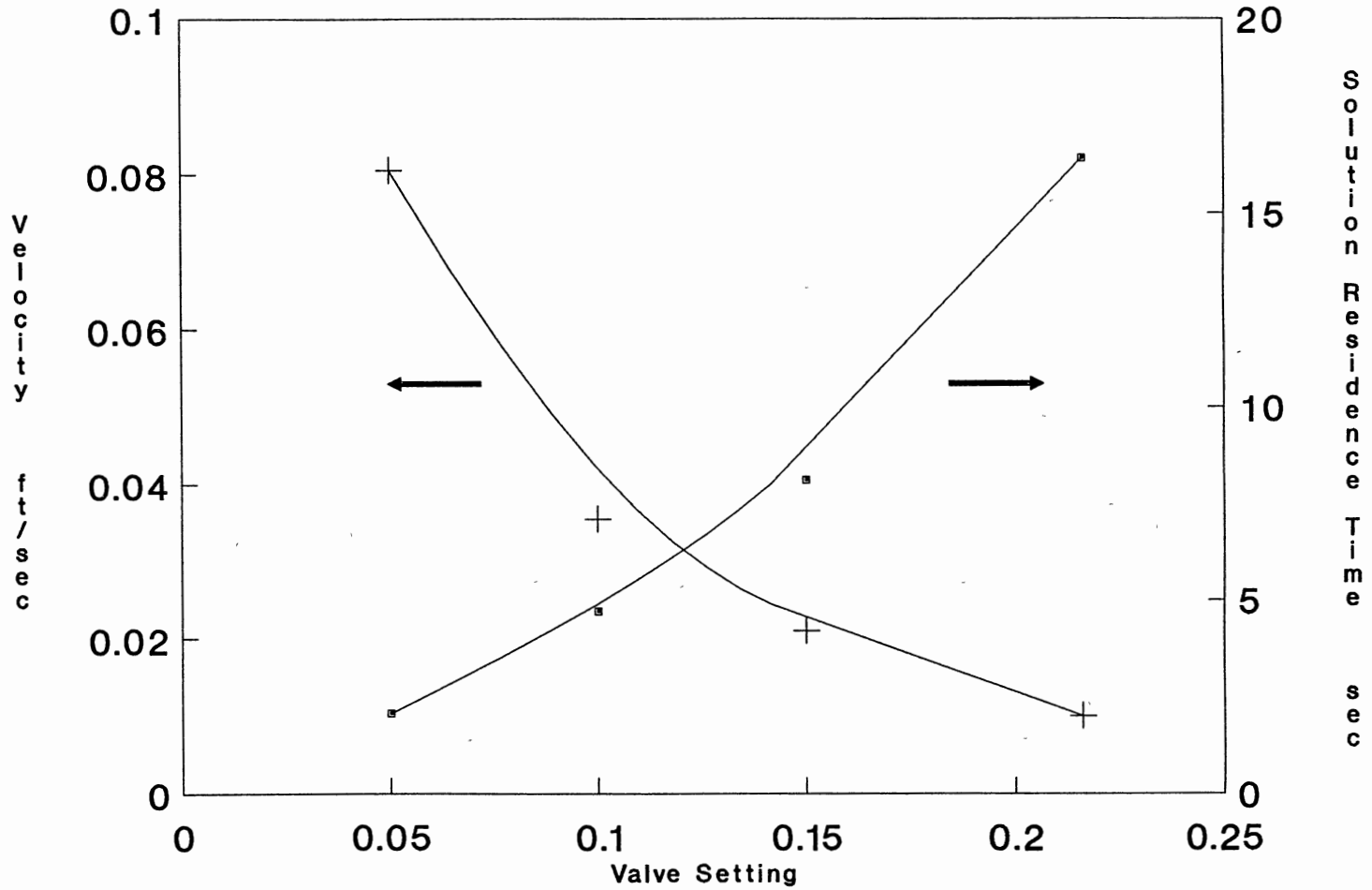

Figure 9. Axial Velocity Calibration Curves

where k is the ratio of the outer cylinder radius to the sample radius, R, and ω_0 is the angular velocity. For this system ω_0 is related to rpm as follows:

$$\omega_0 = \frac{30rpm}{\pi kR} \tag{3.2}$$

If equation (3.2) is substituted into equation (3.1), then

$$\tau_{r\theta} = \frac{-60\mu(rpm)}{\pi kR(1-k^2)} \tag{3.3}$$

The shear stress at the wall for a pipe has been studied by Denpo et al. (1990) and is given from the following correlation:

$$\tau_{wp} = 0.0791 \rho V_p^2 Re^{-0.3} \tag{3.4}$$

where $Re = \rho V_p D_p / \mu$. For equal shear at the wall, the equivalent linear velocity can be correlated to rpm in the concentric cylinder if equations (3.3) and (3.4) are equated:

$$3.6124 + 0.3\ln(Dp) = 1.7\ln(V_p) - \ln(rpm) \tag{3.5}$$

For example, a 1000 rpm rotation using the dimensions of the given concentric cylinder corresponds to an equivalent velocity of 25.5 ft/sec for a 36-inch pipe. Figure 10 is a display of the shear stress and the equivalent linear velocity in a 36-inch pipe as a function of rpm for the concentric cylinder apparatus. High velocities can also be obtained using a rotating cylinder electrode in which the cylindrical sample

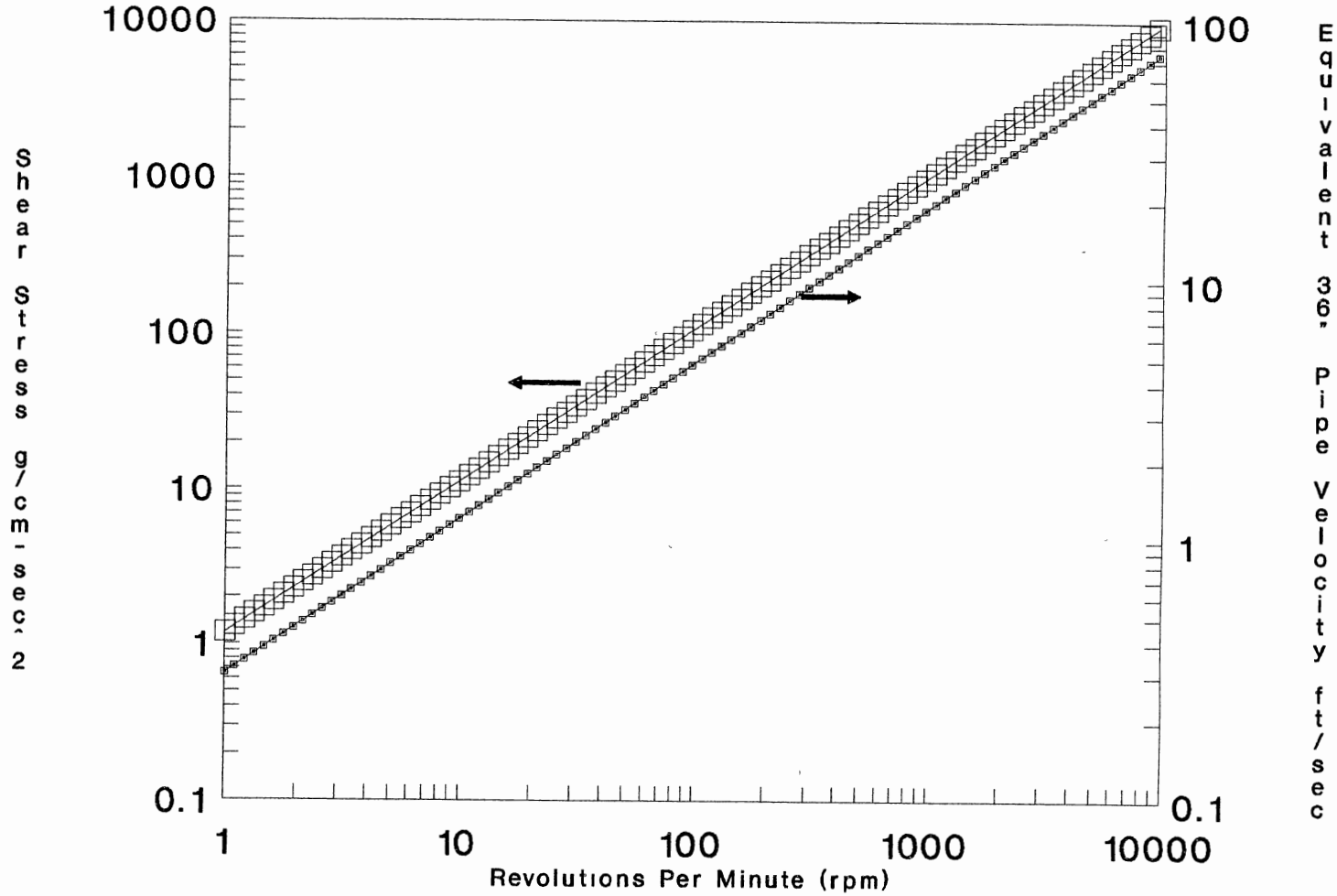

Figure 10. Hydrodynamics in the Concentric Cylinder Test

is also part of the rotating shaft; however, there is no outer cylinder. The kinetic energy from the rotating shaft dissipates in the solution inducing shear at the surface of the sample. The main difference between this system and the concentric cylinder configuration is that the latter offers a greater shear for a given rpm. This higher shear is induced because the kinetic energy is no longer dissipated through the whole kettle solution. It is rather absorbed by the solution trapped in the small gap between the sample and the outer glass cylinder.

Electrochemical measurements

Two electrochemistry software packages have been used: The PARC by Princeton Applied Research - Corrosion; and the Corrosion Monitoring System CMS 100 by Gamry Instruments. The packages offer a variety of electrochemical methods which can be used for uniform and/or localized corrosion measurements. Three main methods were employed within this experimental work: The potentiodynamic option was used to record the free corrosion potential versus time as the sample is contacted with the corrosive solution. The cyclic polarization and the galvanic corrosion options have been used to initiate pitting and measure the propagation rate if repassivation does not occur.

Test Procedures

In the concentric cylinder apparatus, once the system temperature is stable and the solutions are completely purged with CO_2, the sample is placed on the arbor and the seawater solution is continuously pumped through the annulus. The corrosion

process is continued until the sample turns black, an indication of the iron carbonate protective film formation. At this point, both the CO_2 gas flow rate and the angular velocity are increased. This high turbulence environment is maintained for few hours, then the sample is taken out, cleaned, and analyzed by a scanning electron microscope for pit identification.

In the Greene cells experiment, the samples are soaked in the different inhibited and CO_2 saturated solutions over night. After 24 hours immersion time, a cyclic polarization experiment is applied. This technique is traditionally used to evaluate a metal's pitting tendency. The experiment is based on a slow linear sweep of the metal potential towards anodic potentials. When the current reaches a specified level, the sweep direction is reversed. The graphical output of the experiment is a plot of log current versus potential showing both the forward and reverse sweeps on the same curve. Table II shows the parameters of a cyclic polarization test used in this work. Significant hysteresis between the sweeps is an indication of pit formation. Two characteristic potentials may be observed: E_{np}, the potential at which a sudden increase of the current is caused by pit nucleation, and E_{pp}, the potential associated with a drop in current caused by the repassivation of pits. If the output from the cyclic polarization experiment confirms the presence of pitting, the galvanic corrosion technique is applied to test the propagation of the pit(s). This technique is simply based on controlling the potential difference between the pitted sample and a nonpitted sample immersed in the same solution. The output of the technique is the corrosion current versus time.

TABLE II

PARAMETERS OF A CYCLIC POLARIZATION EXPERIMENT

RUN PARAMETERS	
	TechniqueCyclic Poln
	Original NameLOC23
	Initial E (MV)-20 vs. E
	Vertex E (MV)50 vs. E
	Final E (MV)-100 vs. E
	Scan Rate (MV/S)1
	Threshold I (UA/CM^2) 200
	Condition E (MV)Pass
	Condition T (S)Pass
	Init. Delay (MV/S or S)Pass
SAMPLE PARAMETERS	
	Area (CMS^2)5.05
	EQ WT (GM27.82
	Density (GM/CM^3)7.86
	Cathodic Tafel (MV)Pass
	Anodic Tafel (MV)Pass
DATA SCALE	
	E_{CORR}-609
	MV/PT4
	Data Max.291.8812
	Data Min.-.2235643
	ABS Min.0
	ABS Max.291.8812
RESULTS	
	E (I=0) (MV)
	Cathodic Tafel (MV)
	Anodic Tafel (MV)
	I-CORR (UA/CM^2)
	E (I=0) (MV)
	Pol Res. (K-OHMS CM^2)
	I-Corr (UA/CM^2)
	Corr Rate (MPY)
LEGEND	
	Seawater
	10 %oil, CO_2
	120°F
	X-65 Steel
	Green Cell
	Cyclic P.

Results and Discussion

Concentric Cylinder Experiment

Following the testing procedure described in a previous section, a seawater and oil solution saturated with CO_2 at 1 atm and 160 F and flowing at 50 ft/sec has caused pitting of a scaled X-60 steel sample within 6 hours of exposure. The sample showed a large number of pits of varying depths. Figures 11 and 12 show scanning electron micrographs of the sample. Obviously, the sample has experienced severe pitting representative of a flow-induced localized corrosion. This experiment is an approximate simulation of what usually occurs in the lower and upper upsets of a joint in downhole tubing.

Greene Cell Experiment

The cyclic polarization technique has been applied to X-60 steel samples immersed in inhibited seawater-oil solutions containing different inhibitor concentrations. At 0 and 10 ppm inhibitor, no sudden change of current density occurred. Within the time frame of the experiment, uniform corrosion is found dominant at those two inhibition levels. However, the cases of higher inhibitor concentrations display a different behavior as shown on figure 13. The hysteresis effects, i.e., the sudden increase of current density is an indication of pit initiation which has been verified by observing the sample surface after the exposure. It appears that at high inhibitor concentrations, a protective film is formed on the surface. Then, following the electrochemical conditioning process, localized defects

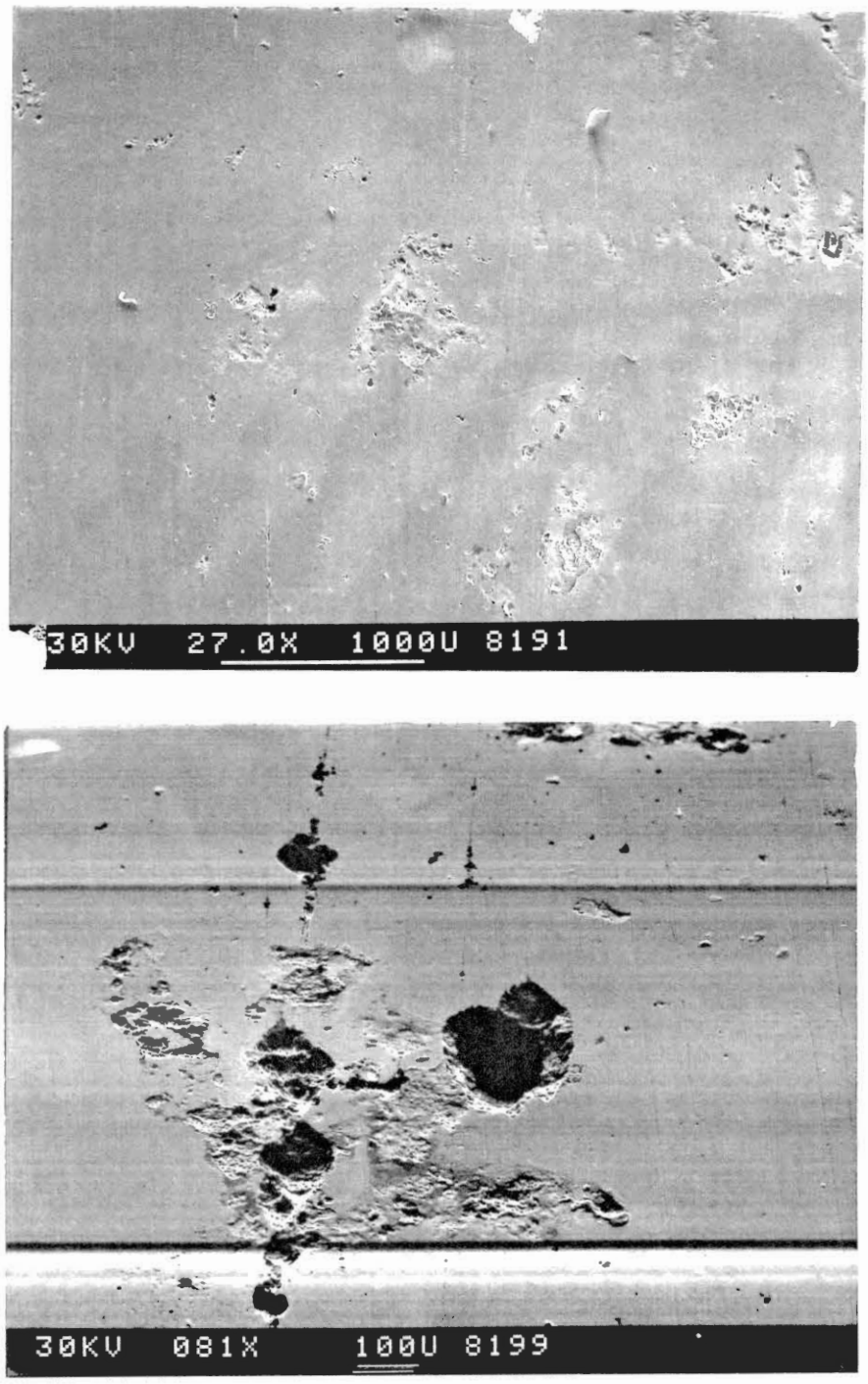

Figure 11. Flow Induced Pitting Corrosion in CO_2 Environment (27x ; 81x)

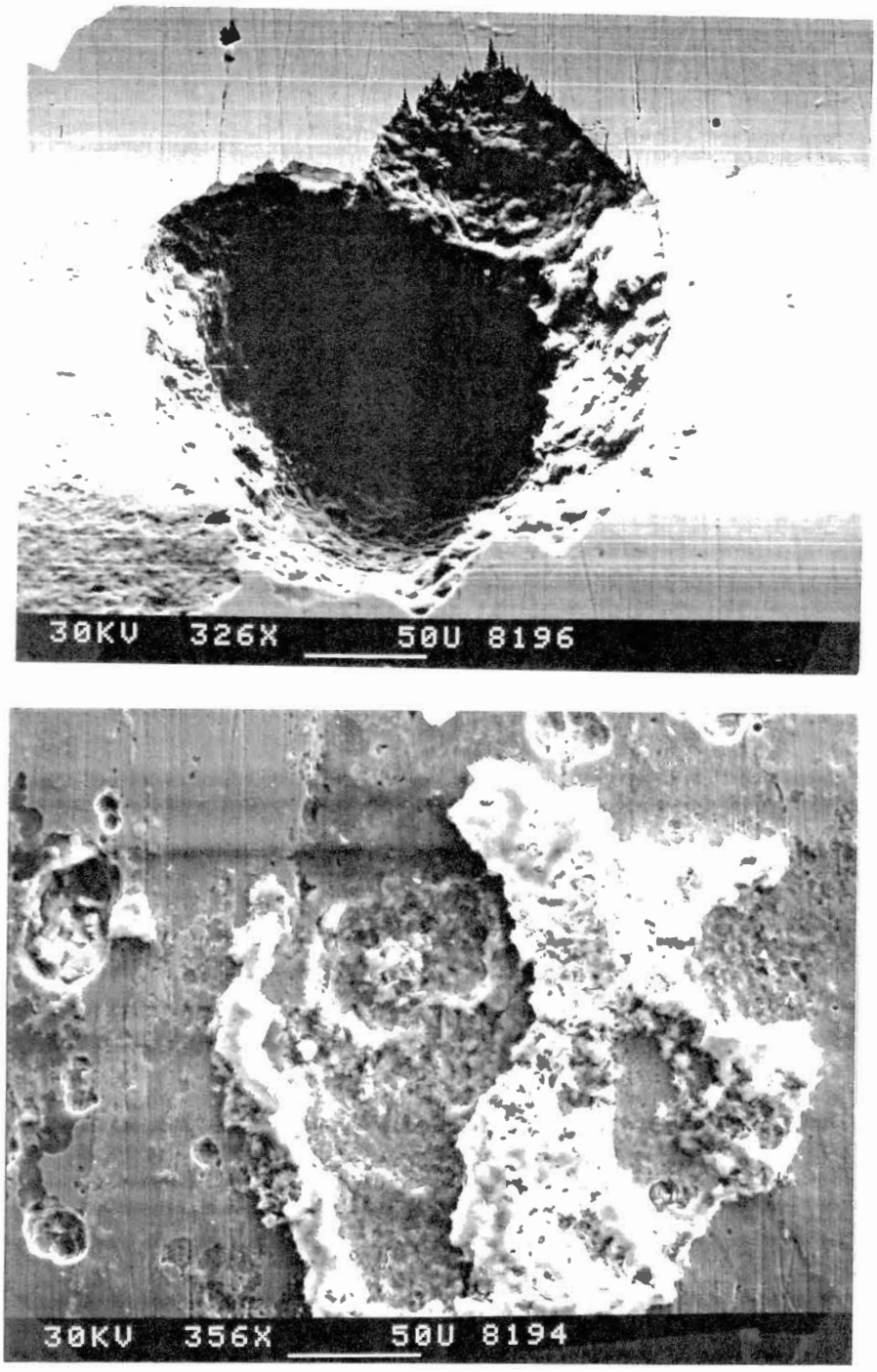

Figure 12. Flow Induced Pitting Corrosion in CO_2 Environment (326x ; 356x)

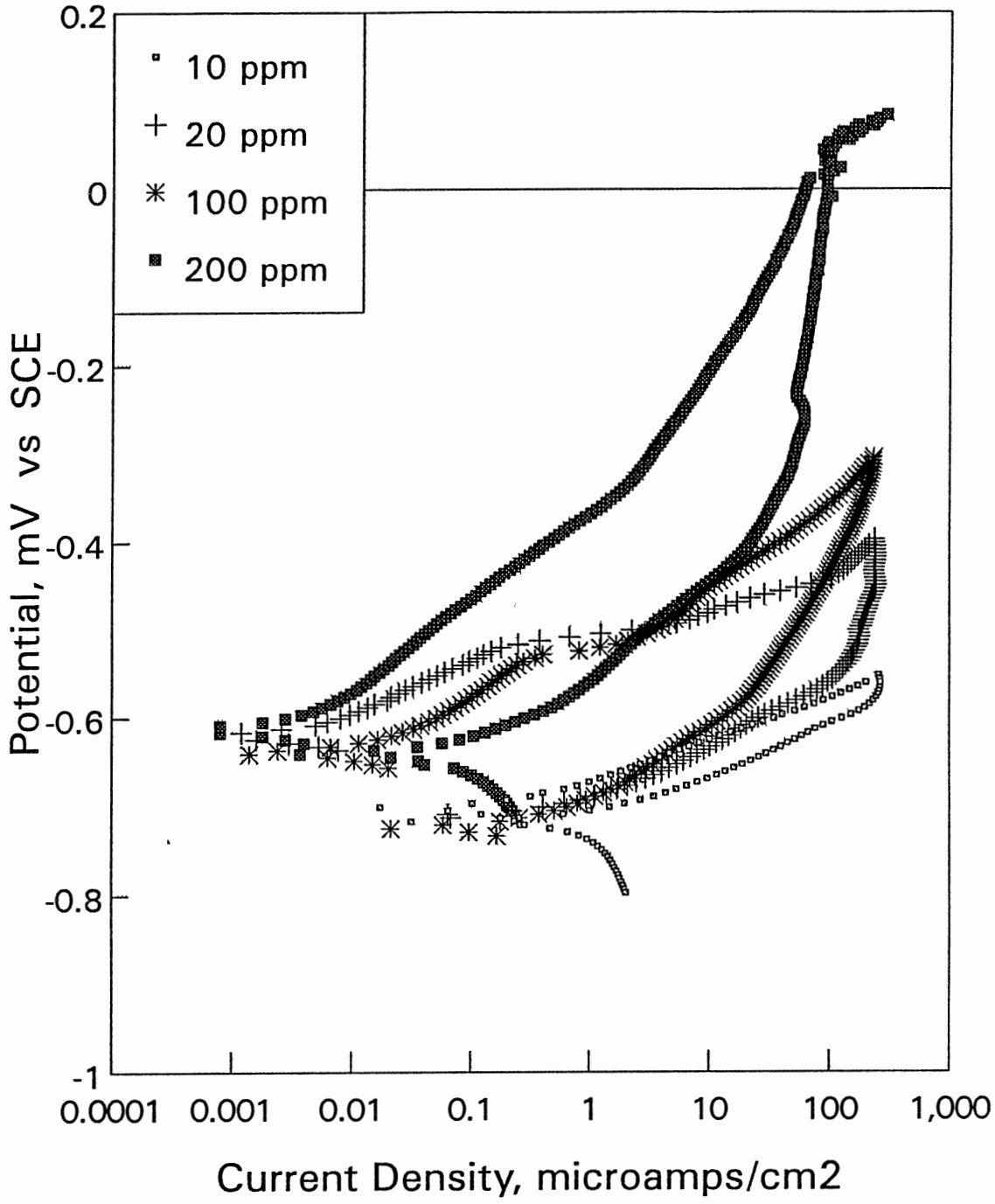

Figure 13. Polarization Curves of X-65 Steel in CO_2 Saturated ASTM Seawater at 100F, Variable Inhibitor Concentration

in the film are induced allowing pit initiation.

In environments where pitting initiation is feasible, attempts have been made to follow the pit propagation rate. In a single Greene cell, two samples of the X-60 steel are immersed in the inhibited environment. One sample has been conditioned by passing 1 mA anodic current for 5 minutes to initiate pitting. The connections of the potentiostat are quickly altered to represent a zero resistance ammeter. If the pits on the preconditioned sample continue to grow, a recording of the galvanic current will represent pit growth. Figures 14 and 15 show the results for two tests. Two inhibitors at several concentrations were been examined, but only very small current flow between the samples was observed, as shown in table III. The conditioned samples experienced pitting in all cases, therefore the initiation step was verified but repassivation of the pits occurred.

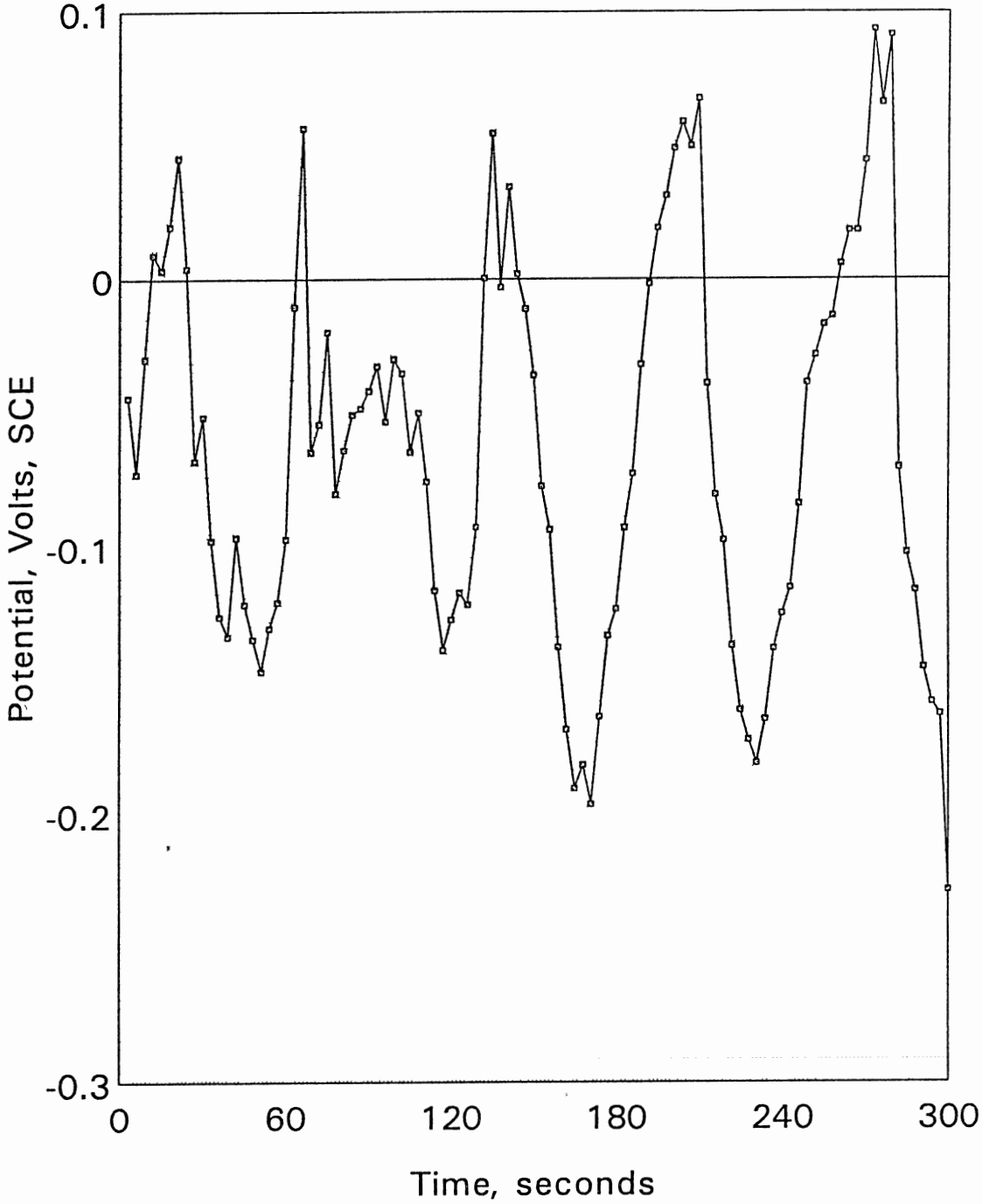

Figure 14. Conditioning Period for Pit Initiation X-65 Steel, ASTM Seawater, CO2, 120F, 200 ppm Inhibitor

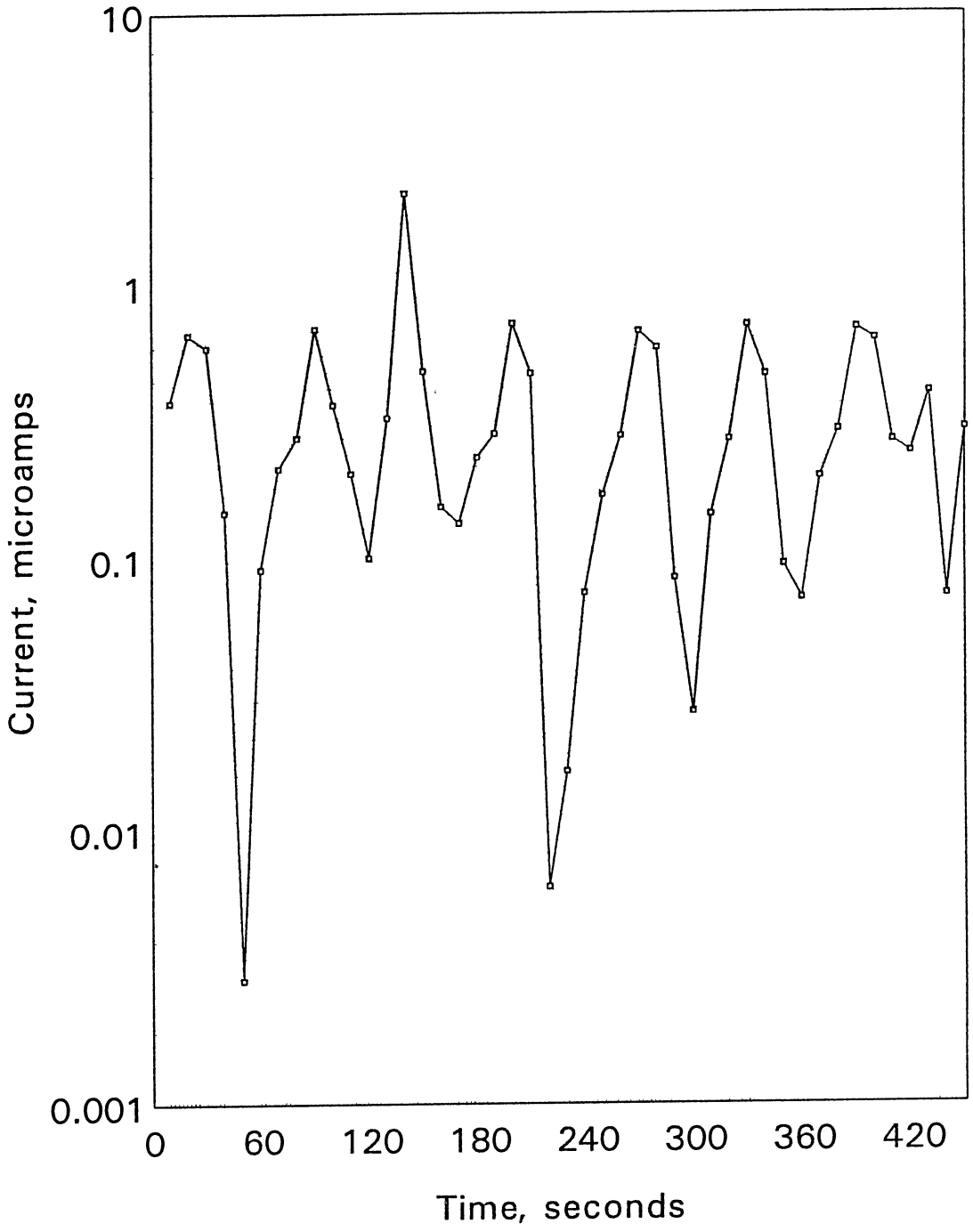

Figure 15. Galvanic Corrosion Test: Pit Propagation, ASTM Seawater, CO2, 10% LVT Oil, 200 ppm Inhibitor, 120 F, X-65 Steel

TABLE III

REPASSIVATION OF PITS IN INHIBITED SOLUTIONS CONDITIONING: 1 mA FOR 5 MINUTES

Inhibitor	Inhibitor Conc. (ppm)	Galvanic Current (μA)
Inhibitor 1	100	0.1
Inhibitor 1	200	0.05
Inhibitor 2	20	10
Inhibitor 2	50	2

Summary and Findings

1. Flow-induced pitting corrosion has been simulated using synthetic seawater and oil solution saturated with CO_2 at 160° F and flowing at 50 ft/sec.

2. The modified concentric cylinder apparatus is found useful for studying flow induced pitting corrosion in CO_2 environments.

3. A correlation has been established, from theoretical derivations, between the angular velocity of the concentric cylinder electrode and the equivalent velocity in a pipe.

5. The cyclic polarization technique can be applied to measure pitting initiation in inhibited environments.

6. The galvanic corrosion technique following the pre-conditioning of one of the samples, to initiate pitting, is a proposed method of measuring pit propagation.

CHAPTER IV

STATISTICAL MODELING OF PITTING CORROSION

Pitting corrosion has been observed to inherently follow a random pattern yet to obey some well defined electrochemical and physical laws. A complete study of such a phenomenon would require a mechanistic treatment at the microlevel and a statistical description and analysis of its behavior at the macrolevel.

Such localized corrosion is described to occur following two distinct steps. First, pits initiate via surface breakdown then expand in depth and volume. Usually, the factors contributing to a pit propagation step are different than those that have led to its initiation. The random behavior can be characteristic of either step. Such behavior can be induced by cracks, holidays, inclusions, insufficient inhibition, coating pinholes, and voids. Likewise, variable flow conditions, such as temperature, ph, pressure, concentration, potential, etc., are a few of the operating parameters which can give pitting corrosion a stochastic behavior within the initiation and/or the propagation step.

For bare tube applications, which are of interest in this work, both non-uniform chemical inhibition and the existence of inherent flaws in the metal combined with the flow conditions can play a role in pit initiation and growth. At the initiation step, the random behavior of pit generation can be attributed either to the inherent

existence of flaws in a probability distribution manner, or to the random variable conditions of a stagnant film or a slug, or to the existence of a localized high turbulence region. At the propagation step, distinct pits usually experience different rates of growth. A tentative explanation is the existence of the corrosion product which results from the pitting reaction and slowly builds up both over and within the pit stifling the reaction and slowing down the rate of pit propagation. The removal and/or the accumulation of the corrosion product from the inside of the pit is certainly affected by the neighboring flow conditions as well as by the thermodynamic equilibrium between the species involved. Depending on its size and location, the pit may grow or repassivate at an early stage. This random behavior, occurring within both steps of pitting corrosion, gives rise to pit-depth distributions, a phenomenon which has been the focus of several research topics and is of interest in this statistical model of downhole pitting corrosion.

The statistical model, developed in this work, requires a set of experimental or field pitting data listing the depths of the deepest pits observed on a metal sample or at a specific location of a pipe. The model analyzes the data by applying Gumbel's Extreme Value Theory and predicts the probability of occurrence of pit depths of interest. The theory is based on the observation that the deepest pits in a given pitting corrosion data set, i.e., the tail end of Figure 16, themselves present a random behavior which can be characterized by an extreme value distribution function. If the input data are time variable, i.e., more than one data set are given at different exposure times, then the model predicts the time-to-first leak and/or the corrosion allowance for an existing or a newly designed structure.

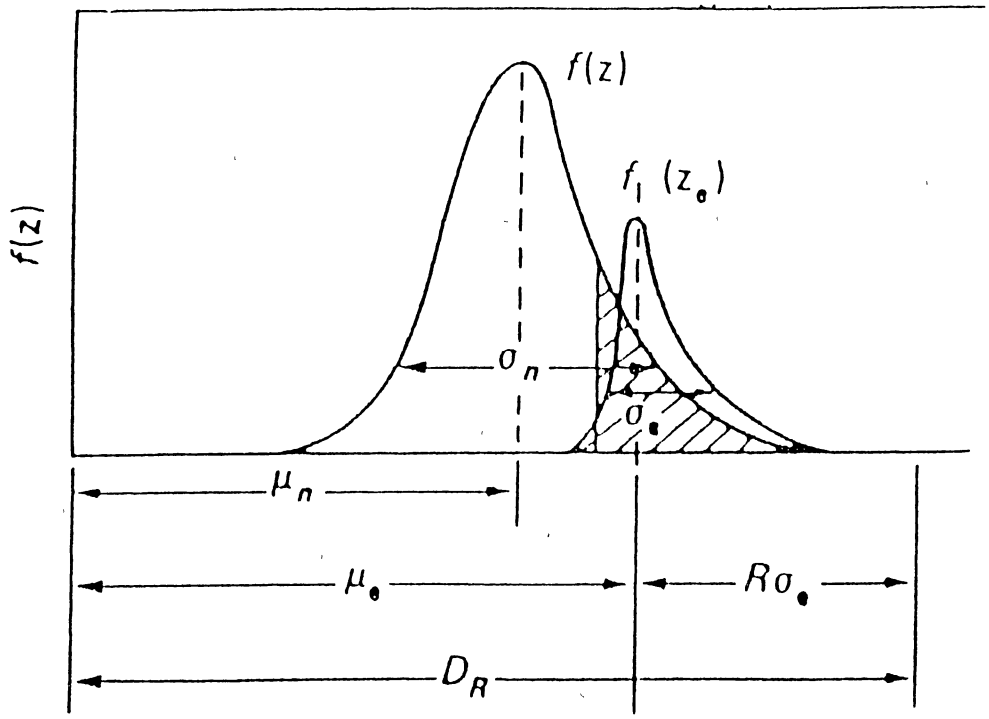

Figure 16. Random behavior of pitting population vs. deepest pits: Probability density functions

Model Description and Development

Before pursuing the development of a statistical model of pitting corrosion applicable to downhole operations, it is imperative to investigate and analyze the modes and forms of pitting data available, whether it is actual data collected from the field or experimental data measured in the lab.

Modes of Pitting Data

If a set of field pitting corrosion data is available, it is usually obtained through a caliper survey. At this point, it would be useful to describe the essence and the important features of such a survey, which will help one to understand and analyze the collected data in a statistical manner. A single caliper device can present as many as twenty operating points of contact with the tube wall; each one measures the depth of the pit beneath it (Chaney 1946). For example the Chaney-Barnes tubing caliper is a mechanical device equipped with at least six independently operating lever arms, to the outer end of which are attached small wheels or rollers to contact the tubing wall. A spring at the end of each lever arm is provided to force the wheels outward against the tubing wall. In order to detect the existence and the extent of pitting corrosion, the inner arms of the six levers contact a polished steel plate on the end of a stylus rod. If several pits of varying depths exist on a single cross section of the tubing wall, the stylus will be actuated by the one arm corresponding to the deepest penetration into the tubing wall and will be lifted free of the other five arms. The output chart consists of a coated sheet of metal foil. The primary data are curves,

traced on the metal foil, whose peaks trace the depths of the pits in the casing. The chart, when removed for corrosion inspection, would show a series of perfect parallel lines if no pits are present. Any pits in the tubing wall will cause longitudinal motion of the stylus, and so produce deviations from the straight and parallel nature of these lines. The depths of the deepest pits at that particular location can be read directly from the chart. If the distance between the lines on the chart corresponds to a change in radius of the tubing of 0.05", then any pit that allows the chart line to advance to the adjacent line is 0.05" deep, or if to the second, is 0.10" in depth. The survey data usually reports the depth of the pit, the number of pits corresponding to that depth, the rank of the pits. Finally, the Chaney-Barnes tubing caliper is claimed to give the measurements of the depth of corrosion pits, as well as internal diameter of the tubing joint within ± 0.01". Such a survey, if carried more than once on the same tubing, would also give time dependent data which could be statistically analyzed to predict the time before the first leak occurs.

The second source of pitting data is through laboratory experimental measurements. First, it is important to mention that the two major problems faced in such laboratory procedures are, first, the elimination of the crevice corrosion at the point between the specimen and mounting material, and second, the simulation of the downhole operating conditions. Assuming that the induced problems from such matters are overcome, there are basically two ways to detect and determine the extent of pitting corrosion experimentally: either electrochemically or by counting the number of pits on a corroded sample and measuring their corresponding depths. The data, generated from the latter, would be similar to the caliper survey data as the

deepest pits at several locations can be listed and ranked accordingly. If the immersion time of the sample in the corroding environment is varied, time-dependent data can be also obtained.

Electrochemically, two basic types of measurements of pitting corrosion are typically done: either the pitting corrosion potential is recorded through sweeping the potential of the electrode and recording the value at which the current flowing through the electrode exceeds a given threshold, or by using polarization resistance measurements to obtain the incubation time necessary to equal the current threshold which is carefully chosen so that it corresponds to one pit growing on the electrode surface. If several samples are mounted together in the same environment, by the random nature of pitting corrosion occurrence, different values for the corrosion potential and the incubation time from the similar samples would be obtained and can be ranked accordingly.

Extreme Value Statistics Applied to Pitting Data

First, it is important to mention that the virtue of using extreme value methods in dealing with pitting corrosion is a necessity rather than a choice. It is unfortunate that the average pit depths, statistically convenient, can not be useful not only because the smaller pits become too indistinguishable to be measured, but also because the large pits are more likely to cause premature failures and therefore they should be detected and followed more closely. The extreme value statistical analysis, developed by Gumbel can be, and has been, specifically applied to predict the extent of pitting corrosion. In this work, an attempt is made to apply such analysis to downhole

applications. Related to pitting corrosion, the aim of a statistical theory of extreme values is to explain the observed deepest pits arising in samples of given sizes and to predict the occurrences of pits with a specified depth on a larger scale sample or within a larger time frame.

According to Gumbel, three main criteria must be verified in order to apply his theory. First, the individual observations must be of statistical nature, i.e., they are dealt with as statistical variates. Second, the initial distribution from which the extremes are drawn and its parameters must remain constant from one sample to the next, or that the changes that have occurred, or will occur, may be determined and eliminated. Third, the observed extremes should be extremes of samples of independent data. The first criterion is verified by the inherent and observed nature of pitting corrosion. In the literature of pitting corrosion, there is substantial experimental evidence indicating that the dimensions of pits (of any type) at a given instant of time and in any of a variety of environments may be characterized by the log normal distribution; such an observation verifies the second criterion. Finally, the third condition is met especially if a large number of samples is used in such a way that the readings of the deepest pits from the various samples are independent.

The Model Calculations

Given a set of data of a random variable, R, measured for various samples collected from the same source and immersed in the same corroding environment, statistical theories will allow us to predict the overall corrosion behavior of the population of interest. Applied to pitting corrosion, the random variable can be either

the maximum pit depth, the corrosion potential, or the induction time depending on the means of measurement of the localized attack. The variable R, mentioned above, can not be described as a single value, rather it is treated as a continuous random variable; in other words, its occurrence can only be described through a probability density function which defines what's referred to as the asymptotic frequency distribution. A full knowledge of such functionality will allow a statistical model to predict how deep the pits are, how large a sampling area is needed before a certain depth can be detected, and how long it would take for a first leak to occur on a pitted structure. Such important information can be provided directly or indirectly from extreme value analysis which involves the following steps:

(1) The samples should be made as identical as possible, i.e., dimensions, surface finish, and the corrosive solution should be well prepared and specified before the immersion is permitted. If a time-dependent data is needed, the set of samples of interest should be removed carefully not to disturb the system.

(2) If pits develop on the surface, the maximum pit depth observed on each sample is recorded and referred to as an element of the population.

(3) The sample elements of extreme values are sorted in an ascending order and ranked from 1 to N, where N is the sample size. The smallest element is ranked first, and the largest pit last. Two new variables are defined for each sample point: The plotting position, $P(X_i)$, is a measure of the frequency of occurrence of a pit with a specified depth, X_i. The second variable is the reduced variate, denoted $Y(X_i)$, and is adequately chosen in order to fit the extreme value probability expression. The two quantities are related as follows:

$$Y(X_1) = -\log\{(-\log[P(X_1)]\} \qquad (4.1)$$

where

$$P(X_1) = \frac{R_1}{N+1} \qquad (4.2)$$

(5) At this stage, for each value of a maximum pit depth, three corresponding quantities have been assigned, i.e., the rank R, the plotting position P, and the reduced variate Y.

(6) For graphical analysis, if the reduced variates $Y(X_i)$'s are plotted against the elements X_i's, a straight line should be obtained, and the slope and the intercept are of importance:

$$Y(X_1) = \alpha X_1 + \alpha\beta \qquad (4.3)$$

α and ß being the shape and scale factors, respectively. These parameters are related to the mean, x_m, and the variance, σ^2, of the sample population as follows:

$$\alpha = \frac{\pi}{\sigma\sqrt{6}} \quad ; \quad \beta = x_m - \frac{0.577}{\alpha} \qquad (4.4)$$

(7) Finally, according to the Gumbel's theory, the extreme value distribution function can be expressed as:

$$\Phi(X) = e^{-e^{-\alpha(x-\beta)}} \qquad (4.5)$$

where α and ß are the parameters of the distribution, X is the random variable maximum pit depth, and x is a specific outcome of X.

(8) Given the above equation, the probability of occurrence of a pit with a specified depth can be determined.

(9) The obtained data can be extrapolated to predict the corrosion behavior of any large scale structure. Such calculations are formulated by defining a new variable called the Return Period, $T(X_i)$. It is the number of observations such that, on the average, there is one observation equalling or exceeding X_i. It is defined as:

$$T(X_i) = \frac{1}{1-\Phi(X_i)} \qquad (4.6)$$

According to Gumbel's theory of extreme value distribution, the return period converges for large values of X_i towards:

$$T(X_i) = e^{Y_i} \qquad (4.7)$$

The return period can be read directly from the Y-axis of the extreme value plot discussed above. Since the axis has a logarithmic scale, the maximum pit depth is found to be proportional to the exposed area.

(10) If the samples' deepest pits are collected for different immersion times, the data

can be correlated to express the time dependency. It has been verified by several authors that the "Arrhenius" law is a good fit for the variation of the characteristic deepest pit with time:

$$\beta = m\log(t) + n \tag{4.8}$$

where m and n are constants, and t is the exposure time. Using equations (4.5) and (4.8), a predictive expression is derived for the survival function of a structure, i.e., the probability that the first sample perforation does not occur before the exposure time t. Such a probability can be expressed as:

$$P_s = \exp[-(t/\Omega)^k] \tag{4.9}$$

The exponent, k, and the characteristic age, Ω, are constant for a given system. Upon statistical analysis, values for α, ß, m, and n can be determined and used to estimate Ω and k as derived below:

Just before the first perforation can occur, the probability of survival would be equal to the cumulative probability of occurrence of a pit with a depth equal to the thickness, δ, of the wall. If the two probabilities from equations (4.9) and (4.5) are set equal, we obtain:

$$\exp[-(t/\Omega)^k] = \exp[-\exp\{-\alpha(\delta-\beta)\}] \tag{4.10}$$

Taking the log of both sides twice,

$$k*\log[t/\Omega] = -\alpha(\delta-\beta) \tag{4.11}$$

Substituting ß from equation (4.8), and rearranging,

$$k*\log(t) - k*\log(\Omega) = \alpha m\log(t) + \alpha(n-\delta) \tag{4.12}$$

Since the equation is valid for all t, equating the coefficients of the time dependent terms, the following relations are obtained:

$$k = \alpha m \quad ; \quad \log\Omega = \frac{\alpha(\delta-n)}{k} \tag{4.13}$$

In summary, if given data describing the deepest pits for several samples immersed in similar corrosive conditions, statistical analysis can provide the probability of occurrence of any size pit, the predicted corrosion behavior of a large scale structure, and finally the time it takes to observe a first leak within the structure.

If the cumulative distribution function of the extreme value is written as

$$F(X_i, \mu_e, \sigma_e) = \exp\{-\exp[(X_1-\mu_e)/\sigma_e]\} \tag{4.14}$$

then μ_e and σ_e, called the location and the scale parameters of the extreme value distribution respectively, can be estimated from the slope and the intercept of the plot

of the reduced variate versus X_i. From equation (4.14), physically, (1-F) can be interpreted as the probability of obtaining a maximum depth measurement greater than some value of depth X_i, i.e., it is a measure of the risk of accepting a given value of X_i as the maximum penetration. In terms of corrosion measurement, suppose it is chosen to define a depth, D_c, for which the risk of accepting D_c as the maximum penetration is α_c. Then

$$\alpha_c = 1-F(D_c) \tag{4.15}$$

$$D_c = \mu_e+\sigma_e R \tag{4.16}$$

$$R = -\log[-\log(1-\alpha_c)] \tag{4.17}$$

Equation (4.16) implies that the maximum penetration depth D_c, using an α_c risk factor, is simply the most probable maximum penetration, μ_e, plus a term $\sigma_e R$ which attributes a safety factor depending on the width of the extreme distribution bell shape.

If time variable data sets are available, different intercepts and slopes from the extreme distribution plots can be obtained. Therefore, the multiple values calculated for the shape and the scale parameters can be correlated with time. In most cases, their time dependence is linear. From equation (4.16), the maximum penetration after an exposure time, t, can be calculated using the time dependencies of μ_e and σ_e, $f_\mu(t)$

and $g_\sigma(t)$:

$$D_c = f_\mu(t) + R\, g_\sigma(t) \tag{4.18}$$

If t is the known life time of a structure, then D_c becomes the corrosion allowance needed to avoid failure after a lifetime with a tolerated risk factor equal to α_c.

The statistical analysis of electrochemical pitting data is performed differently. First, as mentioned in Sato's (1976) pioneering work, a critical pitting potential, E_c, is defined as the smallest potential at which the pit generation probability is practically recognizable. Within an experiment, the pitting potential is found dependent on both the critical potential, E_c, the potential sweep rate, v, and a proportionality constant, α_1, which is experimentally measured:

$$E_p = E_c + \sqrt{\frac{v}{\alpha_1}} \tag{4.19}$$

If a potential sweep experiment is repeated N times for a specific sample, or a single sweep experiment is performed on N identical samples, a potential distribution, $E_1,\ldots,E_i,\ldots,E_N$, is obtained. Each potential, E_i, is associated with the number of samples, i, which have experienced pitting attack before reaching the value E_i. Hence, for each E satisfying

$$E_1 \le E \le E_N \tag{4.20}$$

a pitting probability, Q(E), is defined to be approximately equal to i/N. Thus a survival probability is assigned to each pitting potential, E, as follows:

$$P(E) = 1-Q(E) \approx \frac{N-i}{N} \tag{4.21}$$

For the second type of electrochemical pitting data, a sequence of instants, $t_1,\ldots,t_i,\ldots,t_N$, can be obtained for the incubation times corresponding to the potentiostatic control of N samples with the same apparatus. The incubation time is defined as the time necessary for the sample to experience a current equal to the current threshold imposed in the experiment. A distribution function Q(t) of the incubation times can be evaluated in this case as:

$$Q(t) = Prob\{t \le t_i\} \approx \frac{i}{N} \tag{4.22}$$

and a probability of survival can be, similarly, evaluated from equation (3.26).

An electrochemical data set of pitting potentials and/or incubation times can be analyzed using the extreme value theory by treating the time and/or the potential as a minimum random value as opposed to a maximum for the deepest pit evaluation analysis. The same procedure, outlined for the deepest pit data evaluation, can be used with two modifications. The individual observations X_i's, i.e., the incubation times or the pitting potentials in this case, should be arranged in decreasing magnitude, then equations (4.1) through (4.5) can be used with the following modification in equation (4.4):

$$\beta = x_m + \frac{0.577}{\alpha} \tag{4.23}$$

Following such a procedure, the probability of occurrence of a specified value of a pitting potential or an incubation time can be estimated for a given structure.

Model Results and Discussion

The Dynamics of the Model

Several case studies have been chosen in order to illustrate the dynamics of the statistical model. If a time dependent data set is available, the model performs four main tasks. First, within the section of the statistical analysis of the data, for each given data set, the pit depths are ordered in an ascending fashion and assigned a rank accordingly. Then equations (4.1), (4.2), and (4.3) are used to estimate the probability of occurrence of every pit depth from the data set and its return period. The return period of a pit with a given depth is defined as the number of observations required before a pit, at least as deep, can be observed. It is also referred to as the scale up factor in this work. These two discrete variables are merely an analysis of the data. In terms of predictions, the data is fitted to the basic equations of the Extreme Value Distribution Theory, i.e., equations (4.5) and (4.6), to generate a cumulative distribution function which predicts the probability of occurrence of any given pit depth and its return period. At this point it is important to emphasize that the predicted probabilities and return periods are solely valid within the time frame of the corresponding data set. The longer the exposure time allowed to measure pit depths in a given data set, and the more data points available, the better the prediction. Having determined the behavior of the extreme distribution parameters from the prediction step for each data set, and given a structure thickness, the model tabulates the risk of occurrence and the return period for several fractions of the thickness after an exposure time corresponding to the particular data set. The return

period information is particularly valuable in a laboratory work as it gives an estimate of the surface area required before a pit depth can occur after an exposure time equal to that of the data set. Table IV shows a sample of such output.

If the input data set is from a caliper survey, it is typically a series of pit depths recorded at the distinct joints of the tubing. The model divides the data in groups of fifteen. Such groups correspond to a total depth of about 450 ft of tubing each. The environments in each of these sections are assumed invariant in order to analyze the data as one separate data set and predict the statistical behavior of pits in each section independently. Next, the distribution parameters are determined and used to characterize the random behavior of pits at each section assuming an exposure time corresponding to the time when the caliper survey was performed. A sample of the output is included in Table V.

If more than one data set is given, i.e., time dependent data are available, then the time to first leak of an existing structure or the corrosion allowance, required for a newly designed equipment with a specified lifetime, can be estimated. A typical output of this section is shown in Table VI.

Testing of the Model

Case study I. The following study case, not concerning carbon steel, has been used mainly to test the model dynamics. It also represents typical laboratory pitting data collected in a classical pitting environment. The experimental pitting data of 2S aluminum in tap water have been collected for time periods of two weeks, one, two, four, and six months, and one year respectively (Aziz 1956). The data have been

TABLE IV

STATISTICAL ANALYSIS AND PREDICTIONS FOR A SINGLE DATA SET

FROM DATA SET NUMBER 1 EXPOSURE TIME: 168.0 HOURS

PIT DEPTH (MICRONS)	RISK OF OCCURRENCE	SCALE UP FACTOR
100.0	0.99	1.0
200.0	0.86	1.2
300.0	0.56	1.8
400.0	0.29	3.4
500.0	0.14	7.4
600.0	0.059	17.0
700.0	0.025	40.0
800.0	0.011	94.9
900.0	0.0044	226.1
1000.0	0.0019	539.8

TABLE V

STATISTICAL ANALYSIS AND PREDICTIONS FOR A CALIPER DATA SET

WELL: WELL1
EXPOSURE TIME = 1 YEAR

FROM DATA SET NUMBER 1 0-450 FT FROM SURFACE

PIT DEPTH (INCHES)	RISK OF OCCURRENCE	SCALE UP FACTOR
0.019	0.766	1.3
0.038	0.677	1.5
0.057	0.586	1.7
0.076	0.498	2.0
0.095	0.416	2.4
0.114	0.342	2.9
0.133	0.279	3.6
0.152	0.225	4.5
0.171	0.180	5.6
0.190	0.143	7.0

TABLE VI

PREDICTIONS OF TIME-TO-FIRST-LEAK AND CORROSION ALLOWANCE

Structure thickness: 300.0 Microns
Time to first leak: 0.3 Years

i.e. $X = m * \log(t) + n$ or $t = \exp[(X-n)/m]$
where $m = 124.8989$; $n = -676.8180$
X - pit depth in microns
t - exposure time in hours

*** CORROSION ALLOWANCE SPECIFICATION ***

Life Time: 20.0 YEARS
Wall Thickness: 831.2 MICRONS
% Probability of Failure: 99.5

---

analyzed using the developed model and the different predictions are collected in Table VII. An adequate summary of the predictions is displayed by Figure 17. The figure plots the pit depths statistically predicted to occur after different periods of time. The experimental values are indicated on the same graph. As seen from the figure, the statistical predictions are in a good agreement with the experimental data, especially as the exposure time increases.

Case study II. A study of the corrosion of high level nuclear waste containers, made of carbon steel, in geological disposal has been described by the generation of a set of experimental pitting data. The data have been analyzed by the model, and the fitted distribution function is used to predict the required thickness of the tank wall for a given exposure time. Five sets of samples have been immersed in the corrosive environment for 500, 1000, 2000, 3000,and 10000 hours. For each set of data, the predicted pit depth occurrences are tabulated along with the respective scale up factors (Table VIII). For example, if an experimental metal sample is immersed in the corrosive solution for a chosen exposure time, then for a given pit depth, the third column in the table, i.e., the scale up factor, gives the surface area of a large structure needed before a pit as deep can be observed. This surface area is equal to the product of the sample area and the scale up factor. From the output, as the exposure time increases, more of smaller size pits are observed along with relatively fewer deep pits. This phenomenon can be explained by the probable repassivation of some pits due to the accumulation of corrosion product inside the cavities. When the coupons are first immersed in the corrosive solutions, many pits are initiated and start

TABLE VII

STATISTICAL ANALYSIS AND PREDICTIONS FOR CASE STUDY I

FROM DATA SET NUMBER 1 EXPOSURE TIME: 168.0 HOURS

PIT DEPTH	RISK OF OCCURRENCE	SCALE UP FACTOR
100.0	0.99	1.0
200.0	0.86	1.2
300.0	0.56	1.8
400.0	0.29	3.4
500.0	0.14	7.4
600.0	0.059	17.0
700.0	0.025	40.0
800.0	0.011	94.8
900.0	0.0044	226.1
1000.0	0.0019	539.8

FROM DATA SET NUMBER 2 EXPOSURE TIME: 720.0 HOURS

PIT DEPTH	RISK OF OCCURRENCE	SCALE UP FACTOR
100.0	1.0	1.0
200.0	1.0	1.0
300.0	1.0	1.0
400.0	0.985	1.0
500.0	0.783	1.3
600.0	0.425	2.4
700.0	0.182	5.5
800.0	0.0705	14.2
900.0	0.0262	38.2
1000.0	0.0096	104.3

TABLE VII (Continued)

FROM DATA SET NUMBER 3 EXPOSURE TIME: 2160.0 HOURS

PIT DEPTH	RISK OF OCCURRENCE	SCALE UP FACTOR
100.0	1.0	1.0
200.0	1.0	1.0
300.0	1.0	1.0
400.0	0.999	1.0
500.0	0.929	1.1
600.0	0.659	1.5
700.0	0.354	2.8
800.0	0.163	6.2
900.0	0.070	14.4
1000.0	0.029	34.7

FROM DATA SET NUMBER 4 EXPOSURE TIME: 4320.0 HOURS

PIT DEPTH	RISK OF OCCURRENCE	SCALE UP FACTOR
100.0	1.0	1.0
200.0	1.0	1.0
300.0	1.0	1.0
400.0	1.0	1.0
500.0	1.0	1.0
600.0	0.951	1.05
700.0	0.489	2.05
800.0	0.139	7.20
900.0	0.0328	30.5
1000.0	0.0074	135.0

FROM DATA SET NUMBER 5 EXPOSURE TIME: 8640.0 HOURS

PIT DEPTH	RISK OF OCCURRENCE	SCALE UP FACTOR
100.0	1.0	1.00
200.0	1.0	1.00
300.0	1.0	1.00
400.0	1.0	1.00
500.0	1.0	1.00
600.0	0.986	1.02
700.0	0.749	1.34
800.0	0.361	2.77
900.0	0.135	7.42
1000.0	0.0458	21.8

TABLE VII (Continued)

***** PREDICTION OF TIME-TO-FIRST LEAK ******

Structure thickness:	1000.0	Microns
Time to first leak:	4.4	Years

i.e. $X = m * \log(t) + n$ or $t = \exp[(X-n)/m]$

where $m = 81.4428$; $n = 139.3161$

X - pit depth in microns

t - exposure time in hours

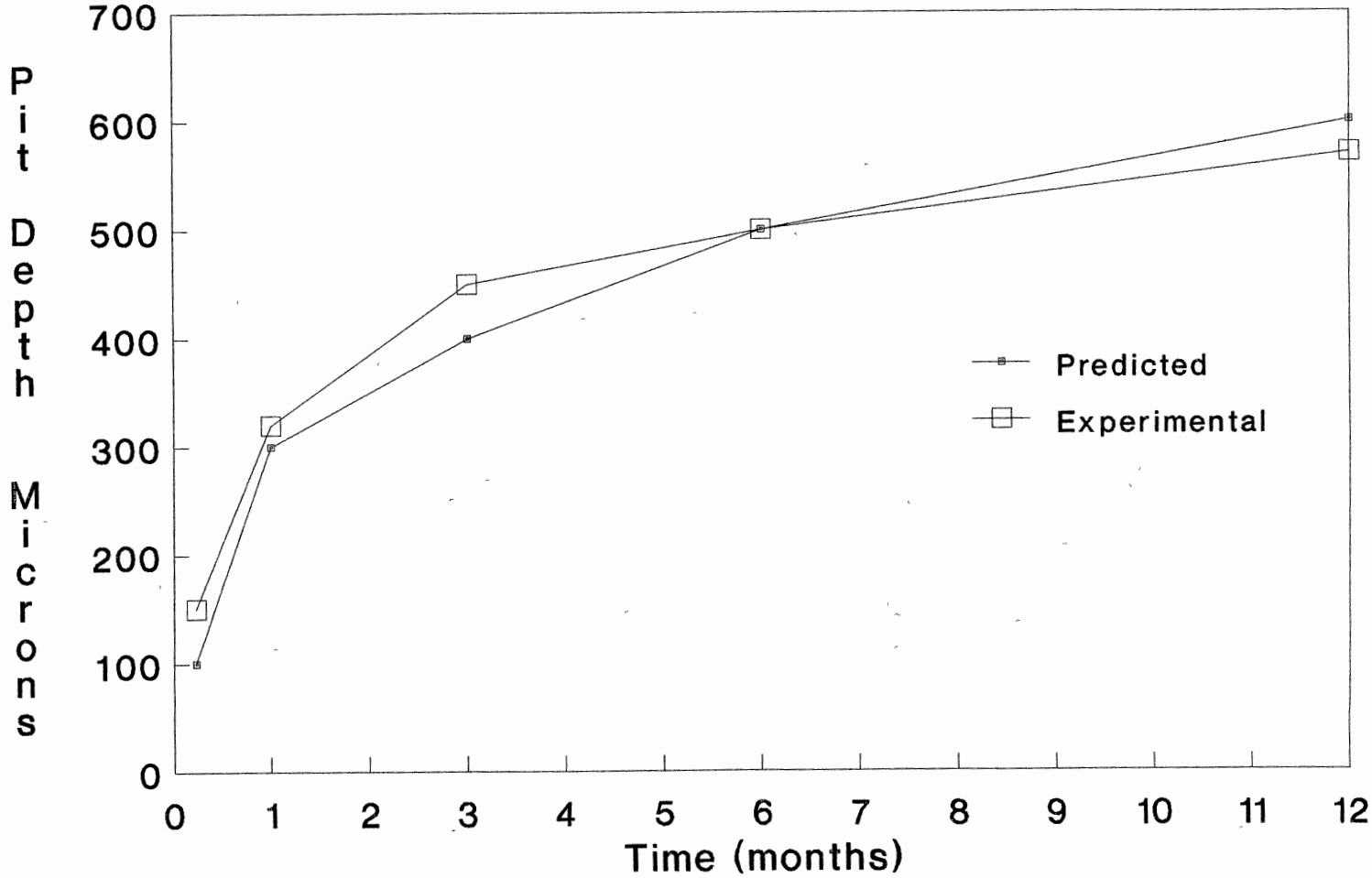

Figure 17. Pit Depth Predictions for Case Study I

TABLE VIII

STATISTICAL ANALYSIS AND PREDICTIONS FOR CASE STUDY II

FROM DATA SET NUMBER 1 EXPOSURE TIME: 500.0 HOURS

PIT DEPTH (MICRONS)	RISK OF OCCURRENCE	SCALE UP FACTOR
500.0	0.416	0.241E+01
1000.0	0.0152	0.658E+02
1500.0	0.00044	0.229E+04
2000.0	0.000012	0.804E+05
2500.0	0.00000035	0.282E+07
3000.0	0.00000001	0.991E+08
3500.0	0.0	0.348E+10
4000.0	0.0	0.122E+12
4500.0	0.0	0.428E+13
5000.0	0.0	0.150E+15

FROM DATA SET NUMBER 2 EXPOSURE TIME: 1000.0 HOURS

PIT DEPTH (MICRONS)	RISK OF OCCURRENCE	SCALE UP FACTOR
500.0	0.947	0.106E+01
1000.0	0.173	0.578E+01
1500.0	0.0122	0.817E+02
2000.0	0.0008	0.125E+04
2500.0	0.000052	0.194E+05
3000.0	0.0000034	0.299E+06
3500.0	0.00000022	0.461E+07
4000.0	0.00000001	0.711E+08
4500.0	0.0	0.110E+10
5000.0	0.0	0.169E+11

TABLE VIII (Continued)

FROM DATA SET NUMBER 3 EXPOSURE TIME: 2000.0 HOURS

PIT DEPTH (MICRONS)	RISK OF OCCURRENCE	SCALE UP FACTOR
500.0	0.999	0.100E+01
1000.0	0.68	0.147E+01
1500.0	0.15	0.653E+01
2000.0	0.024	0.417E+02
2500.0	0.0036	0.282E+03
3000.0	0.00052	0.193E+04
3500.0	0.000076	0.132E+05
4000.0	0.000011	0.903E+05
4500.0	0.0000016	0.618E+06
5000.0	0.00000024	0.423E+07

FROM DATA SET NUMBER 4 EXPOSURE TIME: 3000.0 HOURS

PIT DEPTH (MICRONS)	RISK OF OCCURRENCE	SCALE UP FACTOR
500.0	1.0	0.100E+01
1000.0	0.91	0.110E+01
1500.0	0.33	0.307E+01
2000.0	0.062	0.162E+02
2500.0	0.010	0.981E+02
3000.0	0.0017	0.606E+03
3500.0	0.00027	0.375E+04
4000.0	0.000043	0.233E+05
4500.0	0.000007	0.144E+06
5000.0	0.0000011	0.895E+06

FROM DATA SET NUMBER 5 EXPOSURE TIME: 10,000 HOURS

PIT DEPTH (MICRONS)	RISK OF OCCURRENCE	SCALE UP FACTOR
500.0	1.0	0.100E+01
1000.0	1.0	0.100E+01
1500.0	0.98	0.102E+01
2000.0	0.73	0.137E+01
2500.0	0.36	0.280E+01
3000.0	0.14	0.715E+01
3500.0	0.05	0.200E+02
4000.0	0.017	0.578E+02
4500.0	0.0059	0.169E+03
5000.0	0.0020	0.495E+03

TABLE VIII (Continued)

```
***** PREDICTION OF TIME-TO-FIRST LEAK ******

Structure thickness:        5000.0   Microns
Time to first leak:           16.5   Years

i.e.        X = m * log(t) + n    or  t = exp[(X-n)/m]
where       m =   784.4850 ; n = -4321.2482
            X - pit depth in microns
            t - exposure time in hours
```

propagating, but most of them are progressively stifled and eventually stop growing. This behavior gives the bell shape distribution function which will be discussed in more details in the next study case.

Case study III. In this study case, the corrosion of carbon steel in CO_2 environment is assessed through the statistical analysis of the measured corrosion profiles. Such data are provided by the work of Strutt et al. (1985). Several immersion times have been used in the experiment ranging from 336 to 1176 hours. The data have been analyzed by the model and the results are presented in Table IX. For each exposure time, the probability of occurrence for various fractions of the wall thickness is given. Estimates of both the time to first leak in case of an old structure and the corrosion allowance for design purposes are also given. The distribution parameters from the six data sets are plotted versus the immersion time to give a linear dependency as shown on Figure 18. It is valuable to observe that not only does the most probable maximum depth (i.e. location parameter) increase with time, but also the width of the distribution (i.e. shape parameter) increases with time. This may suggest that pits nucleate on the surface and propagate by lateral growth to expose a new passive surface on which new pits can initiate and survive. With time, more and more pits nucleate giving a rather flat bell shape to the distribution function. Figure 19 displays the estimated continuous pit depth frequency distributions corresponding to the various immersion periods. From an electrochemical prospective, an ideally uniform corrosion process would display a very narrow probability distribution function (pdf) as the anodic and cathodic sites are continually changing in a random

TABLE IX

STATISTICAL ANALYSIS AND PREDICTIONS FOR CASE STUDY III

FROM DATA SET NUMBER 1 EXPOSURE TIME: 336.0 HOURS

PIT DEPTH (MICRONS)	RISK OF OCCURRENCE	SCALE UP FACTOR
30.0	1.0	0.100E+01
60.0	0.38	0.265E+01
90.0	0.0058	0.173E+03
120.0	0.000071	0.142E+05
150.0	0.00000086	0.116E+07
180.0	0.00000001	0.949E+08
210.0	0.0	0.777E+10
240.0	0.0	0.636E+12
270.0	0.0	0.521E+14
300.0	0.0	0.450E+16

FROM DATA SET NUMBER 2 EXPOSURE TIME: 504.0 HOURS

PIT DEPTH (MICRONS)	RISK OF OCCURRENCE	SCALE UP FACTOR
30.0	1.0	0.100E+01
60.0	0.92	0.109E+01
90.0	0.052	0.191E+02
120.0	0.0011	0.876E+03
150.0	0.000024	0.412E+05
180.0	0.00000052	0.194E+07
210.0	0.00000001	0.910E+08
240.0	0.0	0.428E+10
270.0	0.0	0.201E+12
300.0	0.0	0.947E+13

TABLE IX (Continued)

FROM DATA SET NUMBER 3 EXPOSURE TIME: 672.0 HOURS

PIT DEPTH (MICRONS)	RISK OF OCCURRENCE	SCALE UP FACTOR
30.0	1.0	0.100E+01
60.0	0.999	0.100E+01
90.0	0.527	0.190E+01
120.0	0.0794	0.126E+02
150.0	0.0091	0.110E+03
180.0	0.00101	0.991E+03
210.0	0.00011	0.896E+04
240.0	0.000012	0.811E+05
270.0	0.0000014	0.734E+06
300.0	0.00000015	0.664E+07

FROM DATA SET NUMBER 4 EXPOSURE TIME: 840.0 HOURS

PIT DEPTH (MICRONS)	RISK OF OCCURRENCE	SCALE UP FACTOR
30.0	1.0	0.100E+01
60.0	1.0	0.100E+01
90.0	1.0	0.100E+01
120.0	0.744	0.134E+01
150.0	0.180	0.554E+01
180.0	0.0286	0.350E+02
210.0	0.00422	0.237E+03
240.0	0.000617	0.162E+04
270.0	0.000090	0.111E+05
300.0	0.000013	0.762E+05

TABLE IX (Continued)

FROM DATA SET NUMBER 5 EXPOSURE TIME: 1008.0 HOURS

PIT DEPTH (MICRONS)	RISK OF OCCURRENCE	SCALE UP FACTOR
30.0	1.0	0.100E+01
60.0	1.0	0.100E+01
90.0	1.0	0.100E+01
120.0	0.995	0.101E+01
150.0	0.633	0.158E+01
180.0	0.173	0.578E+01
210.0	0.0354	0.283E+02
240.0	0.0068	0.147E+03
270.0	0.00129	0.774E+03
300.0	0.000245	0.409E+04

FROM DATA SET NUMBER 6 EXPOSURE TIME: 1176.0 HOURS

PIT DEPTH (MICRONS)	RISK OF OCCURRENCE	SCALE UP FACTOR
30.0	1.0	0.100E+01
60.0	1.0	0.100E+01
90.0	1.0	0.100E+01
120.0	0.998	0.100E+01
150.0	0.851	0.117E+01
180.0	0.441	0.227E+01
210.0	0.163	0.614E+01
240.0	0.0528	0.189E+02
270.0	0.0164	0.608E+02
300.0	0.00505	0.198E+03

TABLE IX (Continued)

```
***** PREDICTION OF TIME-TO-FIRST LEAK ******

Structure thickness:          300.0   Microns
Time to first leak:             0.3   Years

i.e.        X = m * log(t) + n   or  t = exp[(X-n)/m]
where       m =   124.8989 ; n =  -676.8180
            X - pit depth in microns
            t - exposure time in hours


***** CORROSION ALLOWANCE SPECIFICATION ******

Life Time:                      20.0  YEARS
Wall Thickness:                 831.2  MICRONS
% Probability of Failure:       99.5
```

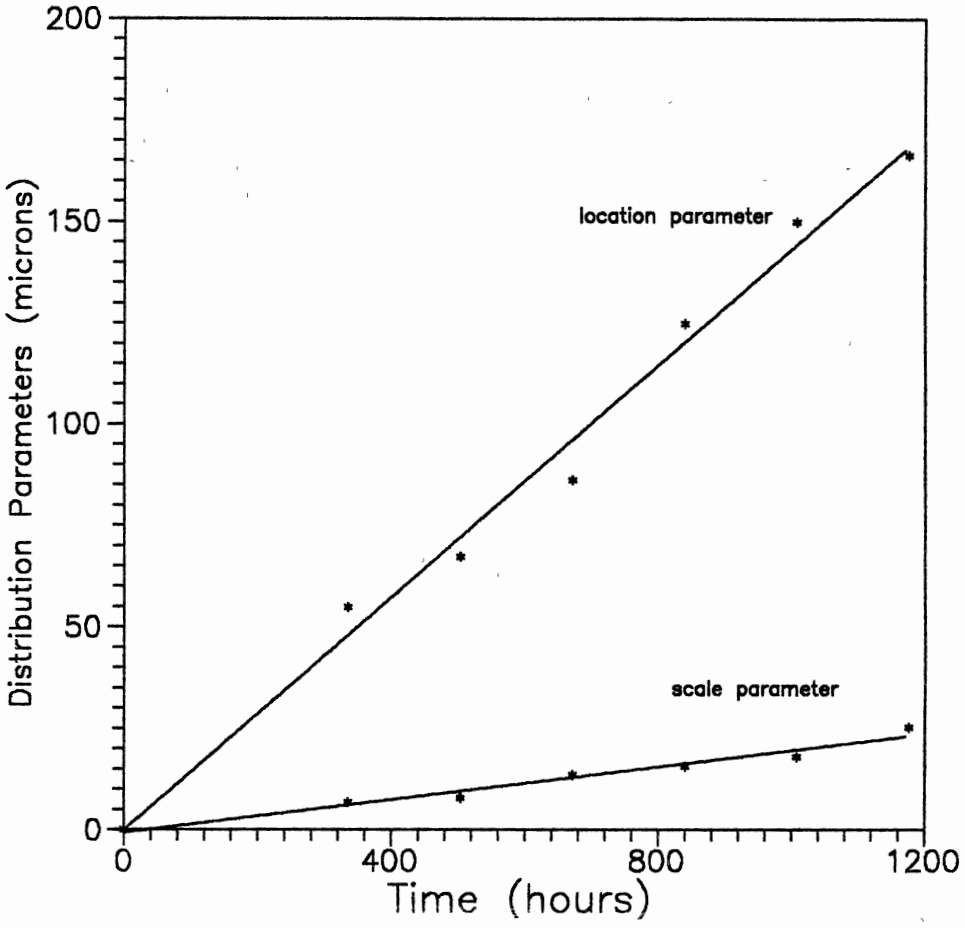

Figure 18. Variation of the Extreme Value Distribution Parameters with Time

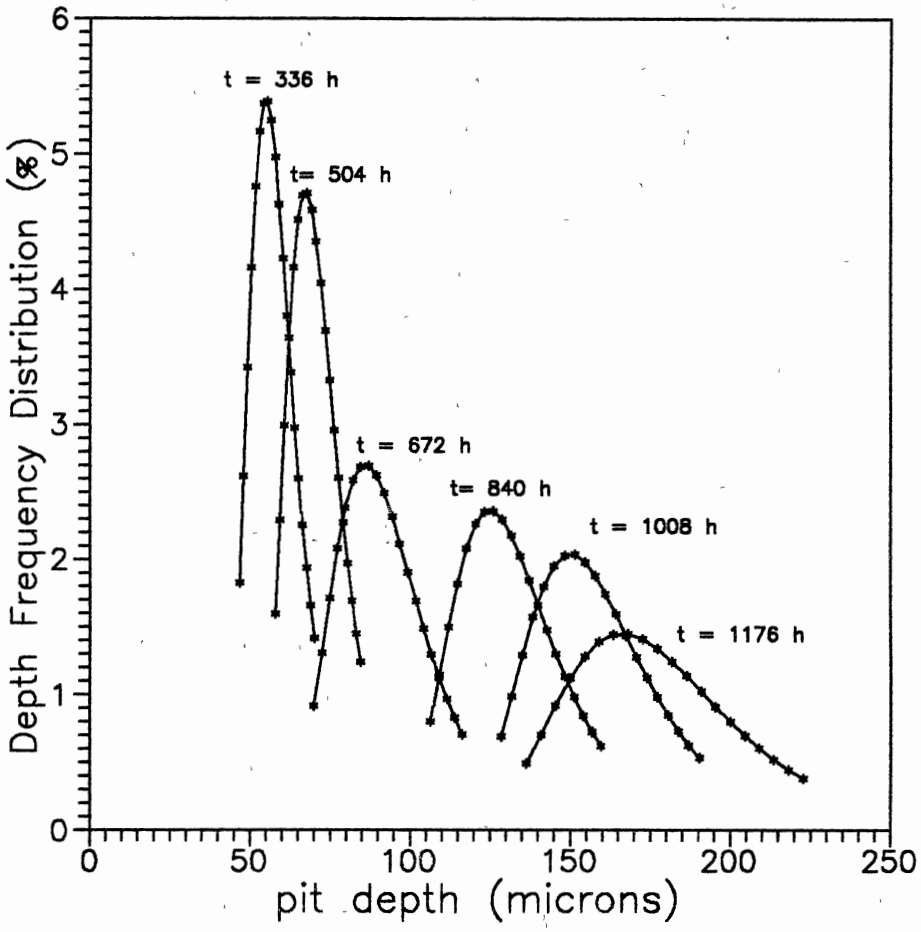

Figure 19. Pit Depth Frequency Distribution as a Function of Exposure Time

manner with time. Conversely, in the case of localized attack, the spacial variations in the cathodic constituents may be changing with time at a slower rate than that of the anodic constituents, which give rise to an accelerating dissociation at the anodic site. Such difference in variations can be caused by the fluid flow regime and/or a localized destruction of the iron carbonate film. The different rate of dissociation results in the broadening of the pdf in the case of pitting corrosion.

Case study IV and V. The model also offers the option of analyzing caliper survey data, such a data source has been fully described in a previous section. This case study displays the results of two caliper survey analyses using the developed model. The outputs, shown in Tables X and XI, are compilations of the predicted probability occurrences of different fractions of the wall thickness throughout the whole tubing. The predictions are given for a 450 ft string at a time. The temperature variation is assumed to be equal to about 1 $^{\circ}$C per 100 ft. Since the conditions of one section might be significantly different than the other, the predictions should be limited for each section independently. The severity of the environment can be compared from one section to the other through the analysis of the probability of occurrence of a given pit depth. The top sections of both surveys show a higher susceptibility to pitting, such degree of attack can be quantitatively compared to other sections through the use of the model output. The main parameters, thought by the author to contribute to pitting occurrence along the tubing can be limited to the water formation, chlorine content, CO_2 and H_2S partial pressures, temperature, and velocity. If a variety of data describing the effects of such parameters can be

TABLE X

STATISTICAL ANALYSIS AND PREDICTIONS FOR CASE STUDY V

WELL: WELL #14
EXPOSURE TIME = 1 YEAR

FROM DATA SET NUMBER 1 0-450 FT FROM SURFACE

PIT DEPTH (INCHES)	RISK OF OCCURRENCE	SCALE UP FACTOR
0.019	0.77	1.3
0.038	0.68	1.5
0.057	0.59	1.7
0.076	0.50	2.0
0.095	0.42	2.4
0.114	0.34	2.9
0.133	0.28	3.6
0.152	0.23	4.5
0.171	0.18	5.6
0.190	0.14	7.0

FROM DATA SET NUMBER 2 450-900 FT FROM SURFACE

PIT DEPTH (INCHES)	RISK OF OCCURRENCE	SCALE UP FACTOR
0.019	0.94	1.1
0.038	0.79	1.3
0.057	0.59	1.7
0.076	0.39	2.5
0.095	0.25	4.1
0.114	0.15	6.8
0.133	0.085	11.7
0.152	0.049	20.4
0.171	0.028	35.9
0.190	0.016	63.4

TABLE X (Continued)

FROM DATA SET NUMBER 3 900-1350 FT FROM SURFACE

PIT DEPTH (INCHES)	RISK OF OCCURRENCE	SCALE UP FACTOR
0.019	0.71	1.4
0.038	0.41	2.4
0.057	0.21	4.8
0.076	0.097	10.3
0.095	0.043	23.0
0.114	0.019	52.0
0.133	0.0084	118.5
0.152	0.0037	270.5
0.171	0.0016	618.6
0.190	0.00071	1415.5

FROM DATA SET NUMBER 4 1350-1800 FT FROM SURFACE

PIT DEPTH (INCHES)	RISK OF OCCURRENCE	SCALE UP FACTOR
0.019	0.98	1.0
0.038	0.69	1.5
0.057	0.28	3.6
0.076	0.09	11.2
0.095	0.026	37.2
0.114	0.0076	131.7
0.133	0.0022	461.3
0.152	0.00062	1619
0.171	0.00018	5685
0.190	0.00005	19968

TABLE X (Continued)

FROM DATA SET NUMBER 5	1800-2250 FT FROM SURFACE	
PIT DEPTH (INCHES)	RISK OF OCCURRENCE	SCALE UP FACTOR
0.019	0.79	1.3
0.038	0.50	2.0
0.057	0.26	3.8
0.076	0.13	6.0
0.095	0.057	17.5
0.114	0.026	39.2
0.133	0.011	88.6
0.152	0.005	201.0
0.171	0.002	456.6
0.190	0.001	1038.0
FROM DATA SET NUMBER 6	2250-2700 FT FROM SURFACE	
PIT DEPTH (INCHES)	RISK OF OCCURRENCE	SCALE UP FACTOR
0.019	0.53	1.9
0.038	0.31	3.2
0.057	0.17	6.0
0.076	0.09	11.6
0.095	0.044	22.9
0.114	0.022	46.1
0.133	0.011	93.1
0.152	0.0053	188.5
0.171	0.0026	382.3
0.190	0.0013	775.9
FROM DATA SET NUMBER 7	2700-3150 FT FROM SURFACE	
PIT DEPTH (INCHES)	RISK OF OCCURRENCE	SCALE UP FACTOR
0.019	0.31	3.22
0.038	0.11	9.28
0.057	0.034	29.1
0.076	0.011	93.7
0.095	0.0033	304.2
0.114	0.0010	990.4
0.133	0.00031	3227
0.152	0.000095	10517
0.171	0.000029	34281
0.190	0.0000090	111741

TABLE XI

STATISTICAL ANALYSIS AND PREDICTIONS FOR CASE STUDY VI

WELL: WELL #8
EXPOSURE TIME = 1 YEAR

FROM DATA SET NUMBER 1 0-450 FT FROM SURFACE

PIT DEPTH (INCHES)	RISK OF OCCURRENCE	SCALE UP FACTOR
0.02	0.84	0.120E+01
0.04	0.48	0.208E+01
0.07	0.21	0.474E+01
0.09	0.082	0.122E+02
0.11	0.031	0.327E+02
0.13	0.011	0.895E+02
0.15	0.0041	0.246E+03
0.17	0.0015	0.680E+03
0.20	0.00053	0.188E+04
0.22	0.00019	0.519E+04

FROM DATA SET NUMBER 2 450-900 FT FROM SURFACE

PIT DEPTH (INCHES)	RISK OF OCCURRENCE	SCALE UP FACTOR
0.02	0.93	0.108E+01
0.04	0.45	0.223E+01
0.07	0.13	0.793E+01
0.09	0.03	0.333E+02
0.11	0.0069	0.146E+03
0.13	0.0016	0.643E+03
0.15	0.00036	0.284E+04
0.17	0.00008	0.126E+05
0.20	0.000018	0.556E+05
0.22	0.0000041	0.246E+06

TABLE XI (Continued)

FROM DATA SET NUMBER 3 900-1350 FT FROM SURFACE

PIT DEPTH (INCHES)	RISK OF OCCURRENCE	SCALE UP FACTOR
0.02	0.54	0.185E+01
0.04	0.27	0.366E+01
0.07	0.12	0.813E+01
0.09	0.053	0.190E+02
0.11	0.022	0.454E+02
0.13	0.0091	0.110E+03
0.15	0.0038	0.266E+03
0.17	0.0016	0.644E+03
0.20	0.00064	0.156E+04
0.22	0.00026	0.380E+04

FROM DATA SET NUMBER 4 1350-1800 FT FROM SURFACE

PIT DEPTH (INCHES)	RISK OF OCCURRENCE	SCALE UP FACTOR
0.02	0.414	0.242E+01
0.04	0.048	0.209E+02
0.07	0.0045	0.222E+03
0.09	0.00041	0.242E+04
0.11	0.000038	0.263E+05
0.13	0.0000035	0.287E+06
0.15	0.00000032	0.312E+07
0.17	0.00000003	0.340E+08
0.20	0.00000000	0.370E+09
0.22	0.00000000	0.403E+10

TABLE XI (Continued)

FROM DATA SET NUMBER 5	1800-2250 FT FROM SURFACE	
PIT DEPTH (INCHES)	RISK OF OCCURRENCE	SCALE UP FACTOR
0.02	0.26	0.379E+01
0.04	0.06	0.169E+02
0.07	0.012	0.826E+02
0.09	0.0024	0.412E+03
0.11	0.00048	0.206E+04
0.13	0.000097	0.103E+05
0.15	0.00002	0.519E+05
0.17	0.0000039	0.260E+06
0.20	0.00000077	0.130E+07
0.22	0.00000015	0.654E+07
FROM DATA SET NUMBER 6	2250-2700 FT FROM SURFACE	
PIT DEPTH (INCHES)	RISK OF OCCURRENCE	SCALE UP FACTOR
0.02	0.60	0.167E+01
0.04	0.22	0.457E+01
0.07	0.065	0.155E+02
0.09	0.018	0.556E+02
0.11	0.005	0.204E+03
0.13	0.0013	0.751E+03
0.15	0.00036	0.277E+04
0.17	0.00010	0.102E+05
0.20	0.000026	0.377E+05
0.22	0.0000072	0.139E+06
FROM DATA SET NUMBER 7	2700-3150 FT FROM SURFACE	
PIT DEPTH (INCHES)	RISK OF OCCURRENCE	SCALE UP FACTOR
0.02	0.41	0.245E+01
0.04	0.09	0.111E+02
0.07	0.02	0.597E+02
0.09	0.003	0.330E+03
0.11	0.0005	0.184E+04
0.13	0.0001	0.102E+05
0.15	0.00002	0.570E+05
0.17	0.000003	0.317E+06
0.20	0.0000006	0.177E+07
0.22	0.0000001	0.983E+07

generated or collected, then a single probability distribution function can be made available to predict pitting occurrences along the tubing. Moreover, if pitting data can be made available from different CO_2 and H_2S environments, then a set of distribution parameters correlated with the operating variables, listed above, can be useful to predict the localized corrosion behavior of an independent well giving a minimum number of inputs. Unfortunately, such task can be difficult since most of the wells, which show signs of pitting failure, are treated with chemical inhibitors to overcome the problem. Therefore, the pitting data from caliper surveys, needed to make time dependent statistical predictions, is not frequently collected. Alternatively, such data can be generated in a laboratory by fixing all the operating parameters except one and study its effects. Once the individual contributions are completed, a general predictive correlation can be developed. While this approach is feasible, it could face the problem of adequately simulating the actual corrosive environment. Nevertheless, with the rapid development of instrumentation, the experimental approach can be viable.

Summary and Findings

1. The random behavior of the deepest pits on a given corroded sample has been found to obey the Extreme Value Distribution theory. Its prediction and analysis are performed upon the estimation of the distribution coefficients.

2. Both laboratory experimental data and field surveys can be analyzed by the model.

3. Given time variable pitting data, the statistical model provides predictions for the time to first leak and the corrosion allowance.

4. If the deepest pits on a laboratory-scale sample are measured and analyzed by the model, an estimate is given for the large scale structure required before a pit with a specified depth is observed at a particular exposure time.

5. Having applied the model to a given well, the generated distribution coefficients could be used to predict the pitting behavior of another well with similar characteristics.

6. A general correlation, capable of predicting the localized corrosion trend for a given CO_2 and H_2S environment, could be formulated if various data sets are collected. Such data sets must span a wide variety of operating parameters, e.g., CO_2 and H_2S contents, temperature, chlorine contamination, water formation, fluid flow characteristics, etc.

CHAPTER V

A THEORETICAL MODEL FOR FLOW INDUCED CO2 AND H2S PITTING CORROSION

In the previous chapter, the statistical modeling of CO_2 and H_2S pitting corrosion in downhole applications has been developed and used to predict the severity of localized attack at a given environment. However, the development of a mechanistic model is necessary in order to fully describe and analyze this phenomenon on a theoretical and sound basis. Furthermore, the use of a mechanistic model of pitting corrosion allows one to predict the severity and the extent of propagation of an existing pit which has been induced at a specific environment. Such models have been scarce and very specific, especially because of the mathematical complexities involved within the formulation. For downhole applications, mechanistic models for pitting corrosion could be very useful to predict the failure analysis of the structure especially with the complete and available information descriptive of the oil and gas wells. In CO_2 and H_2S environments, pitting corrosion of bare steel has been attributed mainly to high turbulence effects, i.e., flow induced localized attack. This phenomenon has also been validated experimentally in chapter II of this work. As a third step, an effort is made to model the effects of flow characteristics and the bulk chemistry on pit propagation rate. Given the hydrodynamics in the main stream and an

initial shape of a pit along the wall, the model predicts the flow conditions inside the cavity and its extent of propagation or repassivation accounting for the equilibrium conditions and the flow characteristics. The criterion of pit passivation or propagation is evaluated depending on the iron carbonate supersaturation kinetics and the concentration of Fe^{++} at the surface of the pit walls. The former is influenced by both the iron dissociation and the mass transfer rates. The activity of a pit is tested all along the downhole tubing by running the localized corrosion calculations at each specified section of the pipe.

Model Description and Development

A theoretical model has been developed in order to predict the propagation rate of an existing pit along the tubing wall under turbulent flow conditions in a CO_2 and H_2S environment. Such a phenomenon has been experimentally validated as part of this work as well as by other authors (Viden and Dugstad 1987). The modelling of the propagation step, rather than the initiation process, is urgent since the premature failure of a structure often occurs because of a high pit growth rate rather than an increasing population of small pits on the metal. On the other hand, the pit initiation step, in CO_2 and H_2S environments, seems to follow a highly random behavior and its theoretical modelling might lead to misleading results unless its probabilistic variations are also accounted for.

Physical Description of the Model

Downhole tubing often experiences the presence of natural gas, with and

without formation water, at high temperatures and pressures. At the higher sections of the tubing, water condensation can occur under considerable temperature and pressure drops. With the presence of a high gas flow rate, the metal walls might be continuously wetted by the liquid phase through which corrosive species, such as CO_2 and H_2S, can diffuse and attack the metal surface. Furthermore, high turbulence regimes might be existent and persistent at certain locations of the piping, e.g., at the joints between the sections or before and after a single slug. The localized high velocity, with the presence of small cavities or defects on the wall, can lead to localized attack, i.e., flow induced pitting corrosion. If the fluid flow conditions are assumed to persist in localized areas, the wall will experience uniform corrosion except at those locations where the corrosion product is being removed under the velocity effects, leaving bare metal exposed to the corrosive solution. The environmental conditions, i.e., the equilibrium state and the fluid flow characteristics, may repassivate the metal surface at the localized sites by the deposition or precipitation of a protective iron carbonate or iron sulfide film. Figure 20 shows three cases representing a uniform attack, an active pit, and a repassivated pit respectively. The development of a model to fully describe the physical phenomenon has to account for the equilibrium thermodynamics in the pipe, the kinetics of the surface reactions on the pit walls, the charge transfer through the possible electrochemical reactions, and the mass transfer and fluid flow occurring around the pit.

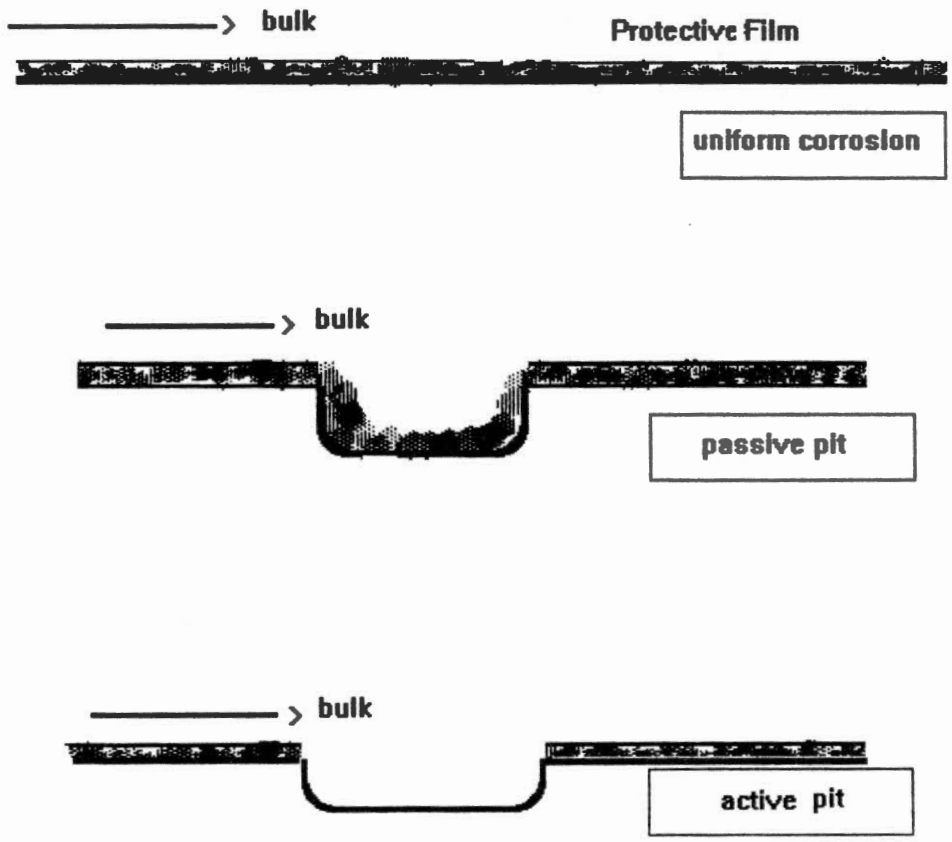

Figure 20. Modes of Carbon Steel Corrosion in CO_2 Environment

The Thermodynamic Equilibrium

The equilibrium calculations performed in the bulk stream are used to determine the composition of the corrosive solution at the mouth of the pit. These calculations are based on the following reactions:

$$H_2O(vap) \leftrightarrow H_2O \tag{5.1}$$

$$H_2S_{(g)} \leftrightarrow H_2S_{(L)} \tag{5.2}$$

$$CO_{2\,(g)} \leftrightarrow CO_{2\,(L)} \tag{5.3}$$

$$H_2S_{(L)} \leftrightarrow HS^- + H^+ \tag{5.4}$$

$$CO_2 + H_2O \leftrightarrow H_2CO_3 \leftrightarrow HCO_3^- + H^+ \tag{5.5}$$

$$HS^- \leftrightarrow S^{--} + H^+ \tag{5.6}$$

$$HCO_3^- \leftrightarrow CO_3^{--} + H^+ \tag{5.7}$$

$$H_2O \leftrightarrow OH^- + H^+ \qquad (5.8)$$

The equilibrium between the vapor and liquid phases is obtained through the following equality

$$y_1 f_i P = m_1 \phi_1 H \qquad (5.9)$$

The concentration of each species is calculated under the equilibrium conditions by expressing the disassociation reactions as follows:

$$K_{H_2S} = \frac{[HS^-][H^+]}{[H_2S]} \qquad (5.10)$$

$$K_{HS^-} = \frac{[S^{--}][H^+]}{[HS^-]} \qquad (5.11)$$

$$K_{HCO_3^-} = \frac{[CO_3^{--}][H^+]}{[HCO_3^-]} \qquad (5.12)$$

$$K_{H_2O} = \frac{[OH^-][H^+]}{[H_2O]} \qquad (5.13)$$

The usage of the above equations along with Equation (9,) applied for the three vapor-liquid equilibrium systems, can only provide eight equations to solve for twelve

unknowns which are H_2S_L, H_2CO_3, HS^-, HCO_3^-, S^{--}, CO_3^{--}, H^+, OH^-, H_2O, Y_{CO2}, Y_{H2S}, and the total amount of vapor. The four additional equations are provided by the electroneutrality relation and three equations set up through an element balance performed on sulfur, carbon, and hydrogen, as shown below:

$$\sum_i Z_i m_i = 0 \qquad (5.14)$$

$$H_2S_{feed} = Y_{H_2S}V + (H_2S_L + HS^- + S^{--} \qquad (5.15)$$

$$CO_{2_{feed}} = Y_{CO_2}V + (H_2CO_3 + HCO_3^- + CO_3^{--}) \qquad (5.16)$$

$$2\,(H_2O+H_2S)_f = 2\,(Y_{H_2S}+Y_{H_2O})\,V + 2H_2O + 2H_2S + HS^- + H^+ + OH^- + HCO_3^- \qquad (5.17)$$

The equilibrium and Henry's constants are expressed as a function of temperature from the work by Edwards et al. (1978) and Kawazuishi and Prausnitz (1987):

$$\ln K_i = \frac{a}{T} + b \ln T + c\,T + d \qquad (5.18)$$

$$\ln H_i = \frac{m}{T} + n \ln T + q\,T + p \qquad (5.19)$$

where the various constants are shown in Tables XII and XIII. The fugacity coefficients are calculated using the SRK equation of state, whereas the activation coefficients are adopted from the work by Kerr (1980):

$$\ln \Phi_i = A_0 Z_i^2 \left[-\frac{I^{1/2}}{1+I^{1/2}} + b_i I \right] \qquad (5.20)$$

where b_i takes the value of 0.3 for all species, with some exceptions: it is equal to 0.4 for H^+, 0.1 for Na^+ and Ca^+, and 0 for CO_3^{--}, HCO_3^-, and HS^-. The Debye-Huckel parameter, A_0, for aqueous electrolyte systems is determined from the temperature correlation by Bradley and Pitzer (1979):

$$A_0 = 0.377388 + 2.5368E\text{-}4\ T + 1.7892E\text{-}5\ T^2 - 3.48184E\text{-}7\ T^3$$
$$+ 4.24739E\text{-}9\ T^4 - 287647E\text{-}11\ T^5 + 1.09781E\text{-}13\ T^6$$
$$-2.20446E\text{-}16\ T^7 + 1.82433E\text{-}19\ T^8 \qquad (5.21)$$

The ion strength is defined as $0.5\Sigma m_i Z_i^2$. Once all the equilibrium calculations are performed, the species' concentrations are fixed and used for the rest of the localized corrosion model.

TABLE XII

EQUILIBRIUM CONSTANT TEMPERATURE COEFFICIENTS

Electrolyte	a	b	c	d	Validity (C)
CO2	-12092.1	-36.7816	0.0	235.482	0-225
H2S	-18034.7	-78.0719	0.092	461.716	0-275
HCO3-	-12431.7	-35.4819	0.0	220.067	0-225
HS-	-496.004	33.8889	-0.054	-214.559	0-225
H2O	-13445.9	-22.4773	0.0	140.932	0-225

TABLE XIII

TEMPERATURE COEFFICIENTS FOR HENRY'S CONSTANTS

Electrolyte	m	n	p	q	Validity (C)
CO2	-6789.04	-11.4519	-.010454	94.4914	0-250
H2S	-13236.8	-55.0551	.0595651	342.595	0-150

Kinetics and Electrochemistry of the System

For the phenomenon at hand, thermodynamics are used to determine how far the given corrosion system can proceed, whereas the rates of chemical and electrochemical reactions are utilized to determine how fast the process can be. For downhole corrosion, iron dissolution is presumed to occur at the bare metal surface of the pit walls:

$$Fe \rightarrow Fe^{++} + 2e^{-} \tag{5.22}$$

The dissolution rate is presumed to follow the following Butler-Volmer expression, usually used to calculate the corrosion current density from which the corrosion rate is estimated:

$$\begin{aligned} i_a &= i_{a0} \exp\left(\frac{\alpha_a F \eta_a}{RT}\right) \\ \Delta i_a &= \left(\frac{-0.5 i_a}{0.434294}\right)\Delta pH + \left(\frac{0.65 i_a}{P_{CO_2}}\right)\Delta P_{CO_2} \end{aligned} \tag{5.23}$$

where i_{a0} is the exchange current density, assumed in this model to be equal to 2.7×10^{-7} A/cm^2, an average value from the literature (Bockris et al. 1961, Gray et al. 1989, Ogundele and White 1986, Liu 1990). α_a ia an experimental constant equal to 0.5 for iron dissolution (Levich 1962). The overpotential, η_a for this system, is estimated by the potential difference between the protected metal at the mouth of the

pit (cathode) and the bare wall surface inside the pit (anode). The value used in this model is 100 mV. In CO_2 and H_2S systems, the iron ion, produced by Equation (22), is mainly consumed by the following equilibrium reactions:

$$\begin{aligned} Fe^{++} + CO_3^{--} &\leftrightarrow FeCO_3 \\ Fe^{++} + S^{--} &\leftrightarrow FeS \end{aligned} \qquad (5.24)$$

For the CO_2 environment, the rate of iron ion consumption is a function of the reaction constants and the species activities were expressed as follows from the work by Wajon (1985):

$$\frac{d[Fe^{++}]}{dt} = k_s\left\{\left[(Fe^{++})\,(co_3^{--})\right]^{1/2} - K_{so}^{1/2}\right\}^2 \qquad (5.25)$$

The forward reaction constant was experimentally measured as a function of temperature and found to fit the following correlation (Wajon 1985):

$$k_s\ (moles/day) = 9.24897*10^{-13}\ \exp(0.142411\ T) \qquad (5.26)$$

Whereas, for the H_2S system, the consumption rate controlled by the chemical reaction between Fe^{++} and hydrogen sulfide is expressed as follows from the experimental work by Tewari and Campbell (1976):

$$\begin{aligned} R_{Fe^{++}} &= k_1[H^+] - k_{-1}[Fe^{++}]^{0.5}[P_{H_2S}]^{0.5} \\ k_1 &= 2.7\pm0.2 * 10^{-6}\ m/\text{sec at } 25^\circ C \\ k_{-1} &= 4.7 * 10^{-9}\ m/\text{sec at } 25^\circ C \\ E_{act} &= 60\pm7\ kJ/mole \end{aligned} \qquad (5.27)$$

Mass Transfer and Fluid Flow in a Single Pit

From the equilibrium calculations and the knowledge of the chemical and electrochemical kinetics, the mobility and reactivity of the species can be fully determined once the hydrodynamics inside the pit are known. In the following derivations, an attempt is made to estimate the mass transfer effects inside the cavity given the bulk flow characteristics and an initial shape of the cavity. The main objective is to obtain an expression for the mass transfer coefficient which, combined with the kinetics and the equilibrium state, will enable to perform a flux balance on the iron ion, a measure of the corrosion rate. Figure 21 is the schematic of an arbitrary pit initially formed at the tubing wall. If the coordinate system is as such,then the flux of iron ion, Fe^{++} designated component A in the equations, can be expressed as follows

$$J_A = -D_{eff}\left(\frac{\partial C_A}{\partial y}\right)+\left(\frac{D_A Z_A F E}{RT}\right)C_A \qquad (5.28)$$

where Z is the charge number and C_A is the activity of component A. The turbulence effects are incorporated through the diffusion coefficient as shown below

$$D_{eff}= D_A+ \epsilon_D \qquad (5.29)$$

and the electric field is defined as

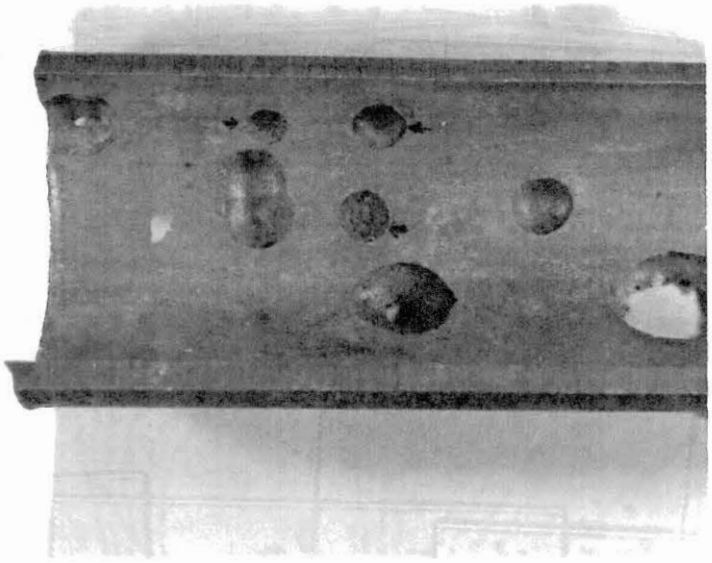

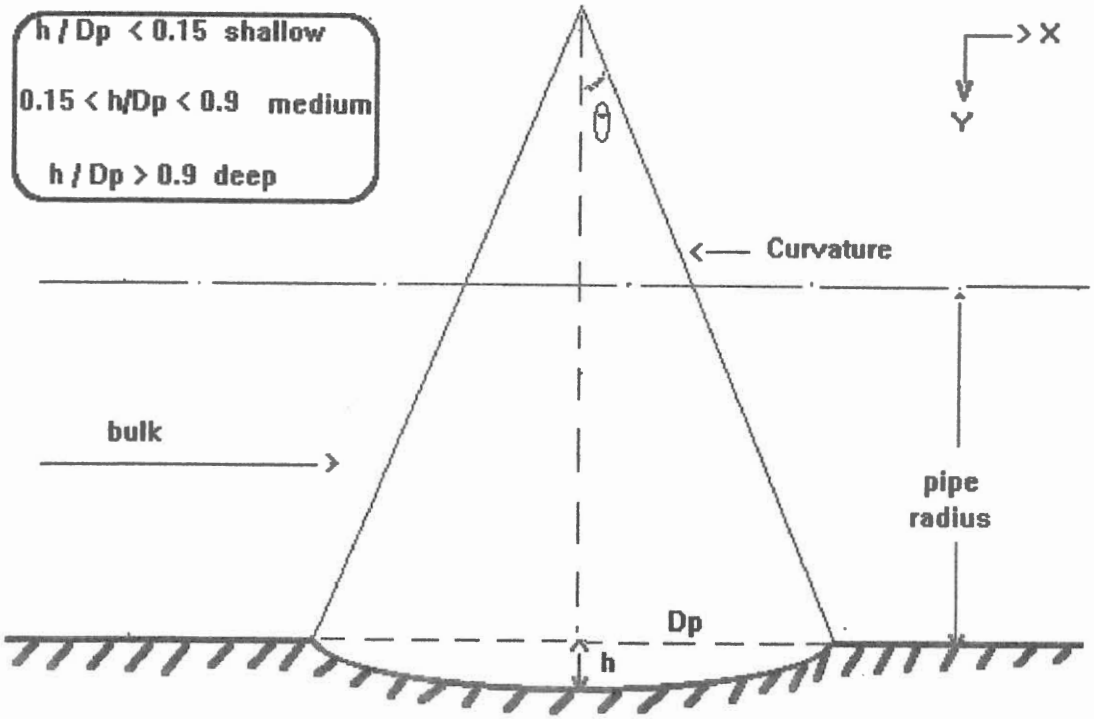

Figure 21. Top: Photo of Actual CO_2 Pits, Bottom: Geometry of a Single Pit

$$E = -\frac{\partial \phi}{\partial y} \qquad (5.30)$$

If expressed as a function of activity, then Equation (28) can be uniquely dependent on C_A. For a binary system A and B, the relation is

$$E = -\frac{(D_B - D_A)\,RT}{F(Z_A D_A + Z_B D_B)}\ \frac{1}{C_A}\ \frac{dC_A}{dy} \qquad (5.31)$$

the above equation is exact for binary systems (Levich, 1962). The relation can be generalized for multicomponent systems as follows

$$E = -\frac{RT}{F}\ G(D_1, Z_1, C_i,)\ \frac{1}{C_A}\ \frac{dC_A}{dy} \qquad (5.32)$$

If the G function is approximately constant, then an analytical solution of the governing equation, Equation (28), can be derived. Such an approximation is validated through the following proof. For a general multicomponent electrolyte solution, Equation (28) can be written

$$J_J = -D_J \nabla C_J + \frac{F D_j Z_J C_j}{RT} \nabla \phi \qquad (5.33)$$

For the corrosion system at hand, no net current flow is present, i.e., the sum of the charged species' fluxes is zero. Therefore multiplying Equation (33) by Z_j and

summing over all j's,

$$\sum_j Z_j J_j = 0 = -\sum_j D_j \nabla C_j + \frac{F}{RT} \sum_j D_j Z_j^2 C_j \nabla \phi \qquad (5.34)$$

From the above equation, the gradient of the electric field is

$$\nabla \phi = \frac{RT}{F} \frac{\sum_j Z_j D_j \nabla C_j / \nabla C_A + Z_A D_A}{\sum_j Z_j^2 D_j C_j / C_A + Z_A^2 D_A} \frac{\nabla C_A}{C_A} \qquad (5.35)$$

Equating Equation (35) to (32), G is expressed as

$$G(D_j, Z_j, C_j) = \frac{\sum_j Z_j D_j \nabla C_j / \nabla C_A + Z_A D_A}{\sum_j Z_j^2 D_j C_j / C_A + Z_A^2 D_A} \qquad (j \neq A) \qquad (5.36)$$

Therefore, G is a function of the concentration gradients. However, for the given system if mass transfer is one-dimensional, then the gradient can be replaced by a 'delta' difference across a thin boundary layer. Therefore Equation (36) can be rewritten as:

$$G(D_j, Z_j, C_j) = \frac{\sum_j Z_j D_j \Delta C_j / \Delta C_A + Z_A D_A}{\sum_j Z_j^2 D_j C_j / C_A + Z_A^2 D_A} \qquad (j \neq A) \qquad (5.37)$$

The ΔC_j's can be calculated by performing an atom balance on the reactive species as follows:

Five equilibrium relations are used along with the expressions obtained from an atom balance performed on H^+, $CO3^{--}$, S^{--}, and Fe^{++} to solve for the ten concentration gradients. Equations (38) through (47) represent such relations respectively:

$$C_{HS^-} = \frac{C_S - C_{H^+}}{K_{HS^-}} \tag{5.38}$$

$$C_{H_2S} = \frac{C_S - C_{H^+}^2}{(K_{HS^-})\,(K_{H_2S})} \tag{5.39}$$

$$C_{HCO_3^-} = \frac{C_{CO_3} - C_{H^+}}{K_{HCO_3^-}} \tag{5.40}$$

$$C_{H_2CO_3} = \frac{C_{CO_3} - C_{H^+}^2}{(K_{CO_2})\,(K_{HCO_3^-})} \tag{5.41}$$

$$C_{OH^-} = \frac{K_W}{C_{H^+}} \tag{5.42}$$

$$D_{H^+}\nabla C_{H^+} + D_{H_2S}\nabla C_{H_2S} + D_{HS^-}\nabla C_{HS^-} + D_{H_2CO_3}\nabla C_{H_2CO_3} + D_{OH^-}\nabla C_{OH^-} = f_1 \tag{5.43}$$

$$D_{H_2CO_3}\nabla C_{H_2CO_3} + D_{HCO_3^-}\nabla C_{HCO_3^-} + D_{CO_3}\nabla C_{CO_3} = f_2 \tag{5.44}$$

$$D_{H_2S}\nabla C_{H_2S} + D_{HS^-}\nabla C_{HS^-} + D_{S^{--}}\nabla C_{S^{--}} = f_3 \qquad (5.45)$$

$$D_{Fe^{++}}\nabla C_{Fe^{++}} = f_4 \qquad (5.46)$$

$$\nabla C_{H_2O} = 0 \qquad (5.47)$$

The f_i's (1 through 4) are the fluxes of H^+, CO_3^{--}, S^{--}, and Fe^{++} from the surface kinetics. After taking the first derivatives of equations (38) through (42) with respect to y and plugging the results into Equations (44) through (47), a system of five equations and five unknowns is generated. Then, once all the concentration gradients are determined, the G function is evaluated from Equation (37).

Back to the governing equation, once the electric potential is substituted in from Equation (32), Equation (28) becomes

$$J_A = -[D_A(1+Z_AG) + \varepsilon_D]\nabla C_A \qquad (5.48)$$

Throughout this model, the pit is assumed to have a spherical shape, therefore Equation (48), in terms of spherical coordinates, becomes

$$\frac{1}{r}\overline{U_\theta}\frac{\partial C_A}{\partial \theta} = \frac{1}{r^2}\frac{\partial}{\partial r}\left\{[D_A(1+Z_AG) + \varepsilon_D]\, r^2 \frac{\partial C_A}{\partial r}\right\} \qquad (5.49)$$

If y is the wall coordinate, then it obeys

$$y=\Re-r \tag{5.50}$$

upon substitution, Equation (49) becomes

$$\overline{U}_\theta \frac{\partial C_A}{\partial \theta} = \frac{1}{(\Re-y)} \frac{\partial}{\partial y}\left[(D'_A+\varepsilon_D)\ (\Re-y)^2 \frac{\partial C_A}{\partial y} \right] \tag{5.51}$$

where

$$D'_A=D_A(1+Z_A G) \tag{5.52}$$

If the mass transfer boundary layer is assumed negligible, then

$$\Re-y \approx \Re \tag{5.53}$$

Therefore, Equation (49) simplifies to

$$\overline{U} \frac{\partial C_A}{\partial \theta} = \Re \frac{\partial}{\partial y}\left[(D_A+\varepsilon_D) \frac{\partial C_A}{\partial y} \right] \tag{5.54}$$

The following velocity profile is assumed to apply within the mass transfer boundary layer,

$$\overline{U}_\theta = \frac{U_*^2 y}{\nu} \tag{5.55}$$

where

$$U_* = \sqrt{\frac{\tau_w}{\rho}} \tag{5.56}$$

Substituting Equation (55) into (54) and introducing the traditional dimensionless variables, the following expression is obtained

$$y^+ \frac{\partial C_A^*}{\partial s^+} = \frac{\partial}{\partial y^+}\left[\left(\frac{1}{S_c} + \frac{\varepsilon_D}{\nu}\right)\frac{\partial C_A^*}{\partial y+}\right] \tag{5.57}$$

where

$$y^+ = \frac{U_* y}{\nu} \tag{5.58}$$

$$S_c = \frac{\nu}{D_A} \tag{5.59}$$

$$C_A^* = \frac{C_A - C_{AS}}{C_{AM} - C_{A^\sigma}} \tag{5.60}$$

$$s^+ = \theta\, \Re^+ \tag{5.61}$$

and

$$\Re^+ = \frac{U_* \Re}{\nu} \tag{5.62}$$

The dimensionless boundary conditions are

$$y^+ = 0, \quad C_A^* = 0 \qquad (all\ s^+) \tag{5.63}$$

$$y^+ \to \infty, \quad C_A^* = 1 \qquad (all\ s^+) \tag{5.64}$$

An initial shape of the pit must be assumed, at this point, in order to predict the appropriate flow conditions. The spherical shape of the pit is fully described if its depth and radius are given. Simple geometry will allow the calculation of the pit curvature. First, the case of a shallow pit (i.e. ratio of depth to diameter is less than 0.15) is treated. The phenomenon of flow separation and reattachment is applied in this case, since a small pit can approximately be simulated as a roughness along the tube. Once the flow sees the pit, it flows in, then separates out of the cavity. In the reattachment region, a boundary layer will be redeveloped, similarly to the traditional entrance region in a pipe. The flow, in this case, is two dimensional. In the separation region, intensive eddy recirculation occurs, hence the concentration gradient along the stream direction is smaller compared with the cross stream direction. Based on the above assessment, Equation (57) can be simplified.

In the boundary layer redevelopment region, the term (ϵ_D/ν) is reasonably set to zero, and Equation (57) reduces to

$$y^+ \frac{\partial C_A^*}{\partial s^+} = \frac{1}{S_c'} \frac{\partial^2 C_A^*}{\partial y^{+2}} \tag{5.65}$$

Introducing a new variable

$$\eta = y^+ \left(\frac{S_c'}{9 s^+} \right)^{1/3} \tag{5.66}$$

Equation (65) translates into the following ordinary differential equation

$$\frac{d^2 C_A^*}{d\eta^2} + 3\eta^2 \frac{dC_A^*}{d\eta} = 0 \tag{5.67}$$

Equation (67), subject to boundary conditions (63) and (64), is analytically solved and assumes the solution

$$C_A^* = \frac{3}{\Gamma(1/3)} \int_0^\eta e^{-\eta^3} d\eta \tag{5.68}$$

By definition, the dimensionless mass transfer coefficient, K^+ is

$$K^+ = \frac{K}{U_*} = \frac{1}{S_c'} \left(\frac{\partial C_A^*}{\partial y^+} \right)_{y^+ = 0} \tag{5.69}$$

Substituting Equation (68) in (69) yields to

$$K^+ = 0.54\,(s+)^{-1/3} S_c'^{\,-2/3} \tag{5.70}$$

The average mass transfer coefficient in the region of boundary layer redevelopment is expressed as

$$\langle K^+ \rangle = \frac{\int_0^{L^+} K^+ ds^+}{L^+} = 0.81 L^{+\,-\frac{1}{3}} S_c'^{\,-\frac{2}{3}} \tag{5.71}$$

where L^+ is the dimensionless length. In terms of Sherwood number,

$$Sh = \frac{KD}{D_A'} = Re\sqrt{\frac{f}{2}}\, S_c'\, K^+ \tag{5.72}$$

The friction factor, f, is defined as

$$f = 2\left(\frac{U_*}{\overline{U}}\right)^2 \tag{5.73}$$

Within the region of boundary layer redevelopment, the friction factor is changing along the stream line direction. Therefore, the local friction factor, is defined as

$$f_{local} = \frac{2\tau_w}{\rho \overline{U}^2} \tag{5.74}$$

The velocity profile in this region is taken from the analysis by Levich (1962):

$$U_t = \frac{2\overline{U}s}{\Re}\zeta \tag{5.75}$$

with

$$\zeta = \left(\frac{2\overline{U}}{\nu\Re}\right)^{1/2}\frac{y}{2} \tag{5.76}$$

By definition, the wall shear stress τ_w is expressed as

$$\tau_w = \mu\frac{\partial U_t}{\partial y}\Big|_{y=0} = \frac{2\sqrt{2}\,\overline{U}^{3/2}\rho\nu^{1/2}}{\Re^{3/2}}s \tag{5.77}$$

Substituting Equation (77) into (74) yields to

$$f_{local} = \frac{4\sqrt{2}\nu^{1/2}}{\overline{U}\,\Re^{3/2}}s \tag{5.78}$$

Therefore, the average friction factor in this region is

$$f = \frac{1}{L}\int_0^L f_{local}ds = \frac{2\sqrt{2}\nu^{1/2}}{\overline{U}\,\Re^{1/2}}\left(\frac{L}{\Re}\right) \tag{5.79}$$

The radius of curvature, $\Re$, is expressed as a function of the pit dimensions for a shallow configuration,

$$\Re \approx \frac{d_p^2}{h} \tag{5.80}$$

For such case, the length of the boundary layer redevelopment is small and can be taken approximately equal to the pit depth. Making these modifications, Equation (79) becomes

$$f = \frac{2\sqrt{2}}{Re_h^{1/2}}\left(\frac{h}{d_p}\right)^3 \tag{5.81}$$

where,

$$Re_h = \frac{\overline{U}h}{\nu} \tag{5.82}$$

if Equation (82) is substituted into Equation (72), then

$$Sh_{rd}=0.96Re\ Re_h^{-1/4}(h^+)^{-1/3}S_c^{/1/3}\left(\frac{h}{d_p}\right)^{3/2} \tag{5.83}$$

Equation (83) is applicable to the region of boundary layer redevelopment.

In the separation region, the concentration gradients in the stream line direction are negligible compared to those in the streamwise direction due to the existence of turbulence eddies. Therefore, the derivative of concentration with respect to S^+ can be set to zero,

$$\frac{\partial C_A^*}{\partial s^+} \approx 0 \qquad (5.84)$$

Once the above assumption is made, then Equation (49), in terms of dimensionless variables, becomes

$$\frac{\partial}{\partial y^+}\left[\left(\frac{1}{S_c'} + \frac{\varepsilon_D}{\nu}\right)\frac{\partial C_A^*}{\partial y^+}\right] = 0 \qquad (5.85)$$

Equation (85) gives

$$K^+ = \int_0^\infty \frac{dy^+}{1/S_c' + \varepsilon_D/\nu} \qquad (5.86)$$

The relation between y^+ and (ϵ_D/ν) for flow over a pit is not well defined. For electrolyte solution with S_c greater than 1000, the mass transfer boundary layer is thin. Therefore, the flow in the separation region can be treated as a plate flow for the thin mass transfer boundary layer. In these derivation, the relation proposed by Lin et al. (1953) is used:

$$\frac{\varepsilon_D}{\nu} = Ay+^3 \qquad (5.87)$$

A is a constant equal 1.43×10^{-3}. Substituting Equation (87) into (86),

$$K^+ = 0.092 S_c'^{-2/3} \tag{5.88}$$

Inserting Equation (88) into (72),

$$Sh_{sp} = 0.092\ Re \sqrt{\frac{f}{2}}\ S_c'^{1/3} \tag{5.89}$$

If a force balance is applied for the flow over the pit, then

$$f = f_w + 2C_D \left(\frac{U_w}{\overline{U}}\right)^2 \frac{d_p}{D} \tag{5.90}$$

Assuming a logarithmic velocity profile, the following expression is obtained:

$$\left(\frac{U_w}{\overline{U}}\right)^2 = 36.0\ f_w \tag{5.91}$$

where U_w is the fluid velocity over the pit mouth. The drag coefficient, C_D, is taken from the case of flow past a sphere in the Newton's law region, i.e., is set equal to 0.44. Then Equation (90) becomes

$$f = 0.079 Re^{-0.25}\left(1+31.7\frac{d_p}{D}\right) \tag{5.92}$$

Inserting Equation (92) in Equation (89) yields to

$$Sh_{sp} = 0.018\ Re^{0.88} S_c^{/\,0.33}\left(1 + 31.7\frac{d_p}{D}\right)^{0.5} \qquad (5.93)$$

The mass transfer rate in the whole pit is a weighted average over the boundary layer redevelopment and separation regions:

$$Sh_{av} = C_1 Sh_{sp} + C_2 Sh_{rd} \qquad (5.94)$$

The constants C_1 and C_2 can be physically explained as the fractional mass transfer area taken by separation region and boundary layer redevelopment region, respectively. Due to the lack of experimental data, C_1 and C_2 are set to 0.6 and 0.4 respectively. Substituting Equations (83) and (93) into (94),

$$Sh_{av} = 0.011 Re^{0.88}\ S_c^{/0.33}\left(1 + 31.7\frac{d_p}{D}\right)^{0.5}$$

$$+0.384 Re\ Re_h^{-0.25} (h^+)^{-0.33} S_c^{/0.33} \left(\frac{h}{d_p}\right)^{3/2} \qquad (5.95)$$

Equation (95) is used to calculate mass transfer coefficients in the shallow pit.

The same treatment is valid for the medium size pits, except a modification of the radius of curvature is needed. For this configuration, the radius of curvature is expressed as follows:

$$\Re = h\left(1 + \frac{d_p^2}{h^2}\right) \qquad (5.96)$$

Following the same procedures, the mass transfer effects are expressed as the following, through Sherwood number:

$$Sh_{av} = 0.011 Re\, S_c^{/0.33} \left(1 + 31.7 \frac{d_p}{D}\right)^{0.5}$$

$$+0.384 Re\, Re_h^{-0.25} (h^+)^{-0.33}\, S_c^{/\,0.33} \left(\frac{h^2}{h^2 + d_p^2}\right)^{3/4} \qquad (5.97)$$

Equation (97) is applicable for the medium size pits.

The case of deep pit is found physically different in terms of fluid flow inside the cavity. In general, flow separation does not occur in such a situation. The flow simply skims the pit. This phenomenon is quite similar to the situation of the flow over very densely packed surface roughness. The concept of skim flow was first proposed by Morris (1954) and later used by Gay and Alcorn (1962) for calculation of the friction factor in single depression. The following treatment is taken from their work. Consider a single spherical eddy shell of r_u and thickness dr_u. The work done in rotating the eddy shell in the unit time can be expressed as

$$dw_u = dm\, r_u^2 \omega^3 = 4\pi\rho r_u^4 \omega^3 dr_u \qquad (5.98)$$

Then the total work done for rotating the whole eddy should be

$$w_u = 4\pi\rho\omega^3 \int_0^{R_u} r_u^4 dr_u = \frac{4}{5}\pi\rho\omega^3 R_u^5 \qquad (5.99)$$

The force balance over the pit yields

$$\Delta p \frac{\pi}{4} D^2 \overline{U} = w_u + \tau_w \pi\, D d_p \overline{U} \qquad (5.100)$$

where,

$$\tau_w = \frac{f}{2}\rho\overline{U}^2 \qquad (5.101)$$

and

$$\Delta p = \frac{2 d_p}{D} f_r \rho \overline{U}^2 \qquad (5.102)$$

Inserting Equation (99), (101) and (102) in Equation (100),

$$f_r - f = \frac{8}{5}\left(\frac{R_u\omega}{\overline{U}}\right)^3 \left(\frac{R_u}{D}\right)\left(\frac{R_u}{d_p}\right) \qquad (5.103)$$

The size of an eddy in the pit can be estimated based on the dimensions of the pit. For simplicity, we use $R_u = h/2$ and further define:

$$R_u\omega = C_w U_w \qquad (5.104)$$

Substitution of these relations into Equation (103) gives

$$f_r - f = \frac{2}{5}\left(\frac{C_w U_w}{\bar{U}}\right)^3 \left(\frac{h}{D}\right)\left(\frac{h}{d_p}\right) \qquad (5.105)$$

The experimental data by Gay and Alcorn for flow over single cylindrical shape of depression showed that (C_w U_w/U) is almost constant and has a value of 0.22. Inserting this value into Equation (105), the following expression is obtained:

$$f_r = f + 4.7x10^{-3}\left(\frac{h}{D}\right)\left(\frac{h}{d_p}\right) \qquad (5.106)$$

Known the friction factor, Sherwood number is calculated from Equation (89), which becomes

$$Sh_{dp}=0.065Re\ S_c^{0.33}\left[0.079Re^{-0.25}+4.7x10^{-3}\left(\frac{h}{D}\right)\left(\frac{h}{d_p}\right)\right] \qquad (5.107)$$

Throughout the above derivations, the influence of fluid velocity on mass transfer in a single pit has been determined. The influence of multicomponent electrolyte solution has been implicitly included through the G function. As a matter of fact, the G

function includes more factors than just correction from binary system to multicomponent system. This assertion can be seen from Equation (31) very clearly. As was described, in order to calculate G function through Equation (31), without solving the system partial of differential equations, all the concentration differences have been determined by element balance through diffusion flux relations. In doing so, the various equilibrium and kinetic relations have been accounted for. To this end, most of the major variables have been taken into account except for the influence of chloride on mass transfer.

The following analysis will provide a correction factor to account for the influence of chloride on mass transfer in the pit. The analysis remains analytical. The influence of chloride on the corrosion rate in a pit has been qualitatively presented by several authors, however most of the work pertained to pitting occurring in stagnant solutions. The emphasis, in this work, is rather mass transfer under flow conditions and the extent of chloride influence on the mass transfer rate.

The electrochemical reaction in the pit is assumed to be

$$Fe \rightarrow Fe^{++} + 2e^{-} \qquad (5.108)$$

In the very close region to the interface, or within the mass transfer boundary layer, the following equilibrium reaction is assumed to occur:

$$Fe^{++} + 2Cl^{-} \rightleftharpoons FeCl_2 \qquad (5.109)$$

The equilibrium constant for reaction (109) is

$$K_{Cl^-} = \frac{[FeCl^2]}{[Fe]^{++}\,[Cl^-]^2} \qquad (5.110)$$

in addition, a reaction front region is defined, which has a distance δ_1 from the wall and in which the following conditions are satisfied.

$$C_A = C_A^e \qquad (at\ y = \delta_1) \qquad (5.111)$$

and

$$C_B = C_B^e \qquad (at\ y = \delta_1) \qquad (5.112)$$

It is assumed that at the reaction front the following mass transfer Equation is satisfied.

$$J_A = (D_A + \varepsilon_D)\frac{dC_A}{dy} \qquad (5.113)$$

and

$$J_B = (D_B + \varepsilon_D)\frac{dC_B}{dy} \qquad (5.114)$$

Within the reaction front, approximately

$$J_A \delta_1 = D_A (C_{AS} - C_A^e) \tag{5.115}$$

Furthermore, if only reaction (109) is considered, then

$$J_A = -\frac{1}{2} J_B \tag{5.116}$$

Substituting Equations (114) and (115) into (116),

$$\frac{D_A (C_{AS} - C_A^e)}{\delta_1} = \frac{1}{2} \frac{C_{BM} - C_B^e}{\int_{\delta_1}^{y_M} \frac{dy}{D_B + \varepsilon_D}} \tag{5.117}$$

From Equation (117),

$$\int_0^{y_M} \frac{dy}{D_B + \varepsilon_D} = \frac{1}{2} \frac{\delta_1}{D_A} \frac{C_{BM} - C_B^e}{C_{AS} - C_A^e} + \int_0^{\delta_1} \frac{dy}{D_B + \varepsilon_D} \tag{5.118}$$

On the other hand,

$$\frac{C_{BM} - C_B^e}{\int_0^{y_M} \frac{dy}{D_B + \varepsilon_D}} = Sh_B \frac{D_b}{D} \left(C_{BM} - C_B^e \right) \tag{5.119}$$

and

$$\int_0^{\delta_1} \frac{dy}{D_B + \varepsilon_D} \approx \int_0^{\delta_1} \frac{dy}{D_B} \approx \frac{\delta_1}{D_B} \qquad (5.120)$$

Further

$$\delta_1 = \frac{D}{Sh_A} \qquad (5.121)$$

Substitution of Equations (119) through (121) into (118) gives

$$Sh_A = \left(1 + \frac{1}{2}\frac{D_B}{D_A}\frac{C_{BM} - C_B^e}{C_{AS} - C_A^e}\right) Sh_B \qquad (5.122)$$

From Equation (122) we have

$$Sh_A = \left(1 + \frac{1}{2}\frac{D_B'}{D_A'}\frac{C_{BM} - C_B^e}{C_{AS} - C_A^e}\right)\left(\frac{D_A'}{D_B'}\right)^{0.33} Sh_A^o \qquad (5.123)$$

In Equation (123), we introduce prime to the diffusivities, which means that we correct the diffusivities for multicomponent effect. Also in Equation (123), Sh_A^o stands for the Sherwood number without chemical reaction between iron ion and chloride ion. Therefore, we obtain the mass transfer enhancement factor as follows:

$$F_{Cl^-} = \left(1 + \frac{1}{2}\frac{D_B'}{D_A'}\frac{C_{BM} - C_B^e}{C_{AS} - C_A^e}\right)\left(\frac{D_A'}{D_B'}\right)^{0.33} \qquad (5.124)$$

This mass transfer enhancement factor can be used for the shapes of pit discussed above.

The Modelling Strategy

In terms of modeling flow induced pitting attack of carbon steel exposed to a CO_2 and H_2S environment, it is assumed that if a surface is uniformally covered with iron carbonate or sulfide film, the corrosion rate is minimal. It is possible that a certain flow regime can cause a localized destruction of the iron protective film. If so, pitting corrosion can initiate at that particular location and may continue to propagate. In this modelling effort, the conditions leading to the continuation of the pit propagation step are investigated. It is therefore assumed that no pit propagation occurs if the pit surface resumes protection by re-accumulating iron carbonate or sulfide scale. If the damaging flow conditions persist, then the 'some how' initiated pit provides an active bare surface. Given an initial geometry of the pit and the equilibrium concentrations of the different species, the fluid flow calculations provide a measure for the extent of mass transfer rate between the pit and the bulk flow. It is presumed that iron metal dissociates at the bare surface following Equations (22) and (23) to produce iron ion. The consumption of Fe^{++} occurs at the metal surface following Equations (24) through (26), and the precipitation of iron carbonate and/or sulfide occurs. However due to the fluid flow, mass transfer from the inside of the pit to the bulk is simultaneously in effect. A mass balance on the iron ion should account for the surface chemical reaction, the electrochemical process at the surface, and the mass transfer contribution. Let J_c, J_e, and J_m denote the three above contributions

respectively, then they are expressed as follows:

$$J_c = \left(\frac{1}{AREA}\right) k_s\left\{\left[(Fe^{++})_s(CO_3^{--})\right]^{1/2} - K_{so}^{1/2}\right\}^2 + R_{Fe^{++}} \quad (5.125)$$

$$J_e = \left(\frac{1}{area}\right) 2Fi_{cor} \quad (5.126)$$

$$J_m = K\left([Fe^{++}]_s - [Fe^{++}]_\infty\right) \quad (5.127)$$

$$J_m = J_e - J_c \quad (5.128)$$

If the expressions from Equations (125) through (127) are substituted into Equation (128), then a quadratic equation is obtained to solve for the iron ion surface concentration. The calculated concentration from the resulting equation is then compared to the supersaturation value given by the iron carbonate and iron sulfide precipitation equilibrium reactions. If the surface concentration is higher than the supersaturation value, the pit is judged passive, else it is presumed to propagate. The growth rate is given using the following flux:

$$J_{cor} = K\left([Fe^{++}]_{supsat} - [Fe^{++}]_s\right) \quad (5.129)$$

The corrosion rate calculated from the above expression fits the modeling philosophy as it reflects the extent of pit propagation in the absence of an iron scale protective film. In other words, this model gives a pit propagation rate with respect to a reference state obtainable if an iron scale film forms and fully remains on the surface of the metal.

Results and Discussion

The model, as developed, is aimed to study the fluid flow effects on the propagation rate of an existing pit along the tubing wall in a corrosive CO_2 and H_2S aqueous environment. The predictions of the model are based on an initial shape of the pit and the equilibrium, chemical, and electrochemical activities of the flowing species. The testing of the model capabilities will be illustrated through the use of several test cases. The input to the model consists of the flowing conditions of a gas well, its gas composition, and its water analysis. At each section of the tubing, the model calculations are performed for three assumed initial penetrations. The three values of 10, 30, and 50 % penetrations have been chosen because, by the caliper survey convention, these three levels are considered small, moderate, and severe respectively. If a caliper survey has been performed on a given well, the model is capable to predict the propagation rate of existing pits along the pipe. Accounting for the flow conditions and the chemistry both outside and inside the pit, the surface concentration of Fe^{++} on the pit wall is determined, from which the pit is judged active or passive, hence a propagation rate is estimated accordingly.

The Dynamics of the Model

Table XIV displays a portion of a typical output from the model. For each section, a descriptive information about the section is printed in the upper left corner, including wall thickness, well depth, percent CO_2 in the well, flow velocity of the liquid phase wetting the wall, and bulk temperature at the section corresponding to the specified well depth. Next, for each penetration level, three pits with different initial penetrations are listed along with the corresponding propagation rates. The corrosion rate, as calculated, is a measure of the ease of corrosion product removal out of the pit. The corrosion rate is assumed zero when the protective film accumulates in the pit. The easier its partial removal, i.e., the higher the mass transfer, the higher the corrosion rate. Such an observation is analyzed through the tabulated data, which displays the variations of growth rate with the initial penetration level and the location within the pipe. As the initial penetration level is raised from 10 to 30 to 50 percent, the propagation rate increases because the corrosion product is easier removed form the pit. A slightly lower severity of propagation rate at the top of the well is observed. This observation, presumably contrary to the overall corrosion picture for a gas well, can be caused by the lack of a very accurate calculation of the adherent liquid film thickness and its velocity and to the lack of corrosion film characterization as a function of temperature.

In terms of the modeling strategy, the corrosion rate mainly reflects the degree of turbulence in the bulk flow, which translates into agitation within the pit to facilitate mass transfer. In the following study cases, the effect of velocity on the

TABLE XIV

A SAMPLE OUTPUT FROM PIT PROPAGATION MODEL

WALL THICKNESS: 0.30 in.
DEPTH: 5700 ft
% CO2: 2.21
VELOCITY: 18.35 m/sec
TEMPERATURE: 208.0 F

% PENETRATION	PIT RADIUS (IN)	GEOMETRY	MPY
10	0.120	2	65.72
30	0.129	2	86.46
50	0.250	2	98.53

GEOMETRY: 1- SHALLOW PIT ; 2- MEDIUM ; 3- DEEP

WALL THICKNESS: 0.30 in.
DEPTH: 5200 ft
% CO2: 2.21
VELOCITY: 18.18 m/sec
TEMPERATURE: 199.8 F

% PENETRATION	PIT RADIUS (IN)	GEOMETRY	MPY
10	0.120	2	58.89
30	0.129	2	77.65
50	0.250	2	87.02

GEOMETRY: 1- SHALLOW PIT ; 2- MEDIUM ; 3- DEEP

various characteristic parameters of the model has been tested. For a given set of well conditions, Figure 22 displays the influence of velocity on the wall shear stress. Such an increasing effect is dependent on the pit shape and yields to a higher mass transfer out of the pit into the bulk stream as shown on Figure 23. The iron ion surface concentration is also plotted as a function of velocity on Figure 24 and shows a decreasing trend with higher turbulence. All these flow and mass transfer parameters quantitatively indicate the detrimental effect of velocity on the buildup of a protective corrosion product inside the pit. Figure 25 illustrates the overall effect of velocity on the propagation rate of an existing pit.

Testing of the Model

In the following section, the model is tested against some actual field data. However, it is essential to precisely state that, in exact terms, the availability of actual or experimental data, which describe pit propagation rate for downhole applications in CO_2 and H_2S environments, is scare. Commonly, the overall corrosion rates for a given gas well can be measured through caliper surveys, corrosion coupons, or iron counts. If available from the former, such rates are usually a collection of penetration rates at the tubing joints. Such information is an indication of the extent of localized corrosion at the various sections of the pipe. The difficulty of matching the predictions from the developed model with the measured rates pertains to the assumption of the initial shape of a given pit at a given location. Therefore a direct comparison of the model results to the actual data is not possible because the initial penetration of the assumed pit is usually unknown, yet required before the model

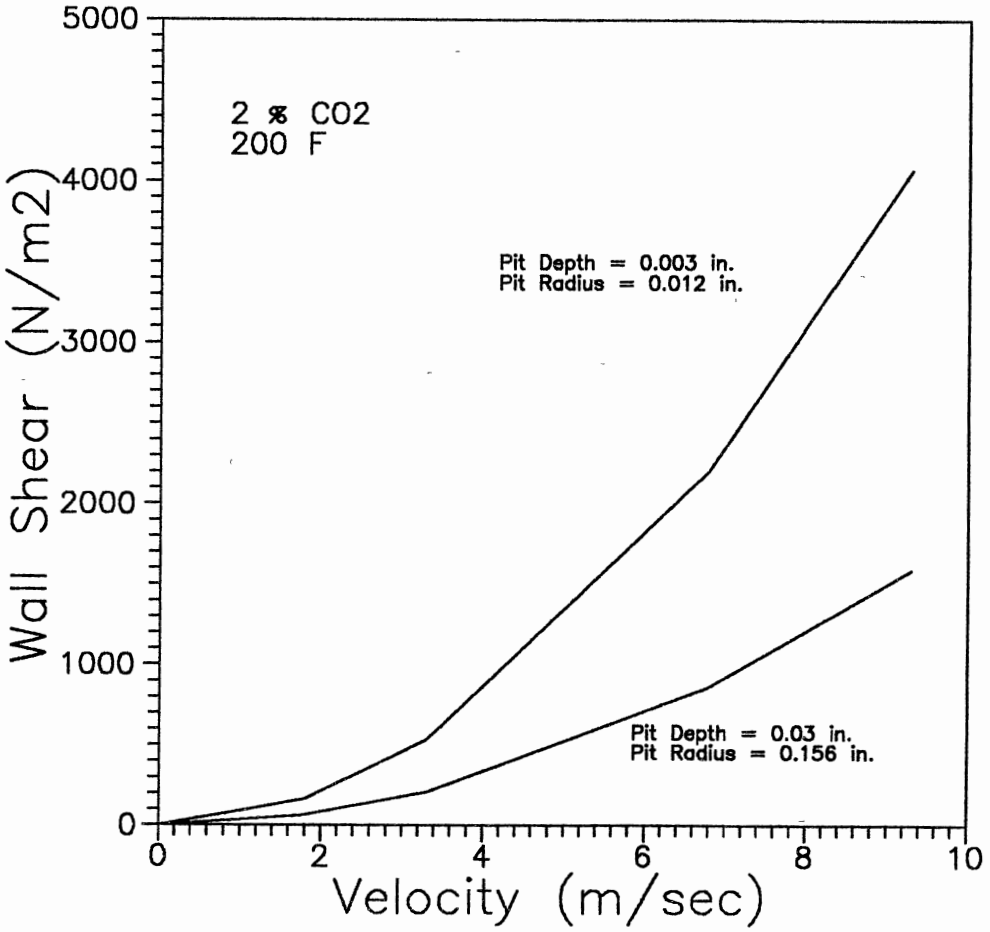

Figure 22. Velocity Effects on Wall Shear in the Pit

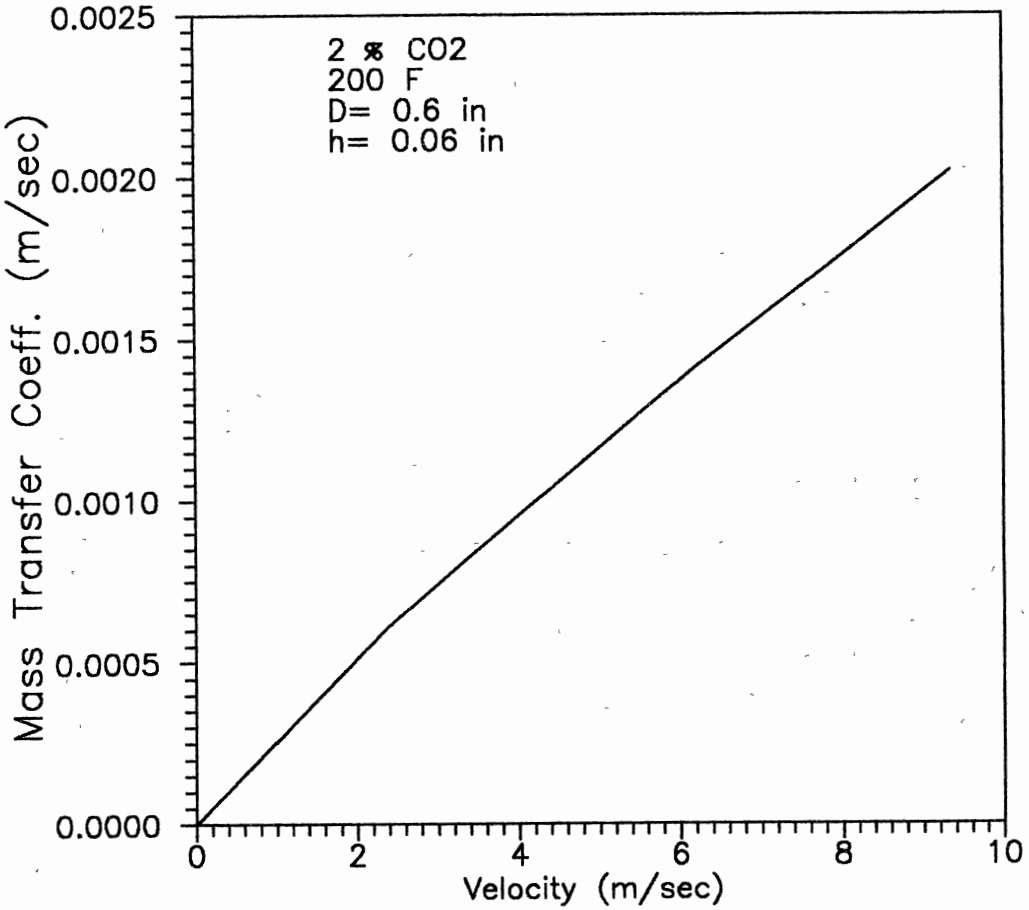

Figure 23. Velocity Effects on Mass Transfer in the Pit

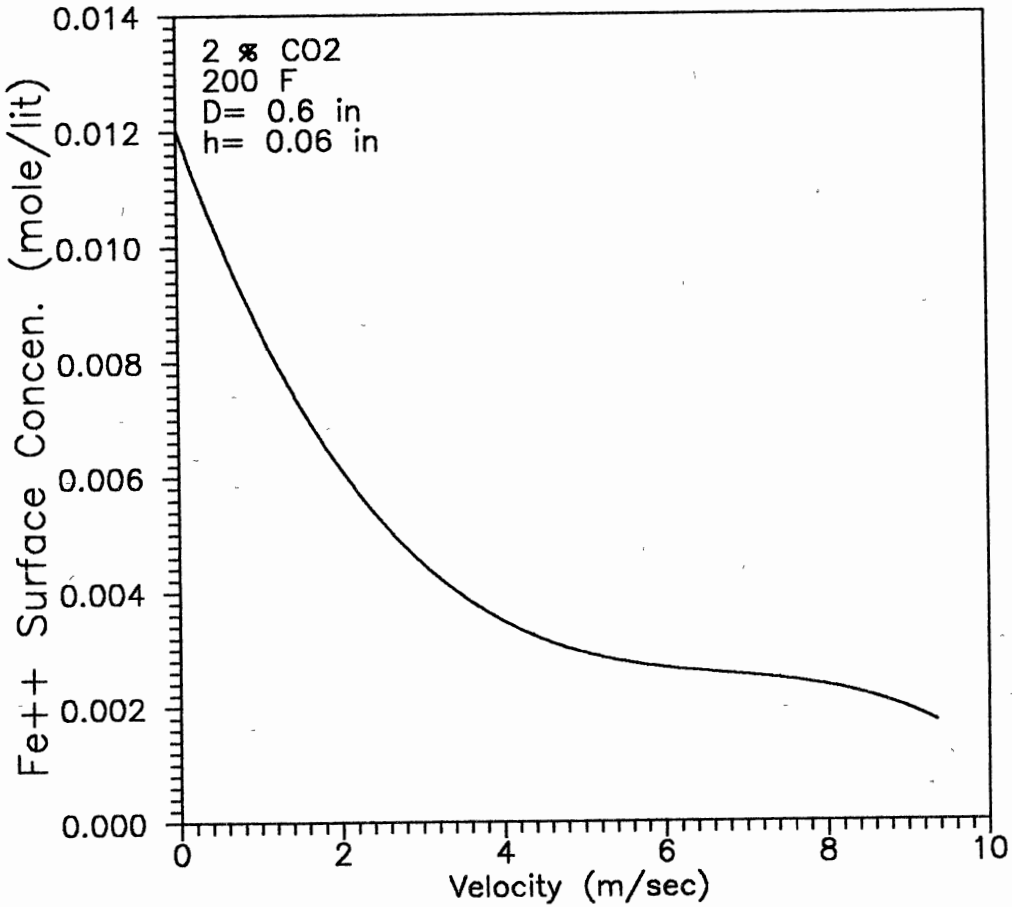

Figure 24. Velocity Effects on Iron Surface Concentration

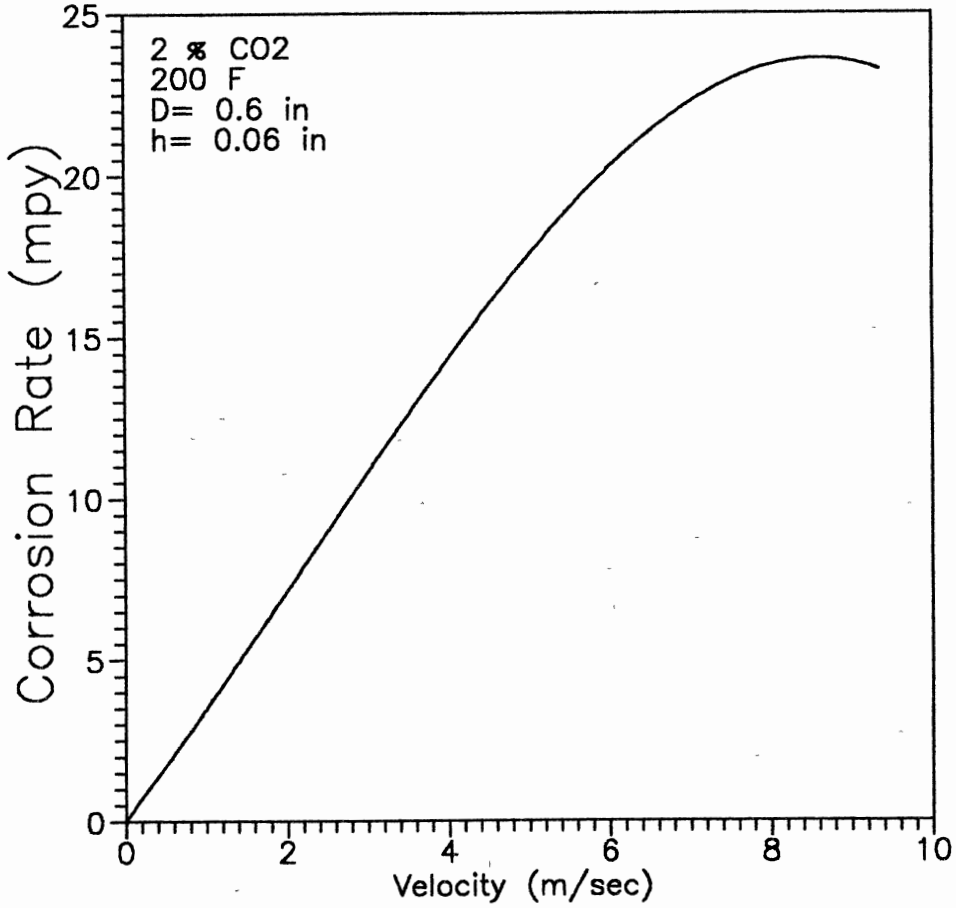

Figure 25. Velocity Effects on Pit Propagation Rate

calculations are performed. However, if a pit size assumed at a specified section of the tubing, then the flow conditions along with the chemistry inside and outside the pit can be used to predict an average propagation rate. Moreover, if the developed model is applied for a given well, it should be able to predict the severity of localized corrosion at least in a comparative way. For any prediction attempts, it is essential to assume that the model pertains to flow induced pitting corrosion only.

Case Study I. The model is used to predict the corrosion behavior of a given well, which failed after four years of service. The failure consists of detecting several holes along the pipe wall at various sections of the string. The flow conditions of the gas well, its gas composition, and the corresponding water chemistry are listed in Tables XV, XVI, and XVII respectively. The well produces about 2150 thousand cubic feet of gas containing 2.2% CO_2, with a water production of 28 barrels per day. The well conditions were used as input to the model. Table XVIII displays the predicted behavior of three pits with different geometries along the pipe wall at two distinct sections. The complete output from the model consists of the same data at the rest of the sections. Figure 26 displays the corrosion profiles along the tubing as predicted from the model, along with the field data. Each curve assumes an initial penetration level. As can be observed from the figure, the predictions span the random field data range. The top curve corresponds to a 21 % initial penetration and the bottom to a 1 % level. The curves can directly be used to predict the future behavior of a given pit size existent after the caliper survey has been performed. However the field data from the caliper survey can not be matched by the model

TABLE XV

WELL CHARACTERISTICS FOR DOWNHOLE CASE STUDY I

Specifications	Units	Values
Water Production	B/D	28
Gas Production	MSCFD	2150
Depth	ft	9700
Tubing Diameter, ID	inches	2.441
Wellhead Pressure	psia	1890
Wellhead Temperature	°F	130
Bottomhole Pressure	psia	4000
Bottomhole Temp.	°F	290

TABLE XVI

GAS ANALYSIS FOR DOWNHOLE CASE STUDY I

Component	Mole Percent
Methane	90.94
Ethane	4.37
Propane	1.14
I-butane	0.27
N-butane	0.23
I-pentane	0.13
N-pentane	0.08
Hexane	0.11
Heptane Plus	0.27
Nitrogen	0.25
Carbon Dioxide	2.21
Total	100.00

TABLE XVII

WATER ANALYSIS FOR DOWNHOLE CASE STUDY I

Constituent	ppm
Sodium	6490
Calcium	298
Magnesium	38
Barium	4
Iron	36
Chloride	10100
Sulfate	111
Bicarbonate	879
Total Solids	17956

TABLE XVIII

SAMPLE OF THE MODEL OUTPUT FOR DOWNHOLE CASE STUDY I

WALL THICKNESS: 0.30 in.
DEPTH: 10200 ft
% CO2: 2.21
VELOCITY: 18.82 m/sec
TEMPERATURE: 282.2 F

% PENETRATION	PIT RADIUS (IN)	GEOMETRY	MPY
10	0.120	2	123.83
30	0.129	2	160.90
50	0.250	2	193.04

GEOMETRY: 1- SHALLOW PIT ; 2- MEDIUM ; 3- DEEP

WALL THICKNESS: 0.30 in.
DEPTH: 9700 ft
% CO2: 2.21
VELOCITY: 18.89 m/sec
TEMPERATURE: 274.0 F

% PENETRATION	PIT RADIUS (IN)	GEOMETRY	MPY
10	0.120	2	116.69
30	0.129	2	151.76
50	0.250	2	181.76

GEOMETRY: 1- SHALLOW PIT ; 2- MEDIUM ; 3- DEEP

WALL THICKNESS: 0.30 in.
DEPTH: 9200 ft
% CO2: 2.21
VELOCITY: 18.92 m/sec
TEMPERATURE: 265.8 F

% PENETRATION	PIT RADIUS (IN)	GEOMETRY	MPY
10	0.120	2	111.15
30	0.129	2	144.69
50	0.250	2	172.93

GEOMETRY: 1- SHALLOW PIT ; 2- MEDIUM ; 3- DEEP

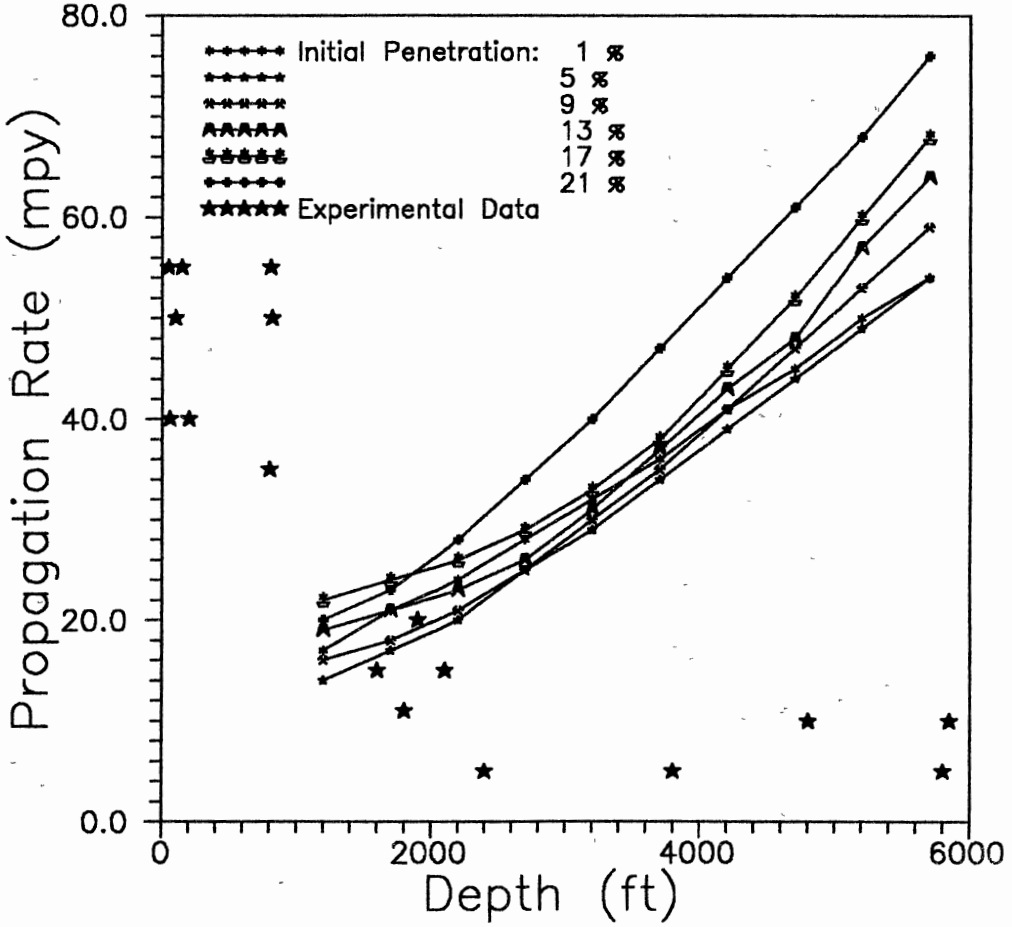

Figure 26. Prediction of Pit Propagation for Case Study I

output because it does not provide the initial penetration levels of the pits. However, the fitted predictions qualitatively match the severity of the well.

Case Study II. A conveniently chosen second case study is analyzed using the developed model. The well produces about the same amount and quality of water as case I and half the amount of gas. The CO_2 content is also about half of the content of the well in case I. The well characteristics, the gas composition, and the water chemistry are listed in Tables XIX, XX, and XXI respectively. A sample of the output for this case study is shown in Table XXII. The model results are presented on Figure 27 along with the corresponding field data for different initial penetration levels. Again, the predictions seem to fit within the data range, reflecting the right magnitude of well susceptibility to corrosion. The curves can be used to predict the behavior of a given pit along each section of the pipe. On the other hand, if compared to the output from case I, the results confirm the field observation indicating that this well is about 40% less corrosive than the well in case I.

Even though a direct comparison between the model results and a given field data is not appropriate, the predictions can be successful in determining the extent of pitting attack severity for a given application. Furthermore, if an initial geometry of a pit can be assumed, detected, or guessed at a given location of the tubing, the model will predict its rate of propagation as a function of the flow parameters inside the pipe and the dominant chemistry of the flowing stream.

TABLE XIX

WELL CHARACTERISTICS FOR DOWNHOLE STUDY CASE II

Specifications	Units	Values
Water Production	B/D	27
Gas Production	MSCFD	1352
Depth	ft	9450
Tubing Diameter, ID	inches	2.441
Wellhead Pressure	psia	1440
Wellhead Temperature	°F	130
Bottomhole Pressure	psia	4000
Bottomhole Temp.	°F	290

TABLE XX

GAS ANALYSIS FOR DOWNHOLE CASE STUDY II

Component	Mole Percent
Methane	91.60
Ethane	4.39
Propane	1.18
I-butane	0.33
N-butane	0.25
I-pentane	0.14
N-pentane	0.09
Hexane	0.13
Heptane Plus	0.33
Nitrogen	0.30
Carbon Dioxide	1.26
Total	100.00

TABLE XXI

WATER ANALYSIS FOR DOWNHOLE CASE STUDY II

Constituent	ppm
Sodium	6280
Calcium	454
Magnesium	50
Barium	2
Iron	0
Chloride	10300
Sulfate	196
Bicarbonate	313
Total Solids	17595

TABLE XXII

SAMPLE OF THE MODEL OUTPUT FOR DOWNHOLE CASE STUDY II

WALL THICKNESS: 0.30 in.
DEPTH: 9950 ft
% CO2: 1.26
VELOCITY: 14.23 m/sec
TEMPERATURE: 277.8 F

% PENETRATION	PIT RADIUS (IN)	GEOMETRY	MPY
10	0.120	2	55.42
30	0.129	2	72.63
50	0.250	2	86.46

GEOMETRY: 1- SHALLOW PIT ; 2- MEDIUM ; 3- DEEP

WALL THICKNESS: 0.30 in.
DEPTH: 9450 ft
% CO2: 1.26
VELOCITY: 14.20 m/sec
TEMPERATURE: 269.4 F

% PENETRATION	PIT RADIUS (IN)	GEOMETRY	MPY
10	0.120	2	48.20
30	0.129	2	63.23
50	0.250	2	75.14

GEOMETRY: 1- SHALLOW PIT ; 2- MEDIUM ; 3- DEEP

WALL THICKNESS: 0.30 in.
DEPTH: 8950 ft
% CO2: 1.26
VELOCITY: 14.16 m/sec
TEMPERATURE: 260.9 F

% PENETRATION	PIT RADIUS (IN)	GEOMETRY	MPY
10	0.120	2	41.44
30	0.129	2	54.43
50	0.250	2	64.56

GEOMETRY: 1- SHALLOW PIT ; 2- MEDIUM ; 3- DEEP

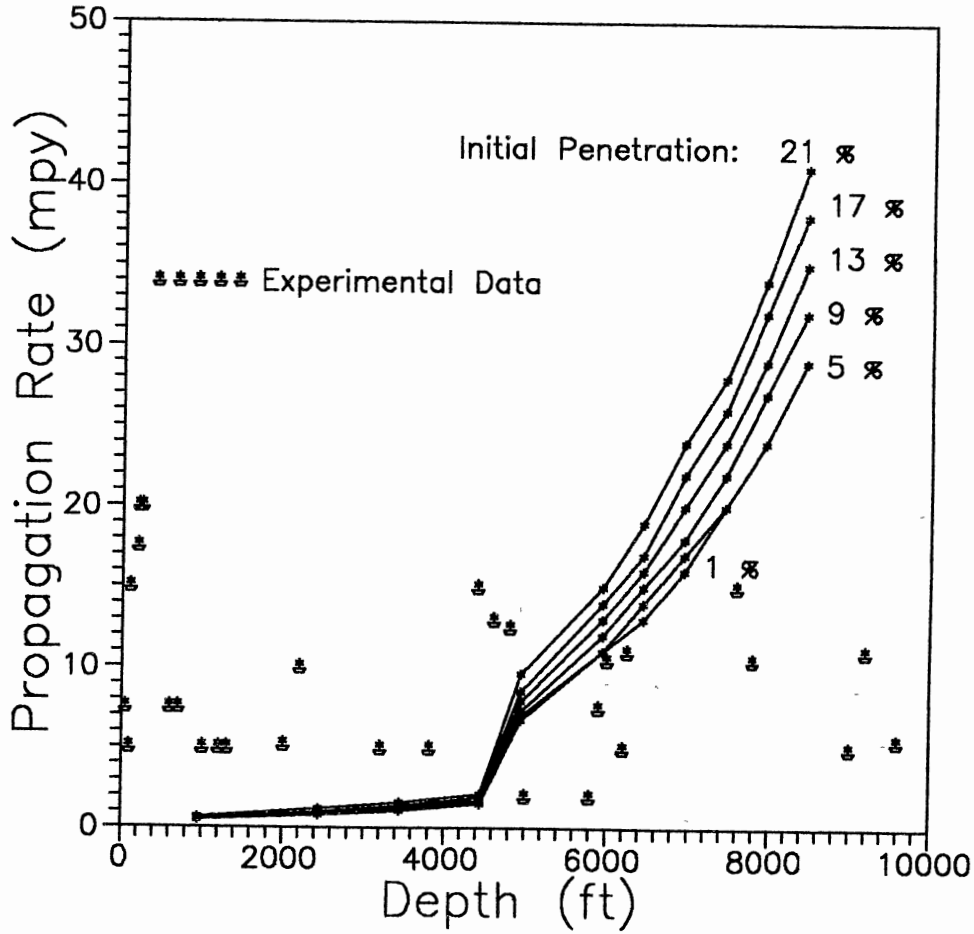

Figure 27. Prediction of Pit Propagation for Case Study II

Summary and Findings

1. Pitting corrosion of carbon steel in CO_2 and H_2S aqueous environments has been modelled in high turbulence regimes, in order to predict the extent of propagation of any existing pit along the pipe.

2. The hydrodynamics inside the pit have been simulated using the concept of flow separation and reattachment for shallow and medium size pits. Deeper pits, however, have been assumed to experience skimming flow.

3. The equilibrium conditions, the surface kinetics, the mass transfer rate, and the electrochemical processes at the pit walls have been used to predict the surface concentration of the ferrous ion, an indication of the extent of corrosion.

4. The supersaturation criterion has been used as an indication of pit repassivation. If the calculated surface concentration of Fe^{++} is higher than the supersaturation state, then the pit is passive.

5. When the pit is active, the corrosion rate has been based on the partial coverage of the pit walls with iron scale, i.e., the propagation rate is proportional to the mass transfer coefficient and the concentration difference between supersaturation and surface.

6. Both the thickness of the liquid film against the wall and that of the mass transfer boundary layer at the bottom of the pit have been assumed a value which can introduce less accuracy to the analysis.

7. An analytical solution has been derived for the mass transfer effects. The multicomponent system has been simulated through the generation of a correction

factor for diffusivities, so called the G function. A better analysis would consist of solving the system of ordinary differential equations for the species concentrations to avoid the error inherent to the analytical assumption.

8. In terms of propagation rate modelling, a reference state has been chosen as a zero point. Such state is obtained when the iron protective film is formed and remains on the metal.

9. The effects of velocity on flow parameters inside the pit have been studied. The mass transfer has been found enhanced with an increasing velocity, hence a higher propagation rate for shallow and medium size pits.

10. The model has been tested to predict the extent of corrosion severity for some actual gas wells in service.

CHAPTER VI

CONCLUSIONS AND RECOMMENDATIONS

This work has provided a study of CO_2 and H_2S pitting corrosion at its initiation and propagation steps caused by high velocity regimes. The initiation process has been studied through an experimental investigation, whereas the propagation rate of an existing pit has been modelled based on theoretical and mechanistic principles. A statistical model has also been developed to statistically analyze and predict the random behavior of pitting corrosion at the macro level. Several conclusions and recommendations, listed below, have been drawn from the three different sections of the work.

1. Flow induced pitting corrosion of carbon steel can be obtained in a simulated environment containing ASTM synthetic seawater and oil solution saturated with CO_2 at 160° F and flowing at 50 ft/sec.

2. A modified concentric cylinder apparatus is found useful for studying flow induced pitting corrosion in CO_2 environments.

3. The cyclic polarization technique can be applied to measure pitting initiation in inhibited CO_2 environments.

4. The technique of a preconditioning period followed by the galvanic corrosion measurement method is found viable for studying pit initiation and propagation in

inhibited CO_2 environments.

5. The random behavior of the deepest pits on a given corroded sample has been found to obey the Extreme Value Distribution theory. Its prediction and analysis are performed upon the estimation of the distribution coefficients.

6. The hydrodynamics inside a pit can be simulated using the concept of flow separation and reattachment if the pit is shallow or medium, whereas skimming flow theory can be applied if the pit is deep.

7. An analytical solution was developed for the mass transfer effects. A better analysis would consist of solving the system of ordinary differential equations for the species concentrations to avoid the error inherent to the analytical solution.

8. Better predictions of pitting corrosion in CO_2 and H_2S environments can be obtained if the random characteristics of the phenomenon are incorporated in a single model which also describes its mechanistic behavior.

REFERENCES

Alkire R. and A. Cangellari, J. Electrochem. Soc., 121, 1000, 1974.

Alkire R., D. Ernsberger, and D. Damon, J. Electrochem. Soc., 123, 458, 1978.

Alkire R. and D. Siitari, J. Electrochem. Soc., 126, 458, 1979.

Alkire R. and E. A. Grens, J. Electrochem. Soc., 116, 177, 1969.

Alkire R. C., H. Deligianni, and J. B. Ju, J. Electrochem. Soc., Vol. 37, No. 3, March 1990.

Ateya B. G. and H. W. Pickering, J. Electrochem. Soc., 129, 453, 1981.

Ateya B. G. and H. W. Pickering, J. Electrochem. Soc., 122, 1098, 1975.

Aziz P. M. and H. P. Godard," Pitting Corrosion Characteristics of Aluminum", Industrial and Engineering Chemistry, Vol.44,No.8, pp. 1791-95, August 1952.

Aziz P. M.,"Application of the Statistical Theory of Extreme Values to the Analysis of Maximum Pit Depth Data for Aluminum", Corrosion- National Association of Corrosion Engineers, Vol.12, pp. 35-46, October 1956.

Batchelor J. K., J. Fluid Mech. 1, 177, 1956.

Beavers J. A. and N. G. Thompson, Corrosion NACE, Vol. 43, No. 3, pp.185-188, March 1987.

Beck T. R. and R. C. Alkire, J. Electrochemical Soc., 26, No. 10, 1882.

Berendson J. and G. Wranglén, Corrosion Science, Vol. 20, pp. 937-940, 1980.

Bockris J. O'M., D. Drazic, and J. M. Despic, Electrochimica Acta, 4, 325-361, 1961.

Boffardi B. P. and H. P. Godard,"Practical Application of Statistics- Part 1 through 6", Material Performance, October 1989 through July 1990.

Bradley D. J. and Pitzer K. S., J. Phys. Chem., 883, 1599-1603, 1979.

Byrd R. B., Stewart, W. E., Lightfoot, E. N., Transport Phenomena, John Wiley and Sons, NY, 1960.

Chaney P. E.," Internal Tubing Caliper Measures- Extent and Location of Corrosion", Oil & Gas Journal, 44, 115, pp. 115-119, April 20, 1946.

Chaney P. E.," Internal Tubing Caliper", The Petroleum Engineer, pp. 122-123, April 1946.

Chilton J. P. and U. R. Evans," The Corrosion Resistance of Wrought Iron", Journal 6 the Iron and Steel Institute", pp. 113-122, October 1955.

Denpo K., and Ogawa, H., Fluid Effects on Corrosion Resistance of Oil- Well Materials, Paper No. 28, Corrosion-NACE '90, 1990.

Edwards T. J., G. Maurer, J. Newman, and J. M. Prausnitz, AIChE J., 24, 966-976, 1978.

Eldredge G. G.," Analysis of Corrosion Pitting by Extreme Value Statistics And Its Application to Oil Well Tubing Caliper Surveys", Corrosion-NACE, Vol.13, pp. 51t-60t, January 1957.

Evans U. R., R. B. Mears, and P. E. Queneau. Engineering, Vol. 136, p. 689, 1933.

Faita G, F. Mazza, and G. Bianchi, Localized Corrsion, Vol. 34, NACE 1974.

Finley H. F. and A. C. Toncre," Extreme Value Statistical Analysis in correlation of First Leak on Submerged Pipelines", Material Protection, pp. 29-35, September 1964.

Findley Howard F.," An Extreme Value Statistical Analysis of Maximum Pit Depths and Time to First Perforation", Corrosion-NACE, pp.83-87, April 1967.

Gabrielli C., F. Huet, M. Keddam, and R. Oltra," A Review of the Probabilistic Aspects of Localized Corrosion", Corrosion Science, Vol.40,No.4, pp. 266-278, April 1990.

Gabriel C., F. Huet, M. Keddam, and R. Oltra, Corrosion Science, Vol. 46, No. 3, pp. 266-278, April 1990.

Galvele J. R., Corrosion Science, Vol. 21, No. 8, pp. 551-579, 1981.

Galvele J. R., J. Electrochem. Soc., 123, 1438, 1976.

Gay B. and T. E. Alcorn, Chemical Engineering Science, Vol. 17, pp. 641-654, 1962.

Godard Hugh P.,"The Corrosion Behavior of Aluminum in Natural Waters", The Canadian Journal of Chemical Engineering, pp. 167-173, October 1960.

Gray L. G. S., B. G. Anderson, M. J. Danysh, and P. R. Tremaine, Corrosion/89, Paper No. 464, New Orleans, Louisiana, 1980.

Greene N. D. and M. G. Fontana,"An Electrochemical Study of Pitting Corrosion in Stainless Steels", Corrosion- NACE, Vol.15, pp.32t-44t, January 1959.

Gumbel Emil J.," Statistical Theory of Extreme Value and Some Practical Applications", National Bureau of Standards, Applied Mathematics Series, 33,Issued February 12, 1954.

Gumbel Emil J., Statistics of Extremes, Columbia Press, New York, NY, 1958.

Gravano S. M. and J. R. Galvele, Corrosion Science, 24, 517, 1984.

Hebert K. and R. Alkire, J. Electrochem. Soc., 130, 1007, 1983.

Johnson B. V., H. J. Choi, and A. S. Green, Paper No. 573, NACE Corrosion'91, 1991.

Kawazuishi K. and J. M. Prausnitz, Ind. Eng. Chem. Res., 26, 1482-1485, 1987.

Kerr C. P., ACS Symposium Series 133, ACS, Washington, D. C., 91-106, 1980.

Kondo Y., Corrosion Science, Vol. 45, No. 1, pp. 7-11, Jan. 1989.

Levich V. G., Physicochemical Hydrodynamics, Prentice-Hall, Englewood, N.J., 1962.

Li J. H. and S. Gregory, Geochimica et Cosmochimica Acta, Vol. 38, pp. 703-714, 1974.

Lin C. S., R. W. Moulton, and G. L. Putnam, Ind. Eng. Chem., 45, 636-640, 1953.

Liu Guohai, PhD. Thesis, Oklahoma State University, Stillwater, OK, 1991.

Marsh G. P. and K. J. Taylor, Corrosion Science, Vol. 28, No. 3, pp. 289-320, 1988.

Mears R. B. and R. H. Brown,"Corrosion Probability", Industrial and Engineering Chemistry, Vol.29,No.10, pp. 1087-91, October 1937.

Melville P. H., Br. Corrosion, J. 14, 15, 1979.

Morris H. M., Proc. Amer. Soc. Civ. Eng., Vol. 80, No. 390, 1954.

Nathan C. C. and C. L. Dulaney," Localized Corrosion as a Statistical Phenomenon", presented at U. R. Evans Conference on localized Corrosion, Williamburg, Virginia, NACE-3, Houston, Texas, pp.184-189, 1971.

Ogundele G. I. and W. E. White, Corrosion, 42, 71-78, 1986.

Oldfield J. W. and W. H. Suttun, Br. Corrosion, J. 13, 104, 1978.

Pan F. and A. Acrivos, J. Fluid Mech, Vol. 28-4, pp. 643-655, 1967.

Pound B. G., G. A. Wright, and R. M. Sharp, Corrosion, Vol. 45, No. 5, pp. 386-392, May 1989.

Pourbaix Marcel, Atlas of Electrochemical Equilibrium, 1974.

Provan J. W. and E. S. Rodriguez III,"Part I: Development of a Markov Description of Pitting Corrosion", NACE Corrosion-Vol.45, No.3, pp.178-92, March 1989.

Rodriguez III E. S. and J. W. Provan, Corrosion Science, Vol. 45, No. 3, pp. 193-206, March 1989.

Sato Norio," Stochastic Process of Chloride Pit Generation in Passive Stainless Steel", Journal of Electrochemical Society, Vol. 123, No. 8, pp. 1197-1199, August 1976.

Silverman D., Corrosion Chemistry within pits, Crevices and Cracks, National Physical Laboratory, 1-3 October, 1984.

Sharland S. M., Corrosion Science, Vol. 27, No. 3, pp. 289-323, 1987.

Sharland S. M., C. P. Jackson, and A. J. Diver, Corrosion Science, Vol. 29, No. 9, pp.1149-1166, 1989.

Sharland S. M. and P. W. Tasker, Corrosion Science, Vol.28, No. 6, 603-620, 1988.

Sheikh A. K., J. K. Boah, and D. A. Hansen," Statistical Modeling of Pitting Corrosion and Pipeline Reliability", NACE Corrosion, Vol. 46, No. 3, pp. 190-197, March 1990.

Shibata T. and T. Takeyama," Stochastic Theory of Pitting Corrosion", Corrosion-NACE, Vol. 33, No. 7, pp. 243-251, July 1977.

Shuck R. R. and J. L. Swedlow, Localized Corrosion, pp. 190, 208, NACE 1974.

Smyrl W. H. and J. Newman, J. Electrochem. Soc., 121, 1000, 1974.

Stetler Frank E.," Accelerating Leak Rate In Ductile Steel Iron Water Mains Yields to Cathodic Protection", Material Performance-NACE, pp. 15-20, October 1980.

Streicher M. A.,"Pitting Corrosion of 18Cr-8Ni Stainless Steel", Journal of Electrochemical Society, Vol.103, No.7, pp. 375-390, July 1956.

Strutt J. E., J. R. Nicholls and B. Barbier,'The Prediction of Corrosion by Statistical Analysis of Corrosion Profiles', Corrosion Science, Vol. 25, No. 5, pp.305-315, 1985.

Tester J. W. and H. J. Isaacs, Journal of physical chemistry, Vol. 80, No. 17, 1976.

Tewari P. H. and A. B. Campbell, Can. J. Chem., Vol. 57, p. 188, 1979.

Turnbull A., British Corrosion Journal, Vol. 15, No.4, pp. 162-174, 1980.

Turnbull A. and J. G. N. Thomas, NPL DMA Report(A), 11, 1979.

Turnbull A. and J. G. N. Thomas, J. Electrochemical Soc., 1412-1422, 1982.

Viden K. and Dugstad, Proc. Symp. Corrosion/87, Vol. 9, pp. 585-603, 1987.

Wajon J. E., G. Ho, and P. J. Murphy, Water Res., Vol. 19, No. 7, pp. 831-837, 1985.

Walton J. C., Corrosion Science, Vol. 30, No. 8/9, pp. 915-928, 1990.

Wranglén Gösta, Corrosion Science, Vol.9, pp. 585-603, 1969.

Wranglén Gösta, Corrosion Science, Vol.14, pp. 331-348, 1974.

Xia Z., K. C. Chou, and Z. S. Smialowska, Corrosion, pp. 636-643, Aug. 1989.

VITA

Mohsen H. Achour

Candidate for the Degree of

Doctor of Philosophy

Thesis: PREDICTION OF DOWNHOLE GAS WELL PITTING CORROSION IN CO2 AND H2S ENVIRONMENT

Major Field: Chemical Engineering

Biographical:

Personal Data: Born in Chebba, Tunisia, September 29, 1962, the son of Mr. and Mrs. Hedi Achour.

Education: Graduated from Homma Charkia-Chebba Primary School, June 1973; Chebba High School: Baccalauriat, June 1981; Oklahoma State University: B.S. in Chemical Enginnering, May 1986; M.S. in Chemical Engineering, December 1987; completed requirements for the Degree of Doctor of Philosophy in Chemical Engineering in May 1992.

Professional Experience: Research Assistant, 1989-1992, School of Chemical Engineering, Oklahoma State University; Research Engineer, summers 1989/1990/1991, Conoco Inc., Ponca City, Oklahoma; Engineer, 1987-1988, STEG, Tunisia; Assistant Engineer, November-February, Masco, Holdenville, OK.